Physics – Uspekhi **51** (4) 319 – 353 (2008)

REVIEWS OF TOPICAL PROBLEMS PACS numbers: **32.80.–t**, **34.50.–s**, **36.40.–c**, 43.25.Cb, 79.20.Rf, **81.07.–b**

Cluster temperature. Methods for its measurement and stabilization

G N Makarov

DOI: 10.1070/PU2008v051n04ABEH006421

Contents

1. **Introduction** 319
2. **Cluster temperature and its influence on cluster properties and processes** 321
   2.1 Cluster temperature; 2.2 Temperature dependence of cluster polarizability; 2.3 Influence of temperature on the magnetic moment of clusters; 2.4 Temperature dependence of the cluster ionization potential; 2.5 Temperature effects on cluster optical properties; 2.6 The effect of internal temperature on other cluster properties
3. **Relation between cluster temperature, cluster structure, and binding energy of atoms (molecules) inside clusters** 328
   3.1 Inner phase and phase transitions in clusters; 3.2 Size and temperature dependence of the cluster structure; 3.3 Relation between cluster temperature and intermolecular interaction potential
4. **Methods of cluster excitation. Measurement and stabilization of cluster temperature** 332
   4.1 Excitation of clusters. Determination of cluster temperature from emission spectra; 4.2 Energy relaxation channels in excited clusters; 4.3 Stabilization of the metal cluster temperature in an inert gas; 4.4 Cluster temperature in a cluster light source; 4.5 Stabilization of cluster temperature on a surface; 4.6 Determination of cluster temperature from infrared absorption spectra of intercalated molecules; 4.7 Methods for measuring cluster melting temperature
5. **Stabilization of cluster temperature by evaporation** 340
   5.1 Association between canonical and microcanonical reaction rates; 5.2 'Evaporative ensemble.' Relation between cluster temperature and evaporation heat; 5.3 Relevant remarks
6. **Excitation of clusters upon collision with a solid surface** 342
   6.1 General remarks; 6.2 Energy transfer in cluster/surface collisions; 6.3 Formation of microshock waves inside clusters; 6.4 Other processes in clusters upon their collision with a surface
7. **Strong heating of clusters by superpower ultrashort laser pulses** 344
   7.1 Cluster ionization; 7.2 Coulomb and hydrodynamic explosions; 7.3 Generation of X-ray radiation and neutrons; 7.4 Characteristics of cluster excitation by vacuum ultraviolet radiation
8. **Conclusion** 348

References 349

Abstract. **Cluster temperature is an important material parameter essential to many physical and chemical processes involving clusters and cluster beams. Because of the diverse methods by which clusters can be produced, excited, and stabilized, and also because of the widely ranging values of atomic and molecular binding energies (approximately from 10^{-5} to 10 eV) and numerous energy relaxation channels in clusters, cluster temperature (internal energy) ranges from 10^{-3} to about 10^{8} K. This paper reviews research on cluster temperature and describes methods for its measurement and stabilization. The role of cluster temperature in and its influence on physical and chemical processes is discussed. Results on the temperature dependence of cluster properties are presented. The way in which cluster temperature relates to cluster structure and to atomic and molecular interaction potentials in clusters is addressed. Methods for strong excitation of clusters and channels for their energy relaxation are discussed. Some applications of clusters and cluster beams are considered.**

G N Makarov Institute of Spectroscopy, Russian Academy of Sciences, 142190 Troitsk, Moscow region, Russian Federation
Tel. (7-495) 334 02 32. Fax (7-495) 334 08 86
E-mail: gmakarov@isan.troitsk.ru

Received 21 June 2007, revised 26 September 2007
Uspekhi Fizicheskikh Nauk **178** (4) 337 – 376 (2008)
DOI: 10.3367/UFNr.0178.200804a.0337
Translated by Yu V Morozov; edited by A M Semikhatov

1. Introduction

Numerous studies of cluster beams are currently underway (see, e.g., monographs and volumes of collected papers [1 – 21] and reviews [22 – 73]). The heightened attention to clusters arises from concomitant dimensional effects. Clusters make up an intermediate link between individual elementary particles (atoms and molecules) and bulk liquids or solids. Due to the discrete structure of energy levels and a high surface-to-volume ratio, their properties are different from the properties of their constituent elements and bulk matter. For this reason, clusters are frequently referred to as 'a new phase of matter' [1].

Studies of cluster structure and dynamics are expected to help establish the lower limit for the number of particles at which the physical properties of bulk matter become apparent. Some authors have determined the number of molecules starting from which clusters exhibit certain char-

acteristics of a macroscopic substance. Specifically, it has been shown that the superfluidity of helium nanodroplets (clusters) [74] first manifests itself when the number of particles in a cluster is $N \geqslant 60-100$ [63, 67, 75–80]. Others have found the approximate number of particles in a cluster at which its structure and selected properties begin to resemble those of macroscopic matter (see Sections 2 and 3). But in the majority of cases, the limiting number of particles is an arbitrary quantity, because different properties of liquids or solids become apparent in clusters containing different numbers of particles.

Scientists appear to be increasingly interested in clusters and cluster beams in connection with the rapid development of nanotechnologies [81–83], a relatively new area of research having important practical implications. Cluster beams are used in micro- and nanotechnologies to manufacture thin films, produce novel materials, and treat surfaces [1–3, 7, 51, 68, 70]. Cluster beams are equally interesting from the standpoint of investigation of cluster properties and processes involving clusters.

Clusters containing $N \geqslant 10^2$ particles are termed nanoparticles. Close links between clusters and other nanoobjects are also underscored by the possibility of characterizing the electron properties and electric conductivity of small-size objects (e.g., nanowires and nanocontacts), which, like clusters, have a high surface-to-volume ratio in the framework of theoretical models and approaches used to describe clusters [84].

Developments in cluster science has given rise to a large number of interesting and practically important lines of investigations, such as the excitation of large van der Waals clusters by superstrong ultrashort laser pulses [85–111] and its use for the generation of X-ray radiation [92–103] and neutrons [104–111]; interaction of high-energy clusters and cluster ions between themselves and with solid surfaces [43, 70]; application of these interactions to nuclear synthesis [119–126] and initiation of chemical reactions [127–146]; film spattering [7, 51, 147–173]; and manufacturing new materials [159–177] and finishing their surfaces [178–196] with cluster beams. Studies of fullerenes or carbon clusters with a closed structure [11, 17, 31, 34, 45–48] and carbon nanotubes [16, 40, 49, 58, 73] have equally important practical implications. It is noteworthy that a group of scientists (R E Smalley, R F Curl, and H Kroto) were awarded the 1996 Nobel Prize in chemistry for the discovery of and research on fullerenes [45–47].

The many lines of cluster studies are highlighted in numerous monographs and reviews [1–73]. They include investigations of gas condensation processes and cluster beam generation [24–27, 54], the structure and dynamics of small loosely bound van der Waals complexes [27, 29, 32, 33, 36] and metal clusters [28], and the physics of small metal clusters [30]. Paper [35] considers the energy structure and quantum effects in large semiconducting clusters (semiconducting nanocrystals). Paper [37] is devoted to the structure, energy characteristics, and dynamics of clusters and cluster ions. Many papers review data on fullerenes [11, 17, 31, 34, 48, 49] (see also [45–47]) and carbon [11, 16, 17, 31, 34, 49] and the carbon nanotube [16, 40, 50, 58, 73] structure. The use of cluster beams in high-energy physics (proton scattering experiments) is considered in [42]. The authors of [39] (see also [43, 44]) discuss applications of clusters in femtochemistry. Reviews [52–57] deal with problems related to the excitation of cluster beams by superstrong ultrashort laser pulses and the use of laser-excited clusters to generate X-ray radiation and neutrons. References [52–57] overview the structure and properties of superfluid helium nanodroplets (clusters) along with spectroscopic characteristics of molecules and clusters embedded in helium droplets [61–63, 66, 67]. Final results of recent studies on surface treatment by gaseous ion cluster beams are reported in [68]. Phase transition in clusters are analyzed in [69], and extreme processes induced by collisions of clusters with solid surfaces are considered in [70]. Recent review papers [71, 72] report results of research on 'nanoscopic' superfluidity of small helium and hydrogen clusters [71] and discuss the possibility of selecting between molecules embedded in superfluid helium nanodroplets (clusters) [72].

This review is focused on the results of investigations on cluster temperature and its influence on cluster properties and physicochemical processes involving clusters and cluster beams. It includes an analysis of research on cluster temperature and describes methods for its measurement and stabilization. The temperature dependence of cluster properties is considered. The mode in which cluster temperature relates to cluster structure and to atomic and molecular potentials in clusters is addressed. Methods for the strong excitation of clusters and their energy relaxation channels are discussed. Some applications of clusters and cluster beams are illustrated.

The review is organized as follows. In Section 2, we define the cluster temperature (internal energy) and analyze its influence on the parameters of clusters and processes with their participation. Results of the studies on temperature dependence of polarizability and magnetic moments for metal clusters are presented. Experimental measurements and theoretical calculations of polarizability are shown to be significantly different; the inner cluster temperature must be taken into account to correlate them. The influence of temperature on the cluster photoionization potential and optical properties is analyzed. The temperature dependence of other cluster properties and processes is discussed.

In Section 3, we consider the phasic states of van der Waals and metal clusters and the structure and temperature of clusters in molecular beams. We show the effect of temperature variations on cluster phase and structure. Temperature-dependent structural changes in van der Waals clusters and neutral and charged carbon and water clusters are addressed. The relation between the cluster temperature and the binding energy of constituent atoms and molecules is considered.

Methods for the excitation, measurement, and stabilization of the temperature of clusters are described in Section 4. The section contains results of experiments on laser excitation of metal and carbon clusters (fullerenes) and an estimation of cluster temperature from emission spectra in the visible and ultraviolet (UV) regions. Similar results on the excitation of carbon clusters by electron impact are briefly discussed. Data on energy relaxation channels in strongly heated clusters are presented along with experimental measurements and theoretical calculations for the stabilization of cluster temperature by collisions with inert gas atoms. We show that the cluster temperature can be stabilized by depositing clusters on a solid surface. Application of strongly heated clusters in cluster light sources is discussed; cluster temperatures in such sources are reported. A method for determining the temperature of intracluster molecules from infrared (IR) absorption spectra is described. Spectroscopically measured temperatures of

large ($N \geqslant 10^3$) superfluid helium clusters (nanodroplets) are presented. Methods for the measurement of cluster temperature and melting heat are considered.

Results of investigations on the stabilization of cluster temperature by evaporation are discussed in Section 5. The notion of an 'evaporative ensemble' is introduced to consider the association between canonical and microcanonical monomolecular reaction (cluster evaporation) rates. The relation between cluster temperature and evaporation heat is analyzed. The analysis is supplemented by relevant notes on the characteristics of the 'evaporative ensemble.' Data on the cluster and cluster ion evaporation rates are briefly discussed.

Analysis of cluster excitation resulting from cluster collisions with a solid surface is presented in Section 6 including characteristics of this process and the concomitant accumulation of energy by excited clusters. Collisions of high-energy clusters and cluster ions with solid surfaces inside a cluster and in the collision zone are shown to lead to anomalously high temperature, density, and pressure accompanied by generation of microshock waves. Physico-chemical processes induced in the clusters and in the zone of collisions under these extreme conditions (ionization, emission of light and charged particles, fragmentation, breakup and formation of chemical bonds, generation of microshock waves, nuclear synthesis, bombardment of the surface) do not occur in thermal equilibrium. The outcomes and possible implications of these processes are briefly discussed.

In Section 7, we present data on the strong heating of van der Waals clusters by superpower ultrashort laser pulses, the excitation of clusters and ions by laser light, induced Coulomb and hydrodynamic explosions, and the electron and ion temperature of clusters obtained in such experiments. The generation of X-ray radiation and neutrons is considered with reference to differences and similarities of cluster excitation upon collision with a surface or under the effect of superstrong ultrashort laser pulses. The closing Section 8 summarizes the most important results of the studies being reviewed and prospects of further research.

2. Cluster temperature and its influence on cluster properties and processes

Before considering cluster temperature and its effects, we recall that clusters are aggregates containing somewhere between a few and millions of atoms and molecules held together by a variety of bonds with energies from tenths of an electronvolt to several electronvolts [1]. The difference between atomic binding energies inside clusters is illustrated by the following example. The binding energy E_b in helium clusters ^4He_N (nanodroplets) is $E_b \leqslant 7.2$ K [77] ($\leqslant 10^{-3}$ eV) compared with 1.1 mK ($\approx 10^{-7}$ eV) in $^4He_2$ dimers [197]. The binding energy of atoms in clusters of metals, carbon, and other refractory materials ranges from roughly 1 eV to 10 eV.

Clusters can be obtained in a variety of ways. Clusters and cluster beams are usually formed in supersonic gas-dynamic jets; metal clusters are generated by laser light. Other common methods include gas aggregation, surface erosion, spraying, laser ablation, pulsed arc discharge, and plasma-based techniques [1–3, 12, 26, 54]. All these methods for cluster and cluster beam production and investigation are comprehensively considered in the wonderful book by Pauly [1] and review papers [22, 26, 30, 54, 70, 198–200].

2.1 Cluster temperature

The internal temperature of a cluster is a function of the energy of random motion of its constituent atoms or molecules relative to the center of mass. When the cluster rotational and translational degrees of freedom are 'frozen,' its internal temperature is given by

$$\frac{3N}{2} k_B T_{cl} = \left\langle \sum_{i=1}^{N} \frac{m_i (v_{c.m.} - v_i)^2}{2} \right\rangle , \tag{2.1}$$

where m_i and v_i are the mass and velocity of the constituent atoms (molecules), $v_{c.m.}$ is the center-of-masses velocity, N is the number of particles in the cluster, and k_B is the Boltzmann constant.

Relation (2.1) is the kinetic definition of the cluster temperature. The cluster temperature can also be represented as a thermodynamic quantity,

$$T_{cl} = \frac{dE}{dS} , \tag{2.2}$$

where E and S are the total internal energy and entropy of the cluster. Temperatures given by Eqns (2.1) and (2.2) are, generally speaking, different quantities, and this may have important implications (see, e.g., [69] and the references therein). In the thermodynamic consideration of clusters, not only the energy of thermal motion of their atoms but also the potential energy of interatomic interactions including the configuration excitation energy is taken into account. For a cluster of N atoms with pair interaction,

$$E = U + K = \sum_{i,j} u(r_{ij}) + \frac{m}{2} \sum_i \left(\frac{dr_i}{dt} \right)^2 , \tag{2.3}$$

where U is the total potential energy, K is the total kinetic energy of atoms, $u(r_{ij})$ is the interaction potential of two atoms separated by the distance $r_{ij} = r_i - r_j$, where r_i and r_j are the atom coordinates, and m is the atomic mass. In this case, the cluster entropy S is given by the general expression [201]

$$S = -\langle \ln P \rangle = -\sum_i P_i \ln P_i , \tag{2.4}$$

where the index i characterizes the state of the cluster and P_i is the probability of its being in this state ($\sum_i P_i = 1$). By configuration excitation, we mean transitions from the cluster ground state to the local minima on the multidimensional surface of potential energy. Specifically, configuration excitation is responsible for variations in the cluster structure and aggregate state [69].

Because a cluster exists near a certain minimum of the potential energy surface longer than the characteristic time of atomic vibrations ($\approx 10^{-14}$ s) [202], the energies of thermal and configuration excitations can be separated. This permits studying atomic dynamics in the cluster [69, 203]. Only the configuration component of the cluster energy is retained at zero temperature; it corresponds to cluster excitation with respect to the global minimum of the potential energy surface. Conversely, at high temperatures, the kinetic energy of atomic motion can be significantly higher than the configuration excitation energy.

We note that the thermodynamic definition of the cluster temperature is more accurate and comprehensive. The thermodynamic consideration of clusters with their overall internal energy and entropy taken into account allows

describing many processes associated with structural transitions; also, it provides a deeper insight into the physics of phase transitions in clusters [69, 203]. For example, the thermodynamic consideration was used to predict negative heat capacity of a cluster near the melting point [204 – 208]. The negative heat capacity of clusters was observed experimentally in [209 – 211] (see also Section 4.7).

Cluster temperature varies over a wide range depending on the type (composition) of the cluster and the mode of its formation and stabilization. For example, the temperature of its ^{3}He and ^{4}He clusters stabilized by evaporation equals 0.15 and 0.38 K, respectively [212, 213]. The temperature of noble gases formed in molecular beams or by aggregation is, as a rule, dozens of degrees Kelvin. Molecular clusters (including clusters with a hydrogen bond) have a temperature from dozens to hundreds of degrees Kelvin. The temperature of metal and carbon clusters (including fullerenes) may be as high as 4000 K; it reaches 4500 – 5000 K for refractory materials. The cluster temperature may increase considerably as a result of excitation, e.g., by electron impact [214 – 218], energetic ions [219], laser radiation [220 – 223] and superstrong ultrashort laser pulses [85 – 93], and collisions of high-energy clusters and cluster ions with a strong surface [43, 70] or between themselves in crossed beams [112 – 118]. For example, the electron and ion temperature in clusters excited by femtosecond laser pulses or by collisions with a solid surface may reach dozens and hundreds of electronvolts [52 – 57, 70]. In equilibrium, the upper limiting temperature of a cluster is given by the boiling point of its material. In other words, the equilibrium temperature in clusters of refractory materials varies over a wide range, whereas the temperature of molecular clusters changes less noticeably and that of helium clusters varies within an even narrower range.

The internal temperature of large clusters can be deduced from electron diffraction measurements. The intersection of an electron beam and a cluster beam produces diffraction rings [224]. The diameters of the rings give lattice parameters that can be used to determine the lattice temperature by comparison with the relevant data for bulk matter (taking cluster dimensional effects into account). However, this method is applicable only to clusters that crystallize into the same phase as the bulk substance. It can be used to determine the temperature of inert gas clusters when each of them contains at least 10^3 atoms, because smaller clusters have an icosahedral rather than crystalline structure (see Section 3.2).

Experimental data suggest that the internal temperature of large clusters formed in nozzle sources in the absence of a carrier gas is virtually independent of the conditions under which they are produced, such as the gas temperature and the pressure inside the source. Temperatures of large clusters are actually characteristic temperatures of the materials of which the clusters are composed.

It is possible to estimate the cluster temperature as described in [225, 226]. The lifetime τ of an atom on the cluster surface with a temperature $T_{\rm cl}$ is given by the well-known expression [227]

$$\tau = \tau_0 \exp\left(\frac{\Delta E_{\rm s}}{k_{\rm B} T_{\rm cl}}\right), \tag{2.5}$$

where τ_0 is the atomic vibration period on the surface and $\Delta E_{\rm s}$ is the sublimation or vaporization heat. Cooling of large clusters as a result of evaporation in a high vacuum is completed within at least 10^{-3} s. This time is comparable with the time of flight from the source to the electron beam

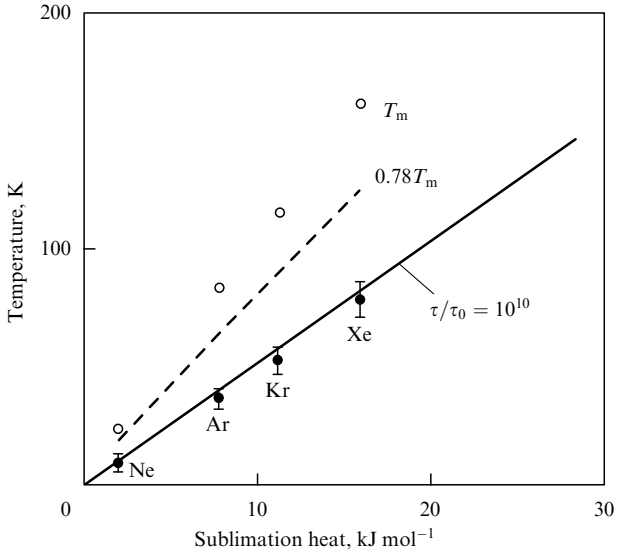

Figure 1. Internal temperatures of clusters formed during pure (undoped) gas expansion calculated by formula (2.6), depending on sublimation heat (solid line). Also shown are experimentally obtained cluster temperatures [224] (black dots), melting temperatures $T_{\rm m}$ of bulk substances (white dots), and low melting temperatures of inert gas clusters containing 1000 atoms [225] (dashed line).

scanning the clusters. The atom stays on the cluster surface for approximately $10^{-2} - 10^{-3}$ s, i.e., as long as the time of flight or slightly longer [225]. Using a typical value 10^{-12} s for the atomic vibration period τ_0 and 10^{-2} s for the atom's lifetime on the cluster surface, it is possible to calculate the internal temperature of the cluster:

$$T_{\rm cl} = (10 k_{\rm B} \ln 10)^{-1} \Delta E_{\rm s}\,. \tag{2.6}$$

Figure 1 presents the internal temperature of van der Waals clusters of noble gas atoms as a function of sublimation heat for bulk matter [225]. It can be seen that relation (2.6) describes experimental results fairly well.

2.2 Temperature dependence of cluster polarizability

Elucidation of the electric, magnetic, and optical properties of clusters is of great interest for the explanation of dimensional effects upon transition from individual particles to bulk matter and for the use of clusters to manufacture thin films and new nanostructural materials with specific properties (see, e.g., [1, 54, 68, 70, 164, 168] and the references therein).

2.2.1 Method for the measurement of cluster polarizability. The measurement of cluster polarizability is one of the few direct methods for the determination of cluster parameters [228]. In this method, a collimated cluster beam passes through a non-uniform electric field created by two curved planes. The typical value of the field strength E is about 10^5 V cm^{-1}; the gradients $\mathrm{d}E/\mathrm{d}z$ are of the order of 10^5 V cm^{-2}. The electric field produces an electric dipole moment in the cluster, while the field strength gradient acts on the dipole normally to its motion. In other words, clusters are deviated by the gradient. The force acting on the cluster (hence, its polarizability α) can be found from the degree of displacement d and the cluster velocity v [30]:

$$d = K \frac{\alpha E}{M v^2} \frac{\mathrm{d}E}{\mathrm{d}z}\,, \tag{2.7}$$

where M is the cluster mass and K is a constant dependent on the geometry of the experiment. The deviation is normally small (fractions of a millimeter) and can be measured by positionally sensitive detectors, i.e., by transversely scanning the beam through a narrow slot in front of the receiver. This method measures the intensity of the cluster beam passing through the slot.

2.2.2 Results of polarizability studies. The majority of polarizability studies have used sodium clusters. Sodium being a simple metal, the size dependence of many clusters is not complicated by the interplay between valence electrons as in more complex chemical elements. Atomic clusters of alkali elements are the most polarizable particles [229]. The statistical electric polarizability of such clusters in the presence of N free valence electrons delocalized outside an ion cage of radius R_N is given by $\alpha_N = (R_N + \delta)^3$ [30, 229]. For a neutral spherical cluster with a filled electron shell, the radius $R_N = r_s N^{1/3}$, where r_s is the Seitz–Wigner radius and δ is the size of the electron cloud outside the ion boundary. For sodium, $r_s \approx 2.1$ Å and $\delta \approx 1.3$ Å [229]. Thus, α_N exceeds even the standard polarizability $\alpha = R^3$ of an ideally conducting sphere.

The authors of [230] were the first to measure polarizability of sodium and potassium clusters. They experimentally observed three characteristic features: (1) polarizability per atom gradually decreases with the cluster size from a value characteristic of a single atom to that of a macroscopic substance; (2) the curve showing the dependence of polarizability on the number N of atoms in the cluster exhibits well-apparent 'dips' at the 'magic' numbers 2, 8, and 18, corresponding to the filled s-, p-, and d-electron shells; (3) the cluster size dependence of polarizability contains an additional structural component, usually attributed to the detailed cluster structure.

Subsequently, numerous calculations have been made in order to understand and explain these experimental results [231–234]. All computed values proved lower than experimental ones (Fig. 2a). Only a rigorous calculation of the structure and polarizability of sodium clusters based on the density functional revealed [235] that the discrepancy between theoretical and experimental findings resulted first and foremost from theorists' disregarding temperature effects on the cluster structure. It was shown that temperature affects the structure of clusters and thus contributes to their polarizability. Taking the real cluster temperature into account substantially decreases the discrepancy between theory and experiment (Fig. 2a).

Many experiments and calculations [30, 229–236] have demonstrated that the polarizability of small ($N \leqslant 10$) metal clusters (Li_N, Na_N, K_N, Al_N) is substantially higher (approximately 1.5–2-fold) than that of macroscopic matter. Polarizability per atom decreases as the number of atoms in the cluster increases; it is much greater (10–15%) for 'hot' clusters. The influence of cluster temperature on polarizability was also observed in large ($N \leqslant 93$) sodium clusters [229]. In this study, clusters formed as the vapor expanded at the nozzle outlet. The polarizability of large clusters decreased with their size but remained higher than for macroscopic substances. It correlated with the structure of the electron shell. Polarizability was susceptible to the vapor temperature above the nozzle, which reflected its dependence on the internal cluster temperature. Thus, enhancement of polarizability with increasing temperature is frequently associated with structural changes in the cluster.

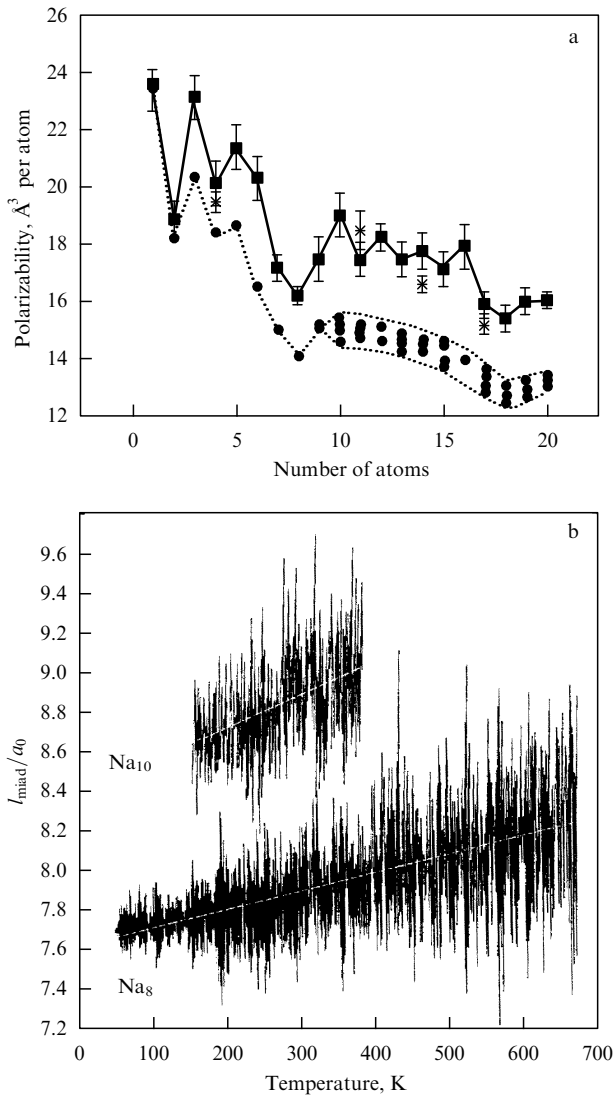

Figure 2. (a) Polarizability of sodium clusters: squares, experimental data [230]; circles, calculated values at $T = 0$ K; asterisks, calculated values at $T = 750$ K [235]. (b) Average interatomic distance in units of the Bohr radius a_0 at different temperatures for Na_8 and Na_{10} clusters. Straight lines, linear approximations to the data obtained (see the text). Note the difference between the line slopes for the two clusters [236].

There is one more phenomenon behind the temperature dependence of cluster polarizability. As shown in [236], such a dependence for small metal clusters is related to an increase in the cluster size. In that work, the molecular dynamics method was used to calculate linear expansion coefficients β for Na_N clusters ($8 \leqslant N \leqslant 40$) and for Al_7, Al_{13}^-, and Al_{14}^- clusters. The parameter β is well known for macroscopic matter:

$$\beta = \frac{1}{l}\,\frac{\mathrm{d}l}{\mathrm{d}T}\,, \tag{2.8}$$

where l is the measure of length and T is the temperature. For crystalline sodium at room temperature and for aluminum, $\beta = 71 \times 10^{-6}$ K^{-1} and $\beta = 23.6 \times 10^{-6}$ K^{-1}, respectively [237]. It has been unknown until recently how small systems undergo thermal expansion. At first sight, it is unclear how the expansion coefficient can be measured in small clusters. The value of the lattice constant may serve as a

measure of length l for bulk matter, but the choice of l in the case of clusters is not equally evident and straightforward, because objects of different geometry need to be compared. Such a situation occurs in metal clusters, where a large number of different isomers arise at increased temperature.

The measure of length in [236] was the mean interatomic distance

$$l_{\text{miad}} = \frac{1}{N(N-1)} \sum_{i,j=1}^{N} |\mathbf{R}_i - \mathbf{R}_j| \,, \tag{2.9}$$

where $\mathbf{R}_i$ is the position of the ith atom in the cluster. Evidently, l_{miad} is a measure of an average 'extension' of the cluster ionic structure. This quantity was computed for all cluster configurations in the framework of the model used in [236]. We here cite the most important results without going into the particulars of the method. Figure 2 shows changes in l_{miad} with varying temperature for Na_8 and Na_{10} clusters. Both dependences exhibit marked fluctuations, as should be expected in the case of small systems. However, the general trend toward the linear increase in l_{miad} with increasing the temperature is fairly well apparent.

Similar results were obtained for aluminum clusters. Thermal expansion in clusters was manifest more readily than in bulk matter. Static electric polarizability of clusters whose shape is given by the structure of their electron shell was found to be linearly dependent on the average interatomic distance. Therefore, thermal expansion leads to higher static electric polarizability. The authors of [236] also showed that theoretical results may agree fairly well with experimental findings if proper account is taken of the aforementioned temperature effect.

To conclude this section, we note that recent works [238, 329] have revealed electric and magnetic moments in niobium clusters Nb_N, as well as their temperature dependence. The temperature of cluster transition to the segnetoelectric state decreased with increasing the cluster size from $T_G(11) = 110$ K to $T_G(100) \sim 10$ K. For comparison, the temperature of transition to the superconducting state was $T_c(\infty) = 9.5$ K for bulk matter. The authors of [238, 239] related the temperature dependence of cluster segnetoelectric properties to the emergence of superconductivity [240, 241]. The data obtained and the conclusion drawn by the researchers are of interest for understanding the mechanisms of superconductivity in small systems [242]. However, further studies [243–245] (see also [246]) have demonstrated that the temperature dependence of the electric dipole moment may have a different origin, even if it is actually related to the structural asymmetry in homonuclear Nb_N clusters. Calculations of cluster deflection in a beam [243] suggest that thermal averaging due to cluster rotation may have an appreciable effect on experimentally measured moments. At the same time, detailed analysis of experimental data in [238, 239] indicates [247] that the dipole moment in small niobium clusters at low temperature is apparent by virtue of the unusual segnetoelectric properties of the clusters. Evidently, further studies are needed to resolve the problem.

2.3 Influence of temperature on the magnetic moment of clusters

The study of the magnetic properties of small-size metal clusters is of interest in view of their possible use in creating mini-systems with large memory reserves [248]. Ferromagnetism is due to the spontaneous mutual orientation of magnetic moments. This phenomenon, underlain by electron – electron interactions in the conductivity region, received a fairly good explanation in the case of bulk matter [249, 250]. But ferromagnetism in small-size systems, such as thin films and small particles or clusters, is poorly known. How the ferromagnetic properties of particles are related to the number of their constituent atoms, from a single atom to bulk matter, remains to be elucidated.

In a magnetic field $\mathbf{B}$, the magnetic moment $\boldsymbol{\mu}$ of a one-domain particle tends to be oriented parallel to the field. This trend is, however, antagonized by thermal motion; as a result, the degree of magnetization M in equilibrium is related to both the temperature and the field strength as $M = \mu L\left[\mu B/(k_B T)\right]$, where $L(x) = \coth(x) - 1/x$ is the Langevin function [250]. By definition, $M = |\boldsymbol{\mu}\mathbf{B}|/B$ is equal to the mean projection of the moment on the direction of the magnetic field. For low argument values, this relation is simplified:

$$M = \frac{\mu^2 B}{3k_B T} \,. \tag{2.10}$$

In this model, particles are assumed to be paramagnetic and have large magnetic moments, i.e., superparamagnetic [251]. This means that a large moment is created by a ferromagnetic array of moments μ_0 of individual atoms, and hence $\mu \approx N\mu_0$ at low temperatures [251], where N is the number of atoms in a particle. However, μ also depends on temperature and tends to vanish when it increases.

The magnetization of a cluster is related to its deflection d in the magnetic field as

$$d = K \frac{\mathrm{d}B}{\mathrm{d}z} \frac{M}{N m_0 v^2} \,, \tag{2.11}$$

where v and Nm_0 are the cluster velocity and mass, K is a constant, and $\mathrm{d}B/\mathrm{d}z$ is the magnetic field gradient. For this reason, the method of Stern and Gerlach for particle deflection in the magnetic field is usually employed to measure magnetic moments [252–257].

Most studies of temperature effects on cluster magnetic moments have been conducted with ferromagnetic clusters of transition metals Fe_N, Co_N, and Ni_N [253–259] (see also [260, 261]). It is worthwhile to note that measurements of magnetic moments depending on the cluster size and temperature are not as unambiguous and definite as the results of polarizability estimation. Nevertheless, the common trends of these dependences are fairly well known. For example [256, 257], the magnetic moment of clusters containing up to several hundred atoms ($N \leqslant 200-500$) is higher than the bulk value (Fig. 3). The magnetic moment per atom is largest in small-size clusters ($N \leqslant 20$) at low temperature ($T \leqslant 100$ K) and decreases as they increase to the size of a bulk solid. Magnetic moments of small ($N \leqslant 20$) Ni_N, Co_N, and Fe_N clusters at low temperature are roughly $1.1\,\mu_B$, $2.4\,\mu_B$, and $3.0\,\mu_B$, respectively, compared with $0.6\,\mu_B$, $1.72\,\mu_B$, and $2.2\,\mu_B$ in bulk matter (see Fig. 3). As the temperature increases to 500–600 K, the magnetic moment per atom in clusters Ni_N and Co_N at $N \leqslant 100$ decreases to the value for a bulk solid. The temperature dependence for iron clusters shows anomalies most probably resulting from the diversity of the magnetic properties of this metal [257].

In-depth studies of magnetic moments in iron clusters are reported in [253, 256, 257]. They included the measurement of magnetic moments $\mu(N)$ in a molecular beam in the

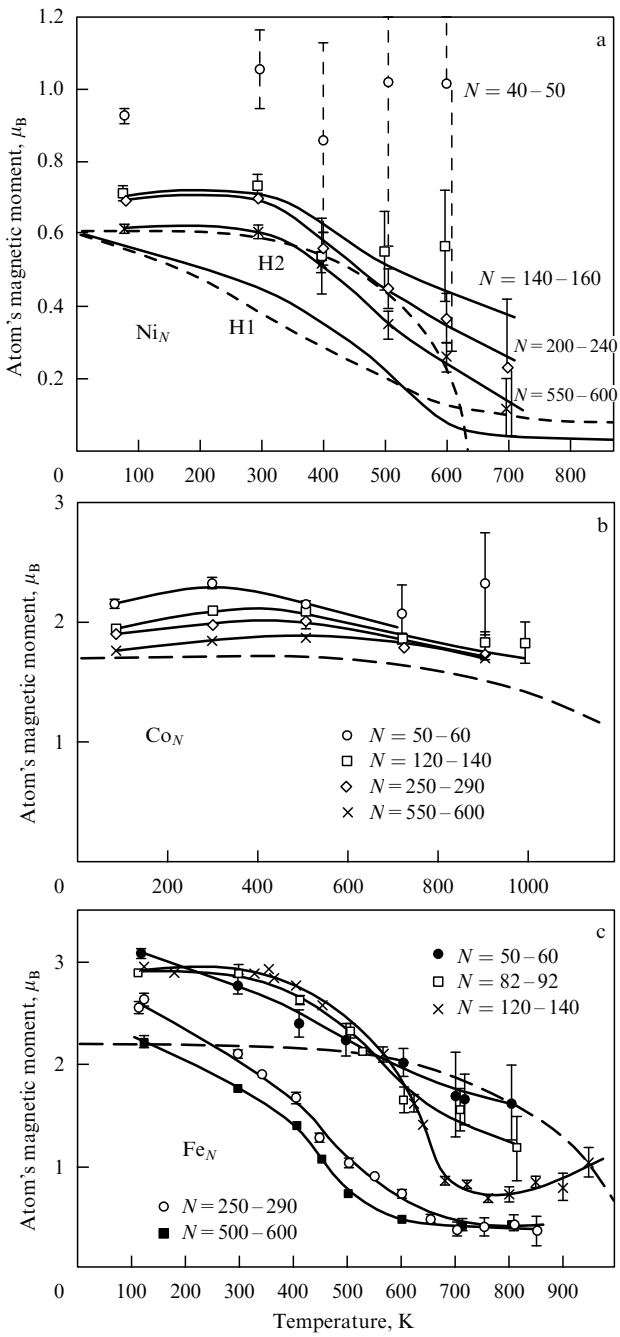

Figure 3. Average magnetic moment as a function of cluster temperature for clusters Ni_N (a), Co_N (b), and Fe_N (c) of different sizes. Magnetization saturation curves for bulk substances are presented for comparison (dashed lines). Curves H1 and H2 in Fig. (a) are plotted based on model calculations for clusters of 128 and 1024 atoms, respectively (from [256]).

temperature range 100 to 1000 K. The magnetic moment $\mu\,(25 \leqslant N \leqslant 130)$ at 120 K was found to be 3 μ_B per atom and decreased with increasing the cluster size to its value in a macroscopic substance (approximately 2.2 μ_B per atom at $N \approx 500$). For all the examined clusters containing $25 \leqslant N \leqslant 700$ atoms, the magnetic moment decreased with increasing the temperature to an almost constant value observed at a certain temperature above $T_c(N)$. For example, $T_c(130)$ and $T_c(550)$ were respectively around 700 K and 550 K, to be compared with $T_c = 1043$ K for bulk matter.

It was also shown [253, 256, 257] that μ decreases as the temperature increases, regardless of the cluster size (see Fig. 3). For example, the magnetic moment in clusters Fe_{50-60} decreases from $3\,\mu_B$ at $T = 120$ K to $1.53\,\mu_B$ at $T = 800$ K and for clusters $Fe_{500-600}$, it decreases from about $2.2\,\mu_B$ at $T = 120$ K to $0.4\,\mu_B$ at $T = 600$ K. The decrease in μ with increasing the temperature can be accounted for by thermal disturbance of mutual spin orientation [250, 262]. The magnetic moment totally disappears at the Curie temperature $T_C = 1043$ K for bulk matter. Also, it follows from Fig. 3 (see the values at $T = 120$ K) that the magnetic moment decreases as the cluster size approaches that of a bulk solid, $\mu = 2.2\,\mu_B$ (at $T = 0$).

Interesting results were recently reported in [263]. The authors studied the magnetic properties of small undoped cobalt clusters Co_N $(N = 7-32)$ and benzene-doped $Co_N(C_6D_6)_M$ in the temperature range 54–150 K. They observed that part of the clusters showed no supermagnetic properties at $T \leqslant 100$ K; their spins were blocked and the magnetic moment was only 1 μ_B per atom. In the supermagnetic regime (at $T = 150$ K), the magnetic moments of Co_{24} and Co_{16} clusters were $1.96\,\mu_B$ and $2.53\,\mu_B$, respectively, i.e., much higher than in the bulk solid ($1.72\,\mu_B$). It was also shown that cobalt clusters containing a layer of adsorbed benzene molecules have a significantly smaller magnetic moment than undoped clusters. Doped and undoped clusters differ 2–5-fold in terms of magnetic moments per atom, depending on size.

To conclude this section, we note that studies on electric and magnetic moments of clusters have become especially important in connection with the development of spintronics, a new science of purpose-oriented electron spin control. The knowledge of cluster moments and their dynamics is paramount for the creation of fast-acting electronic devices operated in the nanometer range. Of special interest in this context are the results of a recent study [264] showing that small ($N \leqslant 100$) magnetic clusters inserted into a metal matrix are capable of a huge magnetic response (in excess of 500%) at low temperature. According to the authors, such a pronounced reaction is based on the electron spin mixing mechanism.

2.4 Temperature dependence of the cluster ionization potential

The ionization potential (IP) or, to be precise, the adiabatic ionization potential (AIP) of a cluster corresponds to the difference between the energies of neutral and ionized clusters in the electron ground state [30]. AIP values are derived from photoionization measurements. If a cluster is assumed to be initially in the ground state and zero nuclear oscillations are neglected, a lowest-energy photon capable of cluster ionization corresponds to the vertical ionization potential (VIP) (Fig. 4).

The geometries of a neutral cluster and a cluster ion in the ground state are normally different, and hence the former appear in the excited vibrational state. Therefore, photoionization measurements of an initially cold cluster give the vertical rather than adiabatic ionization potential. For large clusters, differences in the geometry of neutral clusters and ions are insignificant, accounting for the actually identical adiabatic and vertical the potentials. For small clusters, the difference between the potentials may be appreciably large.

Practical measurements are frequently made on hot clusters, which accounts for the relatively smooth ionization threshold. It requires a thorough analysis of the measurements in order to determine vertical and adiabatic ionization

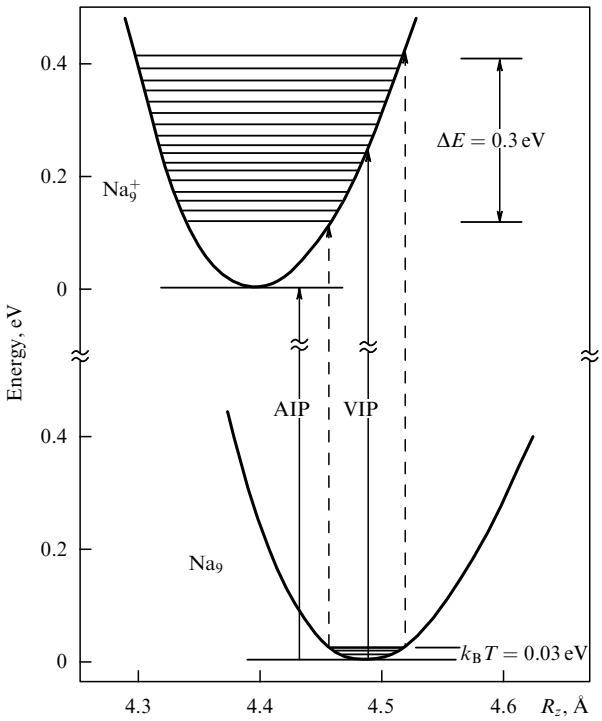

Figure 4. Diagram of the photoionization process $Na_9 \to Na_9^+ + e$. The total cluster energy in the ground state was measured using the ellipsoid shell model; the ionization state is presented as a function of the long cluster axis R_z. Temperature fluctuations in the shape in the ground state account for the widened band of excited vibrational states; hence, wide temperature 'tails' in the photoionization spectra. AIP, adiabatic ionization potential; VIP, vertical ionization potential [30].

potentials (see, e.g., [30]). For example, the process of ionization of cluster Na_9 is illustrated in Fig. 4, where all energy parameters for a neutral cluster and its ion are presented with respect to the shape of the potential. The large difference between the shapes of potentials is typical of small clusters [30]. In accordance with the Franck – Condon principle, the most probable electron transitions are those that occur without a change of geometry. These are vertical transitions, and the energy needed for them is also shown in Fig. 4. On the other hand, the AIP corresponds to transitions from the ground state of a neutral cluster to that of its ion. Such transitions are unlikely when the difference between the potentials is large and the cluster is cold.

The minimal photon energy necessary for cluster ionization decreases at nonzero initial temperatures, leading to the appearance of temperature 'tails' in the curves (spectra) describing the effectiveness of photoionization. Hot clusters produce oscillating efficiency curves. The magnitude of oscillations depends on the location of the points of return of a neutral cluster at a given temperature at which the cluster potential energy equals $k_B T$ [30]. The temperature width of the ionization transition is estimated as the difference between the energies of vertical ionization transitions at two return points. For example, the width of the temperature 'tail' in the case of cluster Na_9 (see Fig. 4) is around 0.3 eV for $k_B T = 0.03$ eV (≈ 300 K). We note that this value is approximately one order of magnitude higher than $k_B T$. Such a substantial increase is due to the large difference in the potential shape between neutral clusters and ions, as well as to the 'friability' of the clusters, which leads to marked oscillations even at relatively low temperatures. Although this picture is only a broad outline, it allows sound estimation of the above effect. Other temperature effects include thermal smearing of electron states, most pronounced when the energy gaps are comparable with $k_B T$, as is the case with large clusters. We note that in the general case, the difference between the VIP and AIP decreases as the cluster size increases. To conclude, hot clusters produce temperature tails in ionization spectra that are much wider than $k_B T$, while the shape of the spectra near the threshold strongly depends on the cluster temperature.

2.5 Temperature effects on cluster optical properties

The temperature dependence of cluster optical properties [265 – 274] is largely due to two main factors, changes of the cluster structure and the phase state. Monte Carlo calculations of absorption cross sections of sodium clusters Na_8 [265] indicate that the equilibrium cluster structure corresponds to the symmetry group D_{2d}. The photoabsorption cross section for this geometry is characterized by two peaks separated by an energy gap of approximately 200 meV (Fig. 5a). The absorption cross section is strongly dependent on the cluster vibrational temperature. The two-peak structure is retained up to 100 K. It changes at higher temperatures, as the new phase space gradually opens, and turns into a spectrum showing a single broad asymmetric peak above the melting point. This situation is in excellent agreement with experimental data obtained at the same temperature (Fig. 5b). The melting temperature of small clusters is much lower than that of a bulk solid [275 – 277] (see Section 4.7).

A strong temperature dependence of a photoabsorption cross section was also reported for cluster ions Na_N^+ in [266] ($N = 4, 7, 11$) and [267] ($N = 9, 21, 41$). The authors of [266] observed six separate absorption bands produced by cold cluster ions Na_{11}^+ ($T \sim 35$ K). They interpreted these lines as individual transitions between electron states of the Na_{11}^+ molecule. At high temperatures ($T > 380$ K), when clusters become liquid, the spectrum contains two broad peaks. Their energy position for clusters with $N > 7$ is fairly well explained in the framework of a model in which almost all free electrons oscillate in a spherical container. In Ref. [267], wide single peaks were found at a high cluster temperature ($T > 300$ K); much narrower lines were recorded at $T = 130$ K. At low temperatures, molecules of Na_9^+ produced two absorption peaks separated by the energy interval 275 meV.

The solid-to-liquid phase transition was deduced from the optical spectra of C_6D_6-doped argon clusters in [268]. It was shown that clusters of solid and liquid phases coexisted in the beam within a certain temperature range; some clusters were solid and others liquid. This conclusion was drawn from the presence of two differently shaped lines corresponding to the absorption by solid and liquid phases at 257.7 – 258.0 nm in the spectrum of dopant C_6D_6 molecules. The integral line intensity was used to determine the relative amount of clusters in liquid and solid states. We emphasize that experiments of this type directly confirm theoretical predictions (based on the quantum-statistical analysis of cluster properties) of two different temperatures, the melting and crystallization temperatures, with a well apparent region between them where the two phases coexist [69, 278 – 280]; in this respect, clusters differ from macroscopic substances. This phenomenon is underlain by configuration (structural) transitions in clusters [69, 280].

Temperature-dependent variations of cluster absorption spectra may be used to determine the temperature of

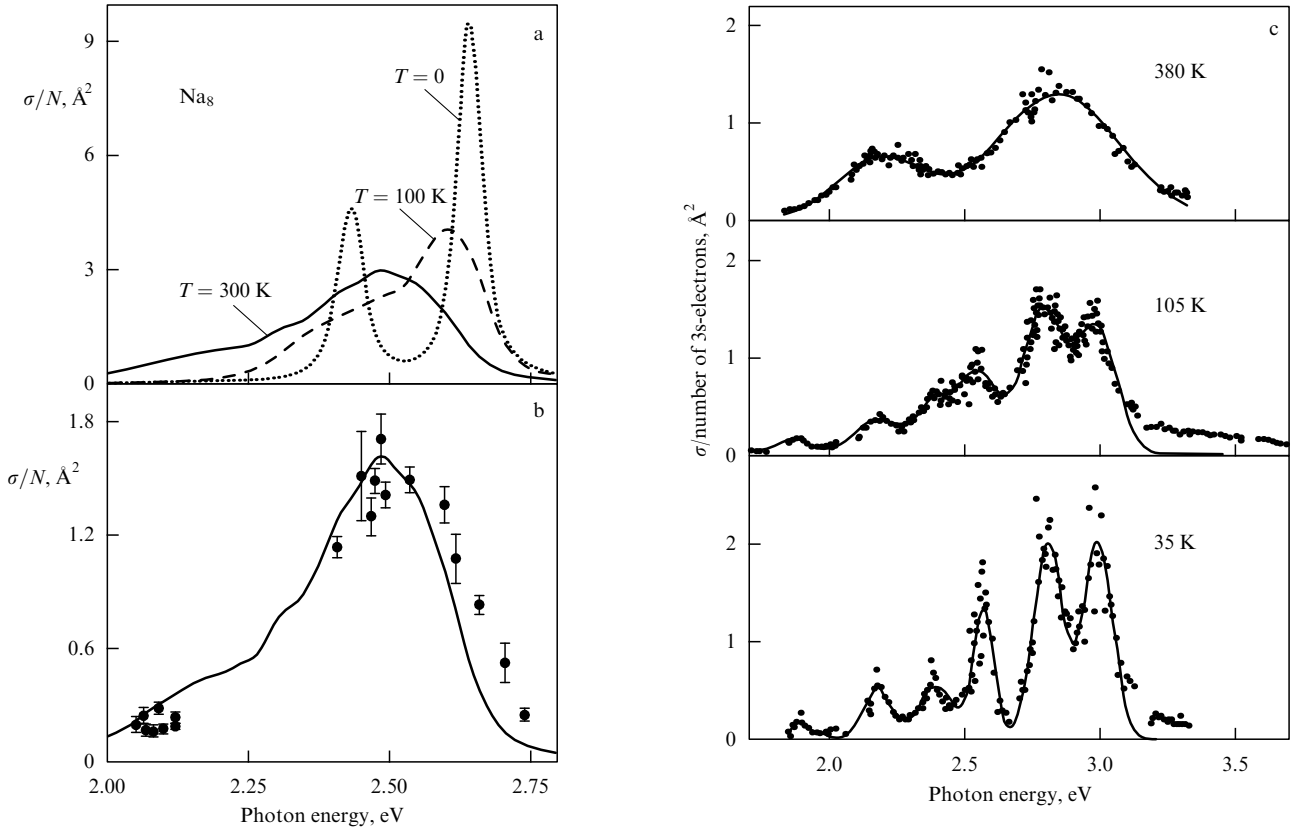

Figure 5. Photoionization cross section of Na_8 clusters (a) at three different vibrational temperatures indicated in the figure and (b) at $T = 300$ K: the theoretical curve and experimental data (circles) obtained at the same temperature in [274]; the theoretical curve is normalized for the computation results to correlate with experimental findings (from [265]). (c) Optical spectra of cluster ion Na_{11}^+ at different temperatures [266].

structural transitions. Analysis of vibrational predissociation spectra of protonated methanol clusters $H^+(CH_3OH)_4$ and $H^+(CH_3OH)_5$ in [270] and their comparison with *ab initio* computed spectra allowed determining the temperature of cluster transition ($T_{cl} = 190$ K) from one isomeric configuration to another. The clusters formed in a molecular beam; their vibrational temperature was 200 ± 20 K [271]. Calculations showed that the redundant proton in these clusters was either localized on one methanol molecule (in the case of cyclic tetramer and linear pentamer) or delocalized between two neighbor molecules, to either of which it was bound with equal probability (in the case of a linear tetramer and a cyclic pentamer). Both cyclic and linear configurations were documented for protonated pentamers of methanol; the isomeric transition between these two structures via a rearrangement of hydrogen bonds occurred at the cluster temperature 190 K. Such a unique behavior of proton delocalization was deduced from vibrational predissociation spectra of a cyclic methanol pentamer in the absorption region for a free OH-stretch (frequency near 3647 cm^{-1}) and hydrogen-linked OH-stretches (3448 and 3461 cm^{-1}). The authors hypothesized [271] that the proton transfer mechanism included sequential breakage and transformation of hydrogen bonds inside the cluster. This mechanism might be closely related to the unusually high proton mobility in liquid methanol. A similar effect of proton delocalization was observed in water clusters [272] when analyzing vibrational predissociation spectra of protonated $H^+(H_2O)_{5-8}$.

2.6 The effect of internal temperature on other cluster properties

Internal temperature affects many other properties of clusters and processes with their participation [281, 282]. In particular, it plays an important role in charge transfer during collisions of metal cluster ions with atoms of metals [283, 284]. Charge transfer is known to underlie many chemical reactions. As the charge is transferred between a cluster and an atom, the former passes to an excited electronic state owing to the collision energy; this leads to evaporation (monomolecular dissociation) of the cluster. It was shown in [283, 284] that results of collision experiments using Li_{31}^{2+} clusters and Cs atoms agreed with the calculated cross sections of charge transfer only when account was taken of the internal temperature of the clusters, which ranged from 400 to 600 K.

The internal temperature of clusters and cluster ions also influences their fragmentation channels in collisions with both atoms and solid surfaces [70]. Calculated molecular dynamics in [285, 286] indicates that the 'population' of fragmentation channels of cluster ions Na_N^+ ($N < 5$) (i.e., fragment distribution) during collisions with He atoms strongly depends on the cluster temperature. Similar results are obtained for clusters Na_9^+ [287] and Na_3^+ [288]. These effects can be accounted for by the fact that an increase in temperature leads to an increase in both the probability of electron excitation of clusters and its energy relaxation rate, followed by the intramolecular vibrational relaxation with a marked effect on cluster fragmentation. Eventually, both

processes strongly affect the population of fragmentation channels of cluster ions. The probability of the fragmentation of 'hot' cluster ions Na_5^+ with the internal energy 0.38 eV via the $Na_3^+ + 2Na$ channel increases almost 1.5-fold compared with 'cold' clusters with the energy 0.04 eV; conversely, the probability of fragmentation via the $Na_4^+ + Na$ channel decreases almost 2.5-fold [286]. A hot cluster is easier to excite, first because a lower energy is needed for the purpose (see Section 2.4) and second because the probability of its collision with helium atoms is higher due to its larger size.

The internal temperature influences the mechanisms of energy relaxation, i.e., fragmentation, emission of electrons, charged particles, and light [70]. Studies with carbon clusters [219, 221] demonstrated that fragmentation and thermoelectron emission are the main energy relaxation channels for clusters at temperatures above 3000 K, while cooling by emission of equilibrium radiation predominates at lower temperatures (see Section 4.2).

The cluster temperature has an appreciable effect on the rate of cluster reactions with other reagents [289, 290] and the rates and channels of chemical reactions at the surface and inside large van der Waals clusters ($N \geqslant 10^3$) (see, e.g., [291–294]). Of special interest in this context are chemical reactions inside nanodroplets (clusters) of superfluid helium [62, 67, 293], providing a unique isolated reaction medium. Such nanodroplets may be regarded as small-size reactors having catalytic activity [62, 67, 293]. Low-temperature reactions provide a new avenue into selective chemistry and may open up prospects for the production of previously unavailable substances.

One more interesting and practically important aspect of temperature dependence emerges in the formation of nanostructures on solid surfaces and film deposition from clusters [295, 296]. Large clusters ($N \geqslant 10^3$) with a high internal temperature readily deform upon deposition on a hot surface, giving rise to two-dimensional structures. Studies with the use of the molecular dynamics method [295] showed that clusters $YBa_2Cu_3O_{7-x}$ ($N = 10^3$) with the internal temperature $T_{cl} \geqslant 2400$ K formed a film of not more than two atomic layers when deposited on the surface of pyrolytic graphite. Also, it was found that hot nanometer clusters were easily deformed on a solid surface due to their high internal energy, undergoing transformation from three- to two-dimensional structures. Such a transformation of hot clusters occurred even at room temperature [296]. High cluster energy makes it easier for atoms to overcome local barriers and be reoriented at the surface with the formation of a high-quality uniformly thick film. This technology opens up prospects for growing homogeneous films from superconducting refractory materials [295, 296].

3. Relation between cluster temperature, cluster structure, and binding energy of atoms (molecules) inside clusters

3.1 Inner phase and phase transitions in clusters

The results of structural studies by the electron diffraction method using clusters of inert gases (except helium) and other van der Waals clusters produced in nozzle sources indicate that all of them occur in the solid state, even if in a different crystalline phase than that characteristic of bulk matter. However, the internal temperature of clusters in a beam is significantly lower than the melting temperature T_m of the corresponding bulk solid [224] (see also Section 2.1 and Fig. 1). The simple correlation between the cluster internal temperature and the corresponding latent heat of sublimation fairly well describes experimental data [226]. This situation is illustrated in Fig. 1, showing melting temperatures of bulk matter (white circles) and clusters of 1000 atoms (dashed line), which are much higher than the cluster internal temperatures. Estimated [297] and calculated values, together with experimental findings [275–277], suggest (see also Section 4.7) that the melting temperatures of clusters depend on their size and are substantially lower than in bulk substances.

Because the basic assumption underlying the above correspondence for van der Waals clusters is that the internal temperature of free clusters in a vacuum depends on evaporative cooling (see Section 5), a similar correlation must be true of metal clusters. Therefore, it is hypothesized [225] that all metal clusters formed during expansion of pure vapor in the absence of a carrier gas have a liquid phase that distinguishes them from van der Waals clusters.

Figure 6 shows the dependence for several typical metals analogous to that presented in Fig. 1. Evidently, the internal cluster temperatures (solid line) given by relation (2.6) are always higher than the melting temperatures of bulk substances. Therefore, they are even higher than the melting temperatures of 1000-atom clusters (dashed lines). Based on the data for gold particles, the melting temperatures of metal clusters are assumed to be 75% of their values for bulk solids [298]. Bearing in mind that the melting temperatures of clusters are lower than those of bulk matter, it is safe to argue that the clusters of all metals included in Fig. 6 must be liquid by virtue of their finite size. We recall, however, that this assertion refers only to clusters formed during the expansion of pure vapor. When clusters form during aggregation in a buffer gas or expansion of a carrier gas, their cooling in collisions may from the very beginning lead to condensation and solidification [226, 299].

It might be assumed that the high internal temperatures predicted by relation (2.6) should result in intense radiative cooling and solidification of clusters. It was shown, however, [225] that radiative cooling is negligibly small compared with evaporative cooling. The reason is that the spectral radiation power of a black body given by the Planck law for small particles (including clusters) is low because the factor of the

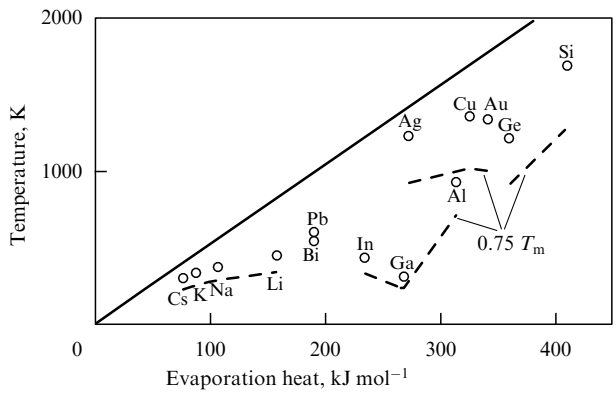

Figure 6. Internal temperatures of metal clusters formed during expansion of pure (undoped) vapor as a function of evaporation heat computed from relation (2.6) (solid line). Circles denote melting temperatures of bulk substances; dashed lines are lowered melting temperatures for clusters of 1000 atoms [225].

spectral efficiency of absorption equals the ratio of the spectral absorption cross section to the cluster geometric cross section (see Section 4.2).

According to [225], the total radiation power in the spectral range 0.5 – 0.7 μm for silver clusters of 1000 atoms approximately 32 Å in diameter at 1500 K is roughly 2.67×10^{-4} of the corresponding radiation power for bulk matter. The energy loss during emission from the cluster surface for the flight time 10^{-3} s is 2.5×10^{-20} J. This energy is an order of magnitude lower than the latent heat of evaporation of a single atom from the cluster surface, which equals roughly 4.5×10^{-19} J at 1500 K [225]. In other words, the size of clusters smaller than the IR radiation wavelength prevents their radiative cooling (see also Section 4.2).

3.2 Size and temperature dependence of the cluster structure

3.2.1 Van der Waals clusters. Variations in the cluster size and temperature lead to phase transitions and structural changes. Numerous experiments with van der Waals clusters (Ar [224, 300 – 307], Kr [307], Xe [307], SF_6 [308 – 310], N_2 [307, 311 – 314], and CO_2 [315, 316]) formed during supersonic expansion of gases in nozzle sources were carried out with the use of the electron diffraction method. Their results taken together with model calculations [303 – 310] unambiguously indicate that the cluster structure strongly depends on the internal temperature. Structural changes at varying temperature also occur in metal [317, 318] and carbon [319, 320] clusters. Structural transitions in van der Waals clusters are most often investigated by the electron diffraction method [224, 300 – 310].

Collectively, experiments and calculations for clusters of inert gases [224, 300 – 307] demonstrated a common sequence of structural changes (amorphous, icosahedral, crystalline) with increasing the cluster size. Structural transitions occur at an approximately equal number of atoms in a cluster, regardless of the nature of the gas under study. This means that the cluster structure of any inert gas depends only on the number of atoms. In contrast, the cluster temperature is independent of the number of atoms. In other words, the cluster temperature is a specific characteristic of individual gases that varies with the depth of the interatomic potential well (see Section 3.3).

A detailed study of argon clusters [224] showed that an increase in their size was accompanied by two transitions in the local order, at $N \approx 50$ and $N \approx 800$. Clusters differ in terms of structure depending on their size; it may be amorphous (polyicosahedral) at $N < 50$ [321], multilayered icosahedral at $50 < N < 800$ [322], or crystalline face-centered at $N > 800$ [301]. Such transitions occur as a result of the high cluster temperature in a beam. Due to the relatively high temperature, a cluster with a given number of atoms N traveling in a beam changes structure so as to minimize its free energy. Calculations by the electron dynamics method indicate that the effective cluster temperature is only slightly lower than their melting temperature. This is a serious argument in favor of the thermodynamic stability of clusters being formed in such experiments.

Because clusters of $N \geqslant 10^3$ atoms have a crystalline face-centered structure, the available diffraction picture [224] permits determining their average size (from the line width), the lattice parameter a (from the diameter of the Debye – Scherer rings), and the mean quadratic displacement of atoms $\langle u^2 \rangle$ (from the decrease in the line intensity with increasing the diffraction angle). Therefore, measurements of these parameters provide a basis for two independent estimates of the cluster temperature, one from the crystal lattice constant a with the use of temperature expansion coefficients, and the other from the quantity $\langle u^2 \rangle$ using the Debye – Scherer temperature θ. In the case of clusters, it should be borne in mind that both estimates depend on N, which should be taken into account in determining the cluster temperature. For argon clusters in [224], $T_{cl} = 38 \pm 4$ K was obtained at $\theta = 85$ K and $\langle u^2 \rangle^{1/2} = 0.25 \pm 0.01$ Å, to be compared with $T = 37 \pm 5$ K for a macroscopic substance. This value is in excellent agreement with the temperature T_{cl} of large argon clusters. Therefore, the authors of [224] used their electron diffraction data to estimate the temperatures of large clusters of other noble gases (see Section 3.3). We note once again that this approach is inapplicable to small clusters with a noncrystalline structure.

The same approach in conjunction with experimental studies was used in [304, 305] to investigate structural transitions in large argon clusters formed during supersonic expansion of a gas at a nozzle outlet. It was found in [304] that clusters of 1000 or fewer atoms have an icosahedral configuration corresponding to the minimal energy, whereas clusters with $N \geqslant 3000$ have a face-centered cubic configuration. Transition from the icosahedral to the face-centered cubic configuration occurs smoothly in the range of N from 1500 to 3500. An interesting result was obtained in [305]. The authors found that the structure of very large argon clusters ($10^3 \leqslant N \leqslant 10^5$) deviates from the face-centered cubic structure characteristic of bulk matter; rather, it is a kind of mixture of face-centered cubic and close-packed hexagonal structures with randomly distributed densely packed regions, implying that large clusters are not monocrystals but consist of numerous domains of different structure. The face-centered structure does not seem to have any advantage over the close-packed hexagonal one.

It is worthy of note that many experimental data on structural transitions in argon clusters depending on the number of atoms are at variance with theoretical results [305, 323, 324] that predict the possibility of a transition from the icosahedral to crystalline structure only at $N \geqslant 10^4$ (taking the binding energy of atoms in the cluster into account). However, direct transition from one close-packed structure to another in such large clusters without their passing into an intermediate liquid state is hardly possible. From this standpoint, experimental results obtained in [305] are in better agreement with theoretical ones. To summarize, the results of the above studies show how diverse and complicated structural (phasic) changes in argon clusters may be (see also [69, 280] and the references therein).

Structural transitions were examined in clusters SF_6, SeF_6, TeF_6 [308], and SF_6 [310] formed in supersonic jets carrying an inert carrier gas. The authors observed differences in the structure of these clusters depending on the carrier being used and the conditions of its expansion (concentration and total pressure at the nozzle outlet). Cubic crystals of SF_6 measuring 50 – 180 Å were formed in a wide range of expansion conditions. Measurement of the lattice constant revealed the dependence of the crystal temperature and size on the conditions of expansion. Crystals with the temperature 100 – 130 K formed in the presence of helium or neon as carrier gases. In argon, the crystal temperature was about 94 K, i.e., close to the phase transition temperature of the bulk substance (94.5 K [325]), even at a relatively high ($\geqslant 3\%$) level of SF_6.

The process of concentration slowed down at a low concentration of SF_6 in the expanding gas, while the condensation temperature decreased, giving rise to colder clusters.

The low-temperature phase of SF_6 with a triclinic structure was obtained using a heavier carrier gas (argon) and a lower concentration of SF_6 [308]. However, the formation of cubic crystals prevailed even under these conditions. The phase transition temperature for SeF_6 and TeF_6 was higher than for SF_6, and their low-temperature phases arose under more moderate conditions. It was also found in [308] that the use of argon as a carrier gas at small SF_6 concentrations produced such a low temperature that SF_6 crystals were not the sole crystals formed in the jet. Concomitantly, cubic face-centered crystals of Ar were identified, having the diameter about 50 Å and temperature 45 – 70 K, i.e., much lower than the temperature of coexisting SF_6 crystals. This finding explained the formation of a low-temperature phase of SF_6 in the presence of argon. At higher SF_6 concentrations in the jet, oversaturation occurred at earlier expansion stages, i.e., at higher temperatures. As a result, the high-temperature phase of SF_6 was formed [308, 310].

Similar phase transition studies by the electron diffraction method involved clusters of Kr and Xe [307], CO_2 [315, 316], O_2 [326], and N_2 [311 – 314]. Experiments with CO_2 showed that the majority of clusters with $N \leqslant 25$ had an icosahedral structure and clusters with $N \geqslant 32$ had a cubic crystalline structure. Clusters of noble gases exhibited a common trend toward transformation of the icosahedral structure into the crystalline one in the course of formation of van der Waals clusters from small molecules. It was shown in [311 – 314] that small nitrogen clusters ($N \leqslant 50$) have an amorphous structure. As the size of the clusters increased, they underwent structural transformations in the following order: quasicrystal (icosahedron) $\rightarrow$ α-phase of N_2 (cubic) with packing defects $\rightarrow$ β-phase of N_2 (hexagonal densely packed, HDP, phase). Transition from the cubic to icosahedral phase occurred via a mechanism characteristic of inert gases, whereas the $\alpha \rightarrow \beta$ transition was associated with an increase in the cluster temperature accompanying their increase in size.

3.2.2 Water clusters. We now consider the results of recent studies on structural and temperature changes in water clusters, bearing in mind the key role of water in the origin and maintenance of life on Earth, which accounts for the great interest shown in the properties of its different forms, including clusters. It was found in experiments [327, 328] that water clusters remain in the liquid overcooled state at temperatures close to 200 K when they exist in the form of crystalline ice having a cubic, rather than hexagonal, structure. Thermodynamic studies revealed the dependence of crystallization on the cluster size. Small clusters with the radius $\leqslant 15$ nm crystallized into ice with a cubic structure at 160 – 200 K, whereas larger ones gave rise to ice crystals of a hexagonal structure [329].

Investigations into the effects of cluster size and temperature on the behavior of water molecules by the molecular dynamics method [330] allowed two (inner and outer) regions to be distinguished in each cluster, in accordance with variations in the local density profile. The region in which molecules behave as they do in a bulk liquid may be regarded as the inner region. Molecules in this region being randomly oriented, their distribution is virtually independent of the cluster size. This, however, has a marked effect on the location of individual molecules outside this region. Surface water molecules in large clusters on the average have many more hydrogen bonds than in small clusters, accounting for the enhanced surface tension in the former. The mean number of hydrogen bonds per molecule in either region decreases and the fraction of surface molecules increases with increasing the temperature.

The molecular dynamics method was used in [331] to observe evaporation of water clusters containing $125 \leqslant N \leqslant 4096$ molecules in a vacuum within a time range from 20 ns to 3 μs. Cooling experiments involved clusters with the initial temperatures 250, 275, and 300 K. The following cluster parameters were measured: temperature, structure, size, number of hydrogen bonds, and cooling rate. The cluster temperature decreased during evaporation, tending toward a common limit ~ 215 K regardless of size. The mean number of molecules evaporated from a unit surface of around 0.9 – 1.0 nm^{-2}, equivalent to a decrease in the cluster radius by 0.16 – 0.22 nm. Evaporation slowed down appreciably after the cluster temperature reached some 240 K.

To conclude this section, we note that the molecular dynamics method was used in [332] to evaluate the effects of temperature on the structure of protonated water clusters $H^+(H_2O_N)$ ($N = 5-22$) at 25 – 330 K. A general tendency was revealed, suggesting the predominance of tree-like structures at high temperatures and the appearance of single-ring structures at low temperatures. Moreover, clusters with $N > 7$ underwent a transition from mono- to multi-ring structures as the temperature decreased. Polyhedral structures started to prevail at low temperatures only in clusters with $N \geqslant 16$. Thus, a high temperature sensitivity of protonated water clusters was demonstrated in [332]. Structural changes in water clusters were also investigated in [333 – 338]. Experiments with water clusters of different sizes [333 – 335] yielded results similar to those considered above.

3.2.3 Carbon clusters. Structural transitions in carbon clusters $(C_{60})_N$ induced by changes in temperature were considered in [319, 320] using neutral and charged $(C_{60})_N$ ($N = 1-150$) clusters. The clusters were heated to a certain temperature in helium-filled cells and thereafter analyzed in a time-of-flight mass spectrometer. Anomalously intense lines corresponded to the most stable structures that underwent only slight evaporation.

The number and character of peaks in the mass spectra depended on temperature. Clusters heated to a moderate temperature (490 K) had mass spectra indicative of their icosahedral structure responsible for highly intense peaks at $N = 13, 19, 23, 26, 35, 39, 43, 46, 49, 55, 55 + 3m$ ($m = 1-14$), 116, 125, 131, 137, and 147 (Fig. 7).

Calculations of molecular dynamics allowed concluding [319, 320] that these icosahedrons were metastable structures that failed to reach thermal equilibrium when heated (approximately 0.5 ms). They proved to be in thermodynamic equilibrium only after heating at much higher temperatures, when they underwent structural modification [319, 320]. Their structure became densely packed (tetrahedral and decahedral) at about 600 K and mass spectra were characterized by a new set of magic numbers, $N = 38$, 48, 58, 61, 64, 68, 71, 75, 77, 84, 91, 96, and 98 (see Fig. 7). Also, it was found [320] that the structure of large $(C_{60})_N$ clusters was insensitive to a change in the charge. In other words, the long-standing hypothesis of charge dependence of $(C_{60})_N$ clusters failed to be confirmed.

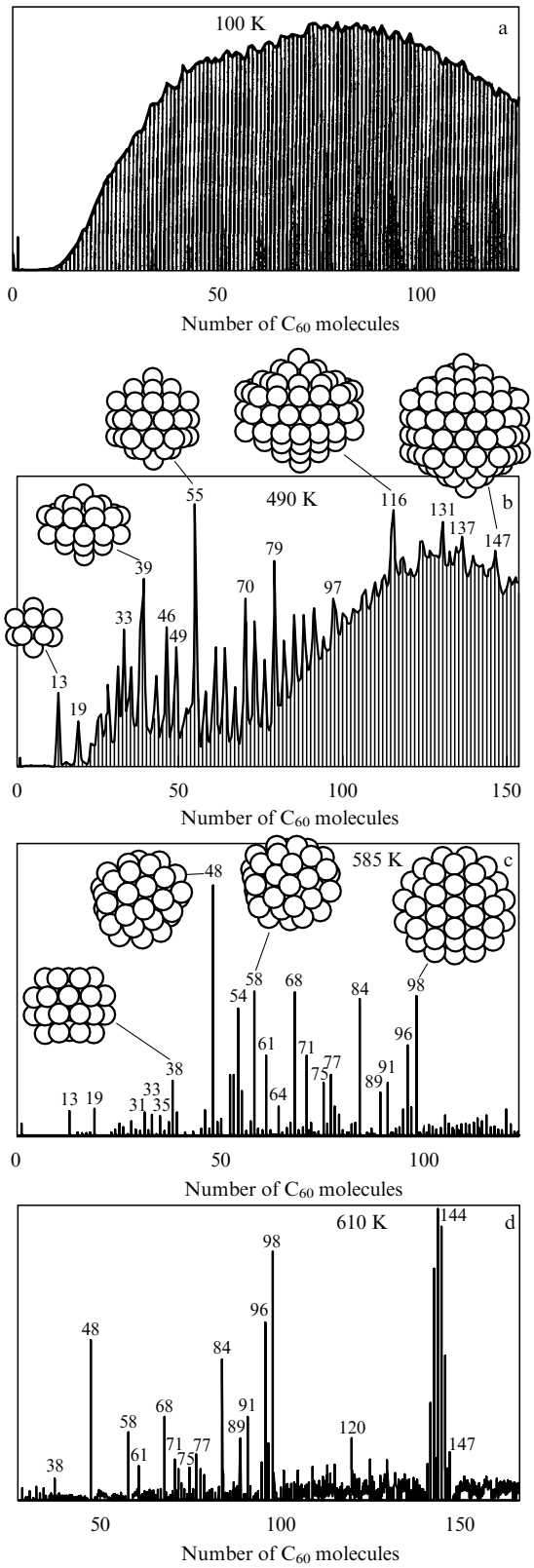

Figure 7. Mass spectra of $(C_{60})_N$ clusters obtained at the heating cell temperatures 100 K (a), 490 K (b), 585 K (c), and 610 K (d). Characteristic structures of the clusters are shown in Figs (b, c), where molecules of C_{60} are depicted as small balls. After heating at 490 K, the clusters had an icosahedral structure (b); more intense heating resulted in densely packed decahedral or tetrahedral structures (c,d) [320].

3.3 Relation between cluster temperature and intermolecular interaction potential

The measurement of crystal lattice parameters in [224] and the use of the known thermal expansion coefficients [339] yielded the following temperatures for van der Waals clusters: $T_{cl}(\mathrm{Ne}) = 10 \pm 4$ K, $T_{cl}(\mathrm{Ar}) = 37 \pm 5$ K, $T_{cl}(\mathrm{Kr}) = 53 \pm 6$ K, and $T_{cl}(\mathrm{Xe}) = 79 \pm 8$ K.

It was found that the stronger the attraction between atoms, the higher is the cluster temperature. This means that the cluster temperature is related to the intermolecular potential, in conformity with condensation and evaporation processes in cluster beams [340]. During cluster growth in an expanding jet, the condensation heat must be absorbed by the gas and the cluster temperature remain increased and almost constant throughout the growth period. The process of expansion being completed, the clusters fly freely in the vacuum, and their condensation stops but evaporation continues. Thus, the cluster temperature decreases until not a single atom can further evaporate. In other words, the smaller the binding energy of atoms in a cluster, the lower its final temperature.

Assuming that the binding energy of atoms in a cluster is proportional to the depth ε of the Lennard–Jones potential well for the inert gas, it can be shown that the cluster temperature T_{cl} is proportional to ε (Fig. 8), suggesting a constant thermal-to-binding-energy ratio for clusters of inert gases in a beam.

We note that condensation–evaporation processes may lead to even lower temperatures for small clusters. The value $T_{cl} = 27 \pm 3$ K was obtained in [321] for small amorphous argon clusters ($N < 50$); this is significantly smaller than the temperature of crystal clusters. The relation between T_{cl} and ε may be extrapolated to clusters of other types. Analysis of diffraction patterns in [341] yielded the temperatures of N_2, O_2, and CO_2 clusters. These results, together with the data for clusters of inert gases, are shown in Fig. 8. There is excellent agreement between them, indicating that the method for

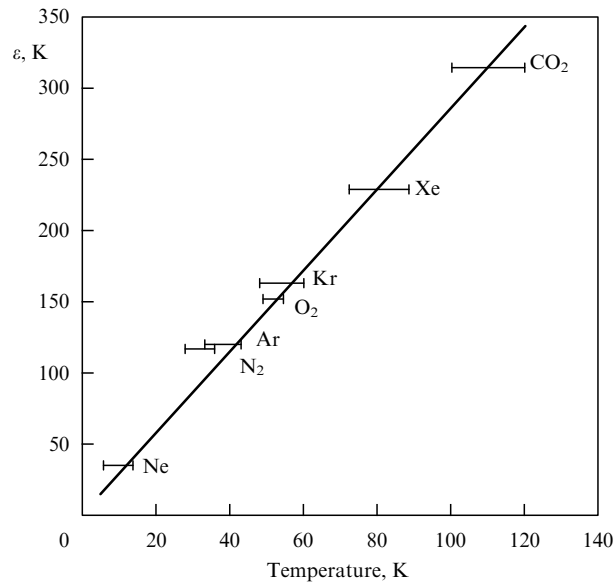

Figure 8. The depth ε of the interatomic or intermolecular potential well as a function of the estimated cluster temperature in a beam. Experimental results suggest a linear dependence (solid line) [224].

measuring the temperature of argon clusters is equally applicable to molecular clusters.

4. Methods of cluster excitation. Measurement and stabilization of cluster temperature

4.1. Excitation of clusters. Determination of cluster temperature from emission spectra

Clusters of metals, carbon, and other refractory elements are characterized by intrinsically strong bonding (1 – 10 eV). This makes them stable, unlike loosely bound van der Waals clusters or clusters with weak hydrogen bonds; they do not dissociate even after strong excitation, when the energy per atom amounts to $\geqslant 1$ eV (see, e.g., [70] and the references therein). It is worth noting that most methods used to form strongly bound clusters (laser irradiation, spraying, pulsed discharge, hot vapor expansion) produce hot clusters unless they are cooled by collisions. Additional excitation by intense laser light [220 – 223, 342 – 344], electron impact [214 – 218], or high-energy ions [219, 345], or as a result of collision with a solid surface [43, 70] and chemical reactions [346] brings clusters to a highly excited state. Due to the high state density, the excitation energy rapidly turns into heat and the clusters become very hot. Such clusters emit light like any 'black body.' Equilibrium emission from excited clusters was observed and investigated in refractory metals [223, 342] and carbon [220 – 222, 343, 344]. The internal temperature of excited clusters, as well as heating and cooling rates, can be accurately determined from their emission spectra. In what follows, we consider concrete examples of excitation and radiative cooling of different clusters observed in experiment and treated theoretically.

Processes of radiative cooling and laser-induced excitation of clusters W_N, Nb_N, and Hf_N are described in [223] and of Nb_N in [342]. Radiation cooling of clusters Nb_N excited in a reaction of oxidation by oxygen is reported in [346]. In all these works, clusters were generated by laser-induced evaporation of the target material. Either the fourth harmonic of an Nd:YAG laser ($\lambda = 266$ nm) [223, 342, 346] or an eximer KrF laser ($\lambda = 308$ nm) [223] was used for the purpose.

Many researchers have studied carbon clusters [220 – 222, 343, 344]. One of the earliest works [220] dealt with particles produced by laser evaporation of graphite in a pulsed helium flow. When the helium stream containing graphite particles passed through a rather long (35 mm) channel prior to expansion, clusters 50 – 100 nm in size were generated. The second harmonic of an Nd:YAG laser (532 nm) was used to evaporate the target and the second, third, or fourth harmonic of another Nd:YAG laser to additionally excite the clusters. Emission of fullerenes C_{60} and C_{70} excited by an eximer KrF laser ($\lambda = 193$ nm) was investigated in [222] and optical emission spectra of C_{60} clusters desorbed by an eximer XeCl laser ($\lambda = 308$ nm, pulse length 20 ns) depending on laser energy density was studied in [221, 344]. In these experiments, laser energy densities were estimated to vary from 10 to 400 mJ cm^{-2} at the pulse length 10 – 20 ns. The equilibrium emission spectra were analyzed in the wavelength range from 350 – 400 to 800 – 850 nm.

Emission spectra (300 – 800 nm) of fullerenes C_{60} excited by a beam with the energy of electrons up to 100 eV were reported in [214 – 217]. The fullerenes were produced by an effusive molecular beam. The authors observed a quasi-continuous emission spectrum (spectral resolution 3 nm) resembling the Planck emission spectrum of a heated body. Both neutral and charged clusters were found to emit radiation. The maximum contribution to radiation was made by charged ions C_{60}^{+} generated after emission of electrons by neutral clusters.

The above studies demonstrated that optical radiation from hot clusters largely consists of broad structureless emission intrinsic to a black body. Analysis of this emission gives the particle temperature. The intensity of emission from a heated particle of radius a (isotropic at a wavelength λ) in the range $\Delta\lambda$ is described by the relation

$$I(\lambda, a) = \varepsilon(\lambda, a)\, P_\lambda(T)(4\pi a^2)\, \Delta\lambda\,, \tag{4.1}$$

where $P_\lambda(T)$ is the Planck distribution function for the black-body emission,

$$P_\lambda(T) = \frac{2\pi c^2 h}{\lambda^5 \{\exp[hc/(\lambda k_{\mathrm{B}} T)] - 1\}}\,. \tag{4.2}$$

Relation (4.1) is actually the expression for the intensity of black-body radiation modified by the introduction of spectral emittance ε of a small particle. This emittance is identical with the absorption efficiency Q_{abs} equal to the ratio of the absorption cross section C_{abs} to the particle cross section, i.e., $C_{\mathrm{abs}} = Q_{\mathrm{abs}}(\pi a^2)$. The quantity Q_{abs} for a given radiation wavelength and particle size can be obtained from the Mie theory of small-particle radiation [347]. In the approximation of Rayleigh criterion $2\pi a \ll \lambda$ (usually, $2\pi a < 0.3\lambda$), Q_{abs} is given by the expression

$$Q_{\mathrm{abs}} = \frac{8\pi a}{\lambda}\, \mathrm{Im}\left(\frac{m^2 - 1}{m^2 + 2}\right), \tag{4.3}$$

where $m = n - \mathrm{i}k$ is the complex refraction index. If m is a weak function of the radiation wavelength in the chosen range, then $Q_{\mathrm{abs}} \propto 1/\lambda$. This assumption leads to a modified formula (4.1) with the factor λ^6 in the denominator, which may be used to determine the temperature of small emitting particles. This relation was used in [214 – 223, 343 – 346] to estimate the temperature of emitting metal and carbon clusters.

The shape of the enveloping emission spectra was found to depend on the temperature of emitting particles. For example, all calculations of a 'hot' spectrum (Fig. 9a) indicate [220] that the carbon cluster temperature falls into the range 3800 – 4000 K. Time evolution of the emission spectra gives an idea of the cooling kinetics of hot clusters. The spectra obtained with a delay relative to the end of the laser pulse are much 'colder' than those obtained immediately after the completion of excitation. Similar results are reported for carbon [220 – 222, 343, 344] and metal [223, 346] clusters (Fig. 9b). The emission spectra and their evolution in time appear to be independent of the mode of cluster excitation [346]. Similar spectra were obtained for clusters excited by laser radiation [220 – 222, 342 – 344] and electron impact [214 – 217], and in a chemical reaction [346].

Experiments [221, 222] demonstrated a weak dependence of the cluster temperature on the energy density of the exciting laser (close to saturation) in the range $\geqslant 30 - 40$ mJ cm^{-2}, in agreement with model calculations [221]. The model predicts that the laser rapidly heats the cluster to a temperature at which cooling by fragmentation (evaporation) competes with

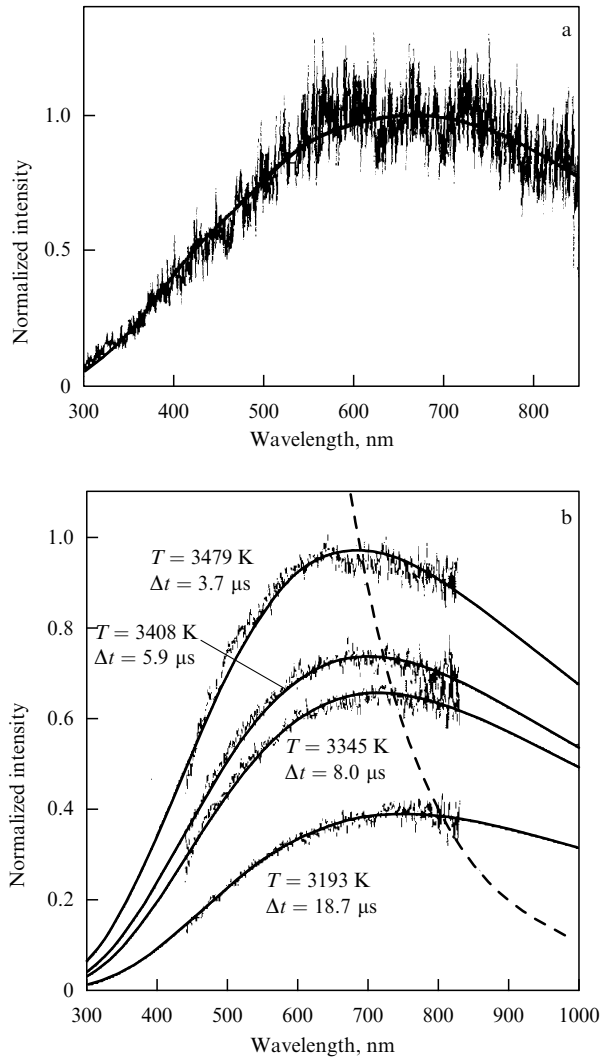

Figure 9. (a) Emission spectrum of carbon clusters (normalized to the sensitivity of the spectrometer) excited by laser radiation (266 nm) at the energy density about 40 mJ cm^{-2}. The clusters were excited at the distance 8.6 cm from the beam source and the emission was detected from the excitation zone. The thick line shows the emission spectrum of a black body calculated from expression (4.1). Experimental and theoretical spectra are normalized at their maxima [220]. (b) The equilibrium emission from niobium clusters ($N \approx 13000$) following excitation by laser radiation (266 nm) at the energy density 37 mJ cm^{-2}. Δt is the time delay between the onset of excitation and the detection of emission. Theoretical spectra are obtained from (4.1). Experimental and theoretical spectra are normalized at their maxima. The dashed line shows the displacement of the spectra according to Wien's law [223].

laser heating, making it difficult to reach a particle temperature above 4000 K. At a moderate energy density of laser radiation, it is possible to heat carbon clusters to the evaporation temperature (approximately 3000 K) [221]. Collisions of clusters with atoms of the cooling gas [348–351] further contribute to the decrease in their temperature. However, equilibrium emission remains the dominant mechanism of energy loss by clusters produced by laser evaporation in nozzle sources.

4.2 Energy relaxation channels in excited clusters

We consider different cooling mechanisms for hot particles (C_{60} clusters) based on the data in [221] (see also [219]). This must give an idea of their importance and provide information about the cooling rates to be expected under concrete experimental conditions. The collisional mechanism of cluster cooling considered in Section 4.3 manifests itself only at high laser energy densities and a high density of particles in a desorbed cloud.

The radiation cooling rate at equilibrium emission can be deduced from the Stefan–Boltzmann law

$$I(T) = c_v \frac{\mathrm{d}T}{\mathrm{d}t} = -4\pi a^2 \varepsilon \sigma_{\mathrm{SB}} T^4 , \tag{4.4}$$

where c_v is the heat capacity of a molecule in C_{60}, a is its radius (3.5 Å), ε is the emittance integrated over the spectrum, and σ_{SB} is the Stefan–Boltzmann constant. Integrating relation (4.4) gives the expression for the time-dependent cluster temperature [221]:

$$T = \left(\frac{1}{T_0^3} + \frac{12\pi a^2 \sigma_{\mathrm{SB}} \varepsilon t}{c_v} \right)^{-1/3} . \tag{4.5}$$

The cluster thermal capacity $c_v = \mathrm{d}E_v/\mathrm{d}T$ ($c_v = 0.0138$ eV K^{-1}) [352] and the integral emittance ε must be known in order to estimate the temperature decrease due to radiative cooling. We use the value $\varepsilon = 4.5 \times 10^{-5}$ obtained in [352]. It follows from (4.5) that the initial cluster temperature 3000 K decreases only by 1.5 K for 10 μs.

Another cooling mechanism for C_{60} clusters is thermoelectron emission [353]. The rate constant for thermoelectron emission can be found using the expression [354]

$$k_{\mathrm{ion}} = 1.9 \times 10^{16} \exp\left(-\frac{U_{\mathrm{i}}}{k_{\mathrm{B}} T} \right) , \tag{4.6}$$

where U_{i} is the ionization potential for C_{60} (7.68 eV [353]).The cooling rate is computed by multiplying the rate constant by the ionization potential. Such an assessment is valid because the concentration of ionized C_{60} remains low compared with that of neutral molecules [221].

An important cooling mechanism for C_{60} clusters is the evaporation or monomolecular dissociation (the loss of C_2 molecules). The rate of this process can be evaluated using the Arrhenius equation with the semi-empiric constant A derived in [356]:

$$k_{\mathrm{frag}} = A \exp\left(-\frac{E_0}{k_{\mathrm{B}} T} \right) , \tag{4.7}$$

where $A = 3 \times 10^{13} N^{2/3} \exp(6/N^{1/3})$ [s^{-1}] with $N = 60$.

A broad range of experimentally obtained values of the dissociation energy E_0 can be borrowed from the literature for neutral C_{60} clusters and positive-charged ions C_{60}^+ (from 4.6 eV in [357] to 7.64 eV [218]). For example, the authors of [221] quote the values $E_0 = 5.77$ eV (C_{60}) from [358] and $E_0 = 7.1$ eV (C_{60}^+) from [218].

Finally, light emission in the IR range by IR-active cluster modes must be taken into consideration. The intensity of this radiation can be estimated from the expression obtained in [359]:

$$I(E) = \sum_n \sum_i h\nu_i n A_i (s-1)\, \xi_{i,E} \left\{ 1 - \left[\frac{a(E)}{2} + n \right] \xi_{i,E} \right\}^{s-2} , \tag{4.8}$$

where $\xi_{i,E} = h\nu_i/(E + aE_0)$, $a(E) = 0.87 + 0.079 \ln(E/E_0)$, E is the total vibrational energy, E_0 is the total zero-point energy, ν_i are normal mode frequencies, n are vibrational

quantum numbers, A_i are Einstein coefficients for spontaneous radiation, and s is the number of vibrational degrees of freedom.

Only four IR-active modes (526 cm^{-1}, 576 cm^{-1}, 1185 cm^{-1}, and 1448 cm^{-1}) must be taken into account, owing to the high symmetry of C_{60} molecules. The Einstein coefficients [221] were found from the IR absorption spectra of a 200-nm-thick film sprayed over a substrate of KBr crystals. Relation (4.8) gives only the lower limit of intensity of the emitted IR radiation because a large number of C_{60} molecules undergo thermoionic emission and/or fragmentation, which leads to the formation of hot fragments with a lower symmetry and a higher number of IR-active modes.

Figure 10a presents the calculated rate constants for different cooling mechanisms in the temperature range 2000 – 4000 K. The temperature dependence of energy loss rates is illustrated in Fig. 10b. It can be seen that clusters are rapidly cooled at temperatures above 3000 K due to thermal ionization and the loss of the C_2 fragment. But the energy loss rate changes dramatically as soon as the system cools to 2500 – 3000 K, when equilibrium emission becomes the dominant cooling mechanism. These data explain why clusters with temperatures 2000 – 3000 K predominate under experimental conditions regardless of the laser radiation density and why the cooling rates of C_{60} clusters are so low.

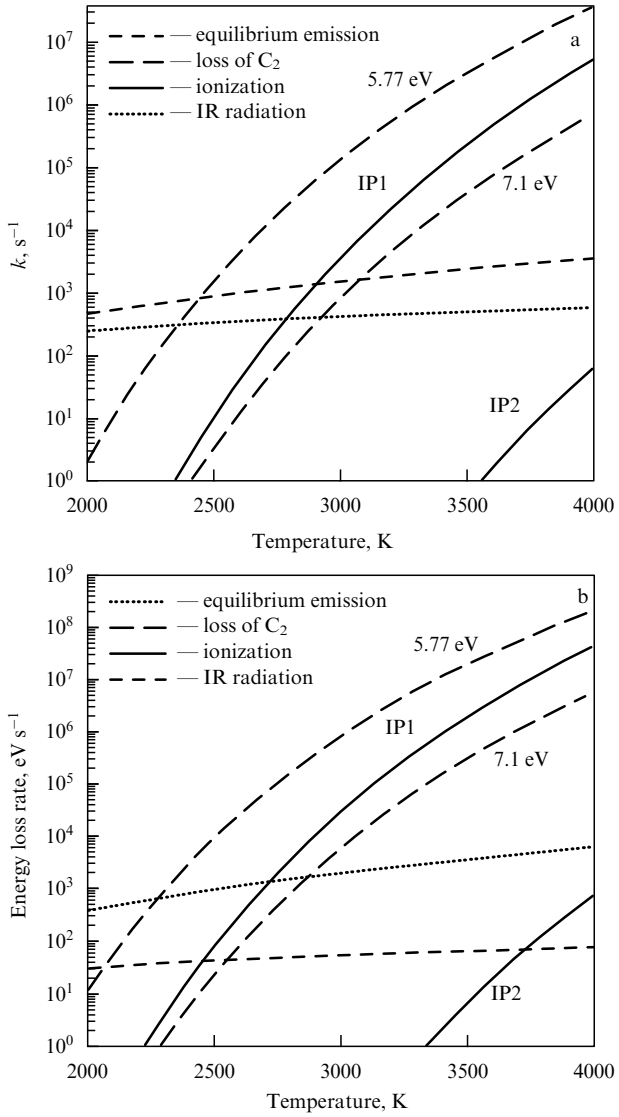

Figure 10. Parameters of the cooling process in superhot C_{60} clusters. The rate (a) and energy loss rate (b) constants for C_{60} molecules depending on temperature. IP1 and IP2 are the first and the second ionization potentials [221].

Thus, studies of optic radiation provide information on the cluster temperature and cooling mechanisms. They show that the electron temperature of desorbed fullerenes varies from 2300 to 3000 K in a rather broad range of energy densities of desorbing laser radiation (20 – 400 mJ cm^{-2}), in good agreement with the cluster vibrational temperature. Analysis of feasible cooling rates via mechanisms such as the thermoelectron emission, fragmentation due to the loss of C_2, and radiation in the IR region leads to the conclusion that the cluster cooling rate at temperatures below 3000 K is low and related to equilibrium emission. At higher temperatures, molecules (clusters) of C_{60} are very rapidly cooled by virtue of thermoelectron emission and/or fragmentation of C_2.

4.3 Stabilization of the metal cluster temperature in an inert gas

In Section 4.1, we considered cluster heating by laser light absorption. The final cluster temperature, dependent on many parameters (e.g., the photon energy, laser power, absorption cross section), is typically unknown. Nevertheless, this method allows obtaining a very high temperature, sufficient for the complete fragmentation of even highly stable clusters. On the other hand, cluster thermalization in an inert gas flow allows varying cluster temperature to a high degree of accuracy. In this method, clusters leaving a nozzle source and the carrier gas (usually helium) undergo heating within several milliseconds. The cluster temperature at this stage amounts to that of the carrier gas due to collisions with its atoms. The main advantage of the collisional thermalization technique over cluster heating by laser light lies in the fact that it permits accurately determining the cluster temperature in a wide range of its values.

4.3.1 Collisional cluster heating and cooling. We consider a heating and cooling technique for $(C_{60})_N$ clusters [361] (see also [319, 320]). The method allows heating a cluster beam to a well-defined temperature between 100 and 800 K. The device has heating and cooling modules (Fig. 11a). Its main part is a 120-mm-long copper tube *1* with an inner diameter of 6 mm attached directly to the nozzle outlet of the cluster source *2*. Clusters enter the heating module immediately after escape from the nozzle. The tube is thermally insulated from the condensation cell by Teflon washer *3* and is heated by virtue of coiled wire resistance *4*. The device is protected by an insulating jacket of thick copper wire *5* in order to stabilize the temperature. The jacket is thermally connected with a condensation cell cooled by liquid nitrogen. The heating module is covered by a stainless steel shield. Cooling the thick copper wire that serves as a cooling line is used to vary the temperature of the heating module in the range 100 to 800 K. Hot clusters leaving the heating module immediately enter the cooling zone. The two modules are mechanically connected by quartz adapter *7* and spring *8*. This flexible connection prevents the beam intensity loss associated with the temperature variation. The central part of the cooling module consists of a stainless-steel tube *9* with the inner diameter 4 mm placed in cryostat *10* cooled by a flux of liquid nitrogen or helium.

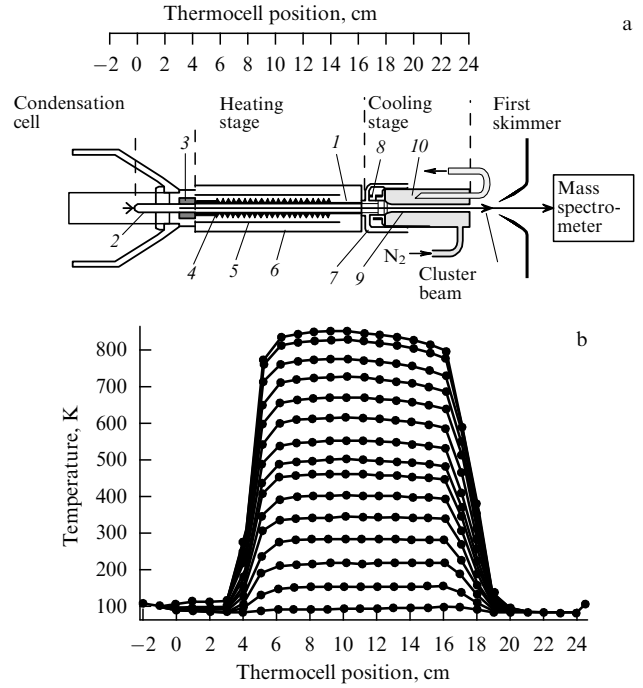

Figure 11. (a) Diagram of the experimental setup. Clusters escaping from the condensation cell consecutively pass through the heating and cooling modules. The scale at the top shows the position of the thermocouplel during measurement of the temperature profile. (b) Temperature profile of the carrier gas (helium) in the heating and cooling regions [361].

The carrier gas temperature is measured by a thermocouple at different points of the heating and cooling regions. Temperature profiles for different heating outputs are presented in Fig. 11b. The positions of the thermocouple on the x axis are shown in Fig. 11a. It was found in experiment that cold helium leaving the source is heated to 840 K over a length of only 3 cm, while the cooling of helium from $T = 840$ K to below 100 K occurs within 4 cm.

We note that the cluster temperature equals the temperature of the carrier gas only if the clusters undergo a large number of collisions with helium atoms. This number depends on the helium pressure, collision cross section, and time spent by the clusters in the collision zone. It was shown in [361] that $(C_{60})_N$ clusters undergo $10^5 - 10^6$ collisions with helium atoms when the gas pressure inside the cluster source is 1 mbar and the temperature in the heating module is 300 K [362]. Also, it was calculated in [361] that the length of the heating cell is sufficient for clusters to undergo the necessary number of collisions and reach the helium temperature. In contrast, in the general case, the cluster temperature in the cooling module exceeds the carrier gas temperature. The authors of [361] ascribe this to a lower helium pressure in the cooling module and its smaller length. This disadvantage is of little importance and can probably be corrected by modifying the device.

4.3.2 Results of calculations. We consider the influence of various parameters on the energy exchange between clusters and an inert gas. The process of energy transfer from Pd_{13} clusters to inert gas atoms was studied by the molecular dynamics method in [348] (see also [349]) depending on (1) the collision parameter, (2) the cluster temperature, (3) the inert gas temperature, (4) the gas – metal interaction force, (5) the metal potential, and (6) the inert gas mass. The results permit evaluating the number of collisions necessary to reach the equilibrium temperature between the clusters and the inert gas.

Without going into the details of computation, we consider data on energy transmission from clusters to atoms. We note at the outset that calculations were performed in the case where all the kinetic energy of the clusters is concentrated in vibrational degrees of freedom, i.e., where the translational and rotational degrees of freedom are not initially activated. This approach facilitates the investigation of energy transfer from the vibrational degrees of freedom to the rotational and translational ones. The total cluster temperature is related to the kinetic energy as

$$\frac{3N}{2} k_B T_{cl} = \left\langle \sum_{i=1}^{N} \frac{m_i v_i^2}{2} \right\rangle, \tag{4.9}$$

where m_i is the mass of metal atoms (106.4 a.m.u. for Pd), v_i is the atom velocity, and N is the number of atoms in a cluster ($N = 13$ in the case under consideration).

The amount of energy transmitted during collision differs for different degrees of freedom. This inference ensues from the dependence of the energy transmitted into different degrees of freedom of a cluster on the atomic gas temperature as shown in Fig. 12a for Pd_{13} clusters colliding with helium

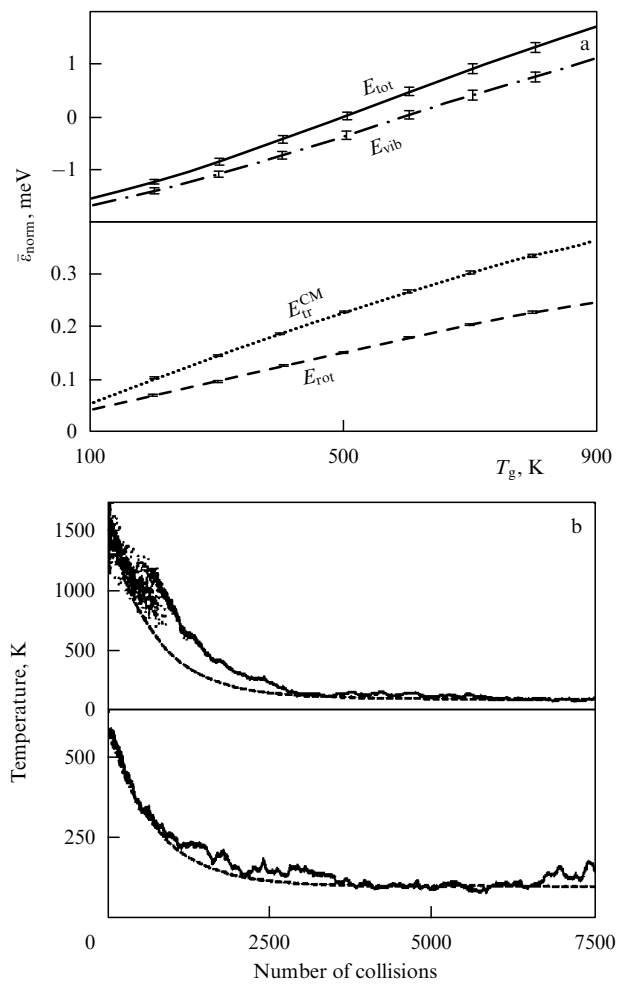

Figure 12. (a) Collisions of helium atoms with Pd_{13} clusters at $T_{cl} = 500$ K. Top: the total transferred energy as a function of the gas temperature. Bottom: the energy transmitted into the cluster rotational and translational degrees of freedom [348]. (b) Cooling of Pd_{13} clusters as a result of collisions with helium atoms [348].

atoms. The cluster temperature is 500 K. The total transmitted energy is zero when the buffer gas temperature is 500 K. The energy transfer from vibrational degrees of freedom is zero at 600 K. This is because all the kinetic energy of the cluster is initially located in vibrational modes. The same fact explains why the energy transmitted into the rotational and translational degrees of freedom is positive. The energy is most effectively transferred into translational degrees of freedom (as is apparent from the slightly sloping curve) and with a roughly equal efficiency into rotational and vibrational ones, although their numbers are significantly different (3 and 33, respectively).

Helium is most frequently used as the carrier gas in cluster sources. However, there is reason to believe that energy transfer would be more efficacious with a heavier inert gas. The authors of [348] examined energy transmission from helium, neon, and argon atoms to Pd_{13} clusters at cluster temperatures of 100 and 500 K. It was found [348 – 351] that the amount of energy transferred to the clusters increased with an increase in the mass of the buffer gas. For example, the energy transferred from argon atoms to Pd_{13} clusters at $T_{cl} = 100$ K and $T_g = 900$ K was approximately 4 times higher than that transferred from helium atoms.

A study of cluster cooling during collisions with inert gas atoms [348] revealed the linear dependence of the amount of energy transferred during the collisions on the buffer gas temperature T_g. Moreover, the dependences for different cluster temperatures T_{cl} had similar slopes. Therefore, the mean transmitted energy can be represented as

$$\varepsilon_{mean} = k(T_g - T_{cl}), \tag{4.10}$$

where k is the slope of a given dependence (the energy exchange constant). It is a function of the atom and cluster masses and of the interaction potentials. Studies of the effect of collisions on the cluster temperature in [348] showed that roughly half of the energy transmitted to a cluster was used to increase its internal potential energy, and the other half to increase the cluster temperature. Hence, the increment of cluster temperature ΔT per collision can be obtained from the relation

$$\frac{3N}{2} k_B \Delta T = \frac{k}{2} (T_g - T_{cl}), \tag{4.11}$$

where N is the number of atoms in the cluster.

The authors of [348] used relation (4.11) to derive a difference equation for the cluster temperature after n collisions:

$$T_{cl}(n) = \left(T_{cl}(0) - T_g\right)\left(1 - \frac{k}{3Nk_B}\right)^n + T_g. \tag{4.12}$$

For example, Eqn (4.12) predicts that some 2500 collisions are needed to cool a Pd_{13} cluster from $T_{cl} = 600$ K to $T_{cl} = 100$ K. We recall that the buffer gas pressure is usually known in such experiments. An equation taking it into account was also derived in [348].

The authors verified Eqn (4.12) by calculating changes in the cluster Pd_{13} temperature depending on the number of collisions [348]. The results for these clusters and helium atoms are shown in Fig. 12b. The lower curve illustrates the case where the initial cluster temperature is 600 K. At the beginning, all the cluster degrees of freedom have equal temperature. The upper part of the figure shows data for the initial cluster temperature 1500 K, i.e., almost 500 K higher than the melting point of Pd_{13}. Rotational and vibrational degrees of freedom have zero temperature. In this case, the cluster temperature also changes in good agreement with (4.12), albeit with a somewhat lower convergence near 1000 K due to the liquid-to-solid phase transition.

To summarize, the results in [348 – 351] permit evaluating the number of collisions necessary to reach the desired cluster temperature in an inert gas. The difference equation obtained with the use of an energy exchange constant allowed determining the cluster temperature. The initially liquid Pd_{13} clusters were found to cool down to 100 K after approximately 3000 collisions (Fig. 12b).

4.4 Cluster temperature in a cluster light source

It was shown in Sections 4.1 and 4.2 that highly heated clusters emit light. This property is used to create cluster light sources. Their key component is cluster plasma, i.e., gas-discharge plasma containing cluster ions. Cluster ions having a positive charge travel from the anode to the cathode in an electric discharge. Such a system has technical implications; in particular, it forms the basis of principally new light sources, 'cluster lamps' [363 – 370]. Thus far, the most widespread light sources have been incandescent bulbs, whose glowing filament emits light, and gas-discharge bulbs, in which light is emitted by excited atoms or in the course of electron – ion photorecombination. Hot filaments have the temperature up to 3000 K, while the plasma temperature in gas-discharge bulbs amounts to 8000 K. Therefore, gas-discharge light sources are more efficacious than conventional electric lamps.

A cluster light source based on tungsten and ruthenium clusters is described in [363 – 365]. In these works, a wave discharge and a regenerative chemical cycle were used to replenish the cluster material, i.e., tungsten or rhenium compounds (WO_2Br_2 and Re_2O_7). The chemical cycle was realized by introducing MX chemicals in the gas discharge, with M = Li, Na, K, Rb, or Cs and X = Cl, Br, or I. The charge was ignited in an inert gas (Ne, Ar, or Xe). Later, a different design of cluster lamps was proposed [366], with cluster ions being driven by the external electric field into a hot ionized gas produced in a low-power plasma generator. This scheme was shown to have a number of advantages [366 – 368]. Cluster light sources are described at greater length in many original papers [363 – 370] and reviews [41, 51]. Here, we briefly consider some of their specific features and the cluster temperatures realized in these devices.

Cluster plasma employed in cluster light sources is usually described in terms of a spherical liquid droplet model where the number of atoms in a cluster is given by

$$N = \frac{4\pi r^3 \rho}{3m}, \tag{4.13}$$

where r is the cluster radius, m is the atomic mass, and ρ is the bulk liquid volume.

Thermal equilibrium between clusters and discharge plasma is maintained by cluster collisions with atoms and electrons. If the gas temperature T_g, the cluster temperature T_{cl}, and the electron temperature T_e are expressed in energy units, it can be assumed [51, 367] that the mean energies of an atom and an electron change after collision with a cluster from $3T_g/2$ to $3T_{cl}/2$ and from $3T_e/2$ to $3T_{cl}/2$, respectively. Such a situation occurs in the case of strong interaction between colliding atomic particles and clusters, especially

when the atoms are trapped at the cluster surface. In the framework of the liquid droplet model for a cluster of radius r and charge Z, the following relations hold for the atom–cluster (k_a) and electron–cluster (k_e) collision velocity constants [51, 367]:

$$k_a = \langle v_a \pi r^2 \rangle = \sqrt{\frac{8T_g}{\pi m_a}} \pi r^2 ,$$
$$k_e = \langle v_e \pi r^2 \rangle \left(1 - \frac{Ze^2}{\varepsilon_e r}\right) = \sqrt{\frac{8T_e}{\pi m_e}} \pi r^2 \left(1 + \frac{Ze^2}{rT_e}\right). \quad (4.14)$$

Here, v_a and v_e are the atom and electron velocities, ε_e is the electron energy averaged over the atom and electron velocity distribution, and Z is the cluster charge. The cluster radius is assumed to be large enough to ensure that collisions obey the classical theory but rather small compared with the free paths of atoms and electrons. For this reason, the cluster interacts with a single particle at any given moment.

The above analysis yields an equation for the cluster temperature [367]:

$$(T_g - T_{cl})\, k_a n_a + (T_e - T_{cl})\, k_e n_e = 0 , \quad (4.15)$$

where n_a and n_e are the atom and electron densities. Hence,

$$T_{cl} = \frac{T_g + \zeta T_e}{1 + \zeta} ,$$
$$\zeta = \sqrt{\frac{T_e m_a}{T_g m_e}} \left(1 + \frac{Ze^2}{rT_e}\right) \frac{n_e}{n_a} . \quad (4.16)$$

Relation (4.16) gives the cluster temperature in plasma. Its value, close to 3600 K, is considered most suitable for a tungsten-based cluster light source when the gas temperature in the discharge tube is about 2000 K and the electron temperature is of the order of 6000 K [51, 367].

Xenon is most frequently used as a discharge gas in cluster light sources by virtue of its small ionization potential (approximately 12.1 eV [371]). It ensures the necessary degree of ionization at a relatively low electron temperature. The data reported in [365–369] indicate that a cluster lamp may be an effective light source because clusters emit light more effectively than plasma electrons. For the same reason, cluster light sources are characterized by a smaller thermal load than gas-discharge sources. In other words, cluster light sources have an advantage of being as efficient as gas-discharge ones at lower temperatures and discharge powers.

4.5 Stabilization of cluster temperature on a surface

Methods of cluster temperature stabilization include deposition (condensation) of clusters an the surface [295, 317, 372–380]. This approach is based on the dependence of the cluster temperature on the temperature of the surface ($T_{cl} = T_s$) at which they condensate. A cold surface also supports cluster formation and growth of cluster layers [374–381]. The surface temperature (hence, cluster temperature) may be varied in a broad range depending on the type (composition) of clusters to be formed and stabilized. Atomic or molecular beams and fluxes of laser-sprayed substances, as well as a rarified gas in a low-pressure chamber, can be used to form clusters on a cold surface. These methods produce not only metal clusters but also carbon clusters, clusters of superconducting elements with strong binding energies in the range 1–10 eV [295, 373, 374], and molecular and noble gas clusters [375–381] having much weaker hydrogen and van der Waals bonds (from 10^{-3} to 0.5 eV).

When clusters with strong bonds are to be formed and stabilized, the surface temperature may be varied from dozens to thousands of degrees Kelvin. Such conditions are frequently realized when clusters of metals and superconducting elements are deposited on the surface to produce nanostructures, thin layers, and new materials [295, 373, 374] (see Section 6.4).

The formation of cluster layers on a cold surface was recently undertaken using molecular beams in [377–381] to study interactions between SF_6 and CF_3I molecules vibrationally excited by intense laser IR radiation in a beam with surface molecular (cluster) layers. The authors studied the reflection of excited and unexcited molecules from a cold surface ($T_s \approx 80-85$ K) covered with molecules (clusters) and their passage through cooled multichannel plates and hollow convergent truncated cones with condensed clusters. The study revealed a much higher probability of reflection of highly vibrationally excited molecules from a cold surface with cluster layers compared to nonexcited molecules. Also, the excited molecules more readily passed through multichannel plates and cones. In all likelihood, this method can be used to select molecules in a beam based on their isotopic and/or component composition.

4.6 Determination of cluster temperature from infrared absorption spectra of intercalated molecules

Cluster temperature is most straightforwardly and precisely determined from the absorption spectra of intercalated molecules. The value of this method was confirmed experimentally using IR spectroscopy of molecules embedded into nanodroplets (clusters) of superfluid helium. Results of these experiments are briefly discussed below. Spectroscopic studies of molecules and clusters inside nanodroplets of superfluid helium are overviewed in [61–63, 66, 67, 72].

In these studies, nanodroplets (clusters) of superfluid helium formed upon gas-dynamic expansion of the gas from the nozzle into a vacuum. The gas pressure over the nozzle usually varied from 1–2 to 50–60 atm. A nozzle with the outlet diameter 5 to 50 μm was cooled to 4–20 K. The cluster beam isolated from the stream passed through a 5–10 cm long scattering chamber containing a molecular gas at the pressure $10^{-4}-10^{-5}$ Torr. On their way through the chamber, the clusters captured the 'guest' molecule of interest. As the clusters moved further toward the mass spectrometer analyzing the beam, they were affected by laser radiation of varying frequencies. When radiation was in resonance with the 'guest' molecule, the absorbed energy promoted the evaporation of helium atoms from the clusters; it thereby the beam and attenuated mass spectrometry signals. This means that the IR spectrum of the molecule of interest inside superfluid helium droplets can be obtained by retuning the laser frequency.

Spectra obtained by this method show a well apparent rotational structure, which can be used to determine the population of the molecule rotational levels and hence the molecule temperature inside the cluster. Comparison of experimental and theoretical spectra allows more precise measurement of the temperature. Figure 13a shows the vibrational absorption spectrum ν_3 of SF_6 molecules inside droplets of ^4He and Fig. 13b shows the vibrational absorption spectrum ν_3 of OCS molecules. The well-resolved rotational structure permits determining the cluster temperature [212,

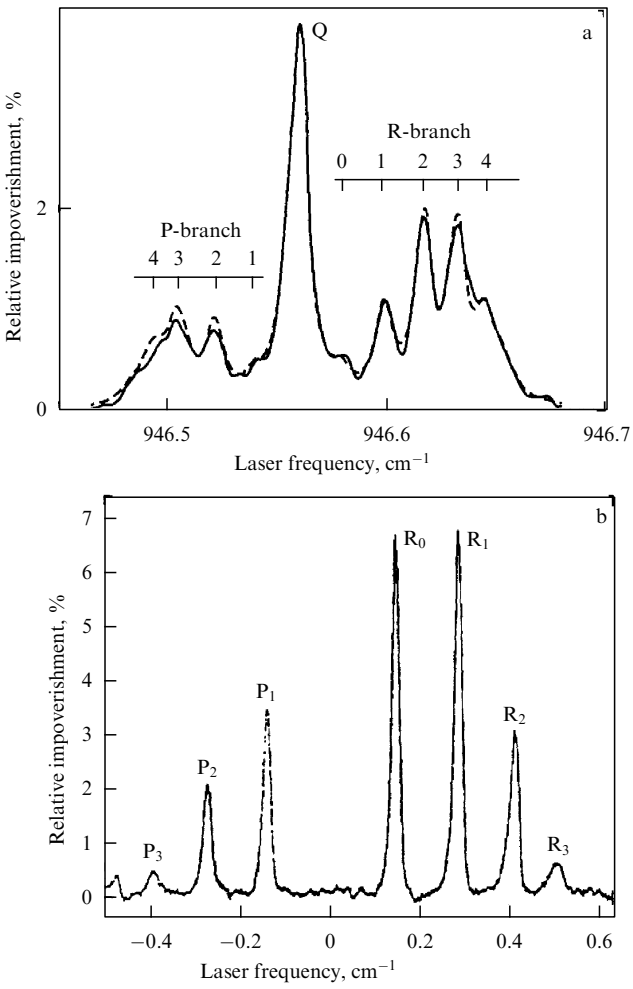

Figure 13. (a) The vibrational IR absorption spectrum ν_3 of SF_6 molecules inside a droplet of ^{4}He ($N = 2700$) (solid curve). The calculated spectrum of a freely rotating molecule is shown for comparison (dashed curve) [63, 382]. (b) The vibrational IR absorption spectrum ν_3 of OCS molecules inside an ^{4}He droplet [383].

382, 383]. The spectra in Figs 13a, b correspond to the molecule temperature around 0.38 K inside the helium droplets. The total width of the vibrational IR absorption spectrum ν_3 of the SF_6 molecules does not exceed 0.5 cm^{-1}, i.e., is significantly smaller than the isotopic shift in the above vibration (≈ 8.5 cm^{-1} [384]). This opens the possibility of selectively exciting molecules inside nanodroplets of superfluid helium by high-power IR lasers and using this process to select intercalated molecules in terms of isotopic (component) composition [72, 385 – 387).

4.7 Methods for measuring cluster melting temperature

4.7.1. General remarks and a brief overview of early methods. Macroscopic matter has a well-defined melting temperature T_m at a given pressure. The melting is manifest as a visually apparent change in the sample shape. Unlike macroscopic substances, clusters have no definite melting temperature; solid and liquid phases coexist in them within a certain temperature range. Melting of clusters reveals a number of their characteristic properties. Measurements of melting temperature and heat in clusters encounter great difficulty. Diffraction methods are applicable to sufficiently large particles with $N = 10^3 - 10^6$ (see Section 3.2). As the particle size decreases, the measurement of the particle temperature becomes progressively more difficult. However, the cluster melting temperature is one of the most important physical parameters, having both scientific and practical implications.

Small particles have a lower melting temperature than bulk matter, as was first predicted in [388] and later confirmed experimentally in [389]. In conformity with the known Lindeman criterion [390, 391], melting starts when the atomic vibration amplitude reaches 10 – 15% of the mean distance between the atoms. Taking this value as the melting criterion, the physical basis of the above phenomenon can be qualitatively described as follows. The fraction of surface atoms in small particles is significantly greater than in macroscopic objects. These atoms have fewer neighbors, and therefore they are weakly bound and less restricted in their thermal motion [392]. At the same time, there are more exact criteria for cluster melting [393, 394], such as Berry's criterion [395, 396]. They are based on the correlation between atom pair distribution functions. When a cluster melts, the corresponding parameters change jump-like, as is the case with the Lindeman criterion, and reflect changes in the thermal motion of melting atoms. At the same time, phase transitions in clusters are related to their configuration excitation. Melting corresponds to the transition to the lowest configuration-excited state of a cluster (see, e.g., [69] and the references therein; see also Section 2.1).

The melting of clusters has been investigated in many experimental [209 – 211, 275 – 277, 397 – 408] and theoretical [204 – 208, 278 – 280, 409 – 420] studies. They have demonstrated that solid – liquid phase transitions in clusters (i.e., systems of limited size) differ from those in macroscopic bodies in three main features: (1) the cluster melting temperature decreases as the particle size decreases, (2) the phase transitions occur in a narrow temperature range, (3) the particle melting heat is lower than that of macroscopic matter. It was also shown that the melting temperature of small clusters ($N \leqslant 200$) varies considerably, depending on their size [277, 404]. The melting heat of certain clusters exceeds that of bulk matter, suggesting their unusually strong structure [421, 422]. Phase transition starts from the melting of the cluster surface layers [412, 419]. Both experimental data [209 – 211] and calculations [69, 204 – 208] indicate that clusters may have negative thermal capacity near the phase transition, meaning that melting at which solid and liquid phases coexist is associated with partial conversion of the cluster kinetic energy into potential energy. The cluster cools as its total energy increases. The essence of this phenomenon is that the energy increases is not an extensive quantity in such complicated systems. Interaction between the cluster subsystems should not be disregarded, bearing in mind its great importance [69, 412, 416].

The first experimental studies of cluster melting temperature [389] were carried out with a transmission electron microscope. The method recorded changes in the diffraction picture at the melting point due to the structural disorder in the clusters. The melting temperature decreased with decreasing the cluster size. It should be noted, however, that the electron diffraction method is inapplicable to small clusters because they produce broadening low-intensity lines (see Section 3.2). Moreover, because this method is sensitive to the cluster structure alone, its use for measuring the melting heat is impracticable.

The melting temperature of lead clusters with a radius 100 – 150 Å was determined in [397] from the measurements

of the reflectivity R of particles inserted into a transparent matrix. This material has different reflectivities in the solid and liquid phases. Therefore, the phase transition temperature can be found from the temperature dependence of reflectivity. The authors of [397] observed a jump in the dependence $R(T)$ for clusters of different types as the temperature increased in the range 390 to 460 K. Analysis of their data gave the cluster melting temperature. It was found [397] that this temperature decreased with a decrease in the radius of the particles. However, the results of the measurements were probably influenced by the surface melting of the clusters.

A colorimetric method for the measurement of melting temperature in large clusters was proposed in [398]. The authors examined the melting of tin particles with the radius 50 – 500 Å (containing up to 10^7 atoms). The particles were deposited on the surface of a thin-film SiN calorimeter. Measurements were made by delivering an electric pulse to a heater made of a thin Ni film. The pulse heated the system composed of the heater, the SiN membrane, and an Sn sample. Current and voltage across the system were measured in real time. The energy consumption rate increased abruptly as soon as the tin particles began to melt. Subsequent analysis of variations in the heater resistance in time gave exact temperatures of the system and the total energy put into it. The melting temperature was found to decrease sharply (from approximately 220 °C to 150 °C) with a decrease in the mean cluster radius from 500 Å to 50 Å. For bulk matter, $T_m = 232$ °C. The melting heat of the clusters also decreased significantly from the bulk value 58.9 J g^{-1} to ≈ 16 J g^{-1}, i.e., by roughly 70%.

The solid-to-liquid phase transition can be detected from the structure of cluster fragmentation [399]. When dissociating clusters are in the liquid phase, magic numbers are not apparent in their fragmentation structure because cluster stability depends on the structure and liquids have no ordered structure. Conversely, the presence of well-apparent magic numbers in the fragmentation structure suggests a solid structure of the cluster undergoing fragmentation. Dissociation of a solid particle is regarded here as an analog of sublimation. The melting of clusters was also recorded in [400, 401] from the altered spectral characteristics of free combined clusters composed of a large molecule embedded into an inert gas cluster (see also Section 2.5). In Sections 4.7.2 and 4.7.3, we consider the recently developed methods in which clusters themselves serve as energy-measuring instruments ('ultrasensitive calorimeters'). These methods use two mass spectrometers, one for the selection of clusters of the desired size and the other for the analysis of their fragmentation.

4.7.2 Measuring the caloric curve from the photofragmentation of clusters. The most straightforward method for the diagnostics of phase transitions in clusters consists of the elucidation of characteristic features of their heat capacity $c(T)$, defined as the partial derivative of the internal energy with respect to temperature:

$$c(T) = \frac{\partial E}{\partial T}\,. \tag{4.17}$$

The temperature – energy relation $E = E(T)$ is called the caloric curve. Caloric curves for mass-selected sodium clusters were obtained in studies of cluster thermal properties [209, 277, 402, 404, 405].

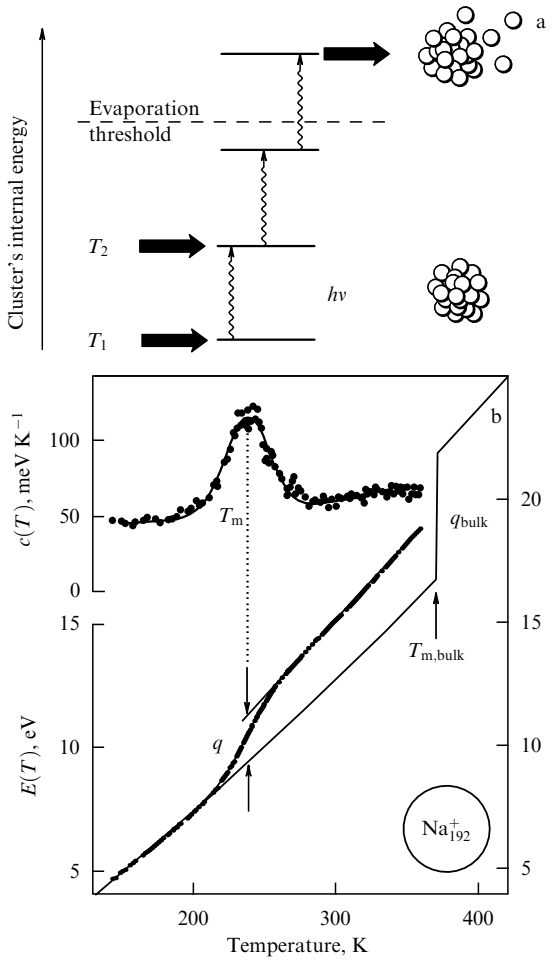

Figure 14. (a) Schematic representation of a cluster laser heating experiment. (b) Temperature dependences of the thermal capacity and melting heat for positive-charged sodium clusters of 192 atoms. Black dots are the experimental data. The melting point of the cluster, T_m, can be obtained from the maximum of the dependence $c(T)$ and the latent melting point q from the jump on the caloric curve. The solid line is the caloric curve for bulk matter (normalized to 192 atoms) [276].

The idea behind experiments in [209, 277, 402] designed to measure $E = E(T)$ is as follows (Fig. 14). A cluster with a temperature T_1 is heated to T_2 when it absorbs a photon with the energy $\delta E = h\nu$. The steady-state cluster temperature T_2 is determined from the temperature of the cluster source at which the photon-heated clusters have fragmentation patterns (mass spectra) similar to those of laser-heated structures.

The clusters' thermal capacity is measured in four stages.

1. Preparation of mass-selected cluster ions with the temperature T_1 in a vacuum.

2. Irradiation of the clusters by laser photons. The absorbed energy ($h\nu = 3.1$ eV $\approx 10^{-18}$ J) relaxes and heats the clusters to the temperature T_2 at which they do not yet emit atoms within the experimental time scale (for approximately 100 μs). The cluster temperature increases so as to trigger evaporation of atoms only after each cluster absorbs several additional photons from the same laser pulse (two in the case shown in Fig. 14a).

3. Evaluation of the distribution of cluster ions by size after fragmentation with the help of the second mass spectrometer. This distribution is highly susceptible to the cluster internal energy.

4. Increasing the cluster temperature to T_2, at which the absorption of only two laser photons induces evaporation of the same number of cluster atoms. In other words, an increase in energy by δE results in a temperature increase by $\delta T = T_2 - T_1$. For relatively small δT, the ratio $\delta E/\delta T$ equals the heat capacity $c(T)$. The melting point of a cluster is the temperature at which the function $c(T)$ has a maximum (Fig. 14b).

This method was used in [209, 277, 402, 404, 405] for in-depth studies of the heat capacity and melting temperature of sodium cluster ions. As shown in [402], the melting temperature of Na^+_{139} ions is $T_m = 267$ K compared with 371 K for bulk matter. The width of the phase transition is 12.6 K, and the latent melting temperature is 1.98 eV, i.e., significantly lower than the latent melting temperature of bulk matter (3.69 eV).

4.7.3 Ionic colorimetry. We consider the ion colorimetry technique recently developed [407, 408] for the measurement of cluster temperature and melting heat. The method is based on the dissociation of cluster ions induced by their multiple collisions with inert gas (helium) atoms. The method consists of reproducing a similar degree of cluster ion dissociation (similar internal energy) by modulating the cluster thermal energy (as a result of heating in the source) and the energy generated by collisions with buffer gas atoms. Measurements were made for cluster cations of aluminum with the number of particles $N = 49-63$ [407] and $N = 63-83$ [408]. The cluster thermal capacity was assessed in the temperature range 150 – 1050 K.

The clusters were generated by the laser evaporation method using a liquid metal sample in an atmosphere of the buffer gas (helium). The cluster ions thus formed entered an expansion chamber, where their temperature could be modulated and stabilized as a result of collisions with the buffer gas (see Section 4.2). Thereafter, the clusters were mass-selected using a quadrupole mass spectrometer and driven to a collisional cell containing helium at the pressure 1 Torr, where multiple collisions between the clusters and helium atoms occurred. Each collision caused the transformation of a small translational energy fraction of a cluster into the internal energy. Given a sufficiently high translational energy of cluster ions entering the cell, some of them were heated to a temperature that induced their dissociation. Intact parental ions and ion fragments formed in subsequent collisions were cooled to the helium temperature, extracted from the cell by a weak electric field, and directed to the second quadrupole mass spectrometer for analysis. The resulting mass spectra were used to determine the fraction of the dissociated cluster ions.

The energy needed to dissociate clusters decreased with increasing the temperature as a result of their increasing thermal energy. When the temperature increased to $T_{cl} = T_m$, the energy necessary for cluster dissociation dropped sharply due to the latent melting heat [407, 408]. The translational energy $E_{tr}^{(50\%)}$ at which 50% of the ions dissociated was measured experimentally depending on the cluster temperature in the expansion chamber. It gradually decreased as the cluster temperature increased and fell dramatically at the melting temperature. The derivative of $E_{tr}^{(50\%)}(T)$ with respect to the temperature was proportional to the cluster thermal capacity with a high degree of accuracy. It was shown using this method that the cluster melting temperature was approximately 40% lower than the bulk value. It underwent marked fluctuations depending on the cluster size; for the majority of clusters, it was significantly smaller than in the bulk. For example, $T_m = 586$ K for the Al^+_{79} cluster ion compared with 934 K for a macroscopic substance. The width of the peak in the temperature dependence of heat capacity for Al^+_{79} was 150 K [408]. This suggests the co-existence of the liquid and solid phases in a rather wide (150 K) vicinity of the melting point.

To summarize, the above method is applicable only to clusters that dissociate in the liquid phase. It cannot be used to measure the melting temperature if clusters dissociate (sublimate) in the solid phase at $T < T_m$ (such behavior is characteristic of tin clusters).

5. Stabilization of cluster temperature by evaporation

5.1 Association between canonical and microcanonical reaction rates

As a rule, the available methods for cluster generation (see [1 – 3, 12, 24, 26, 30, 54, 70]) cannot be used to obtain large clusters with a desired energy and temperature. Evaporation is one of the methods to stabilize the cluster temperature (internal energy). The process of evaporation of atoms or molecules from clusters is usually described [354, 423 – 428] in terms of the theory of monomolecular reactions [429, 430], which allows deriving the microcanonical and canonical reaction rate constants. There are two strategies for the computation of the microcanonical rate constants of monomolecular reactions. One takes the properties of the transient state into account [431] and the other is based on microscopic reversibility [432]. A third approach, proposed in [423], is a combination of these two methods. It assumes the following relation between microcanonical and canonical rate constants:

$$k(E) = k(T)\left[\frac{\omega^*(E-E_0)}{\omega^*(E)}\exp\left(\frac{E_0}{k_B T}\right)\right], \tag{5.1}$$

where $k(T)$ is the canonical rate constant at the temperature at which the system undergoing fragmentation has the mean energy $\overline{E}(k_B T)$ equal to the specific energy E of interest. In Eqn (5.1), the terms in square brackets describe the relation between the canonical and microcanonical rate constants: $\omega^*(E-E_0)$ and $\omega^*(E)$ are the sums over the states of the transient complex at energies $E - E_0$ and E, and E_0 is the activation energy at zero temperature. Equation (5.1) relates the microcanonical and canonical rate constants and permits deriving the former from the latter [423 – 428].

5.2 'Evaporative ensemble.' Relation between cluster temperature and evaporation heat

To characterize clusters produced in nozzle sources, Gspann [226] hypothesized that they should evaporate intensively with the evaporation rate constant given by the inverse time interval between consecutive events in the evaporation process. This hypothesis looks valid, assuming that each cluster undergoes at least a single evaporation act and each step requires more time than the preceding one to be completed. Gspann also suggested [226] that the expression for the evaporation rate constant k_{ev} has a form similar to the Arrhenius formula:

$$k_{ev} = A\exp\left(-\frac{\Delta}{k_B T}\right), \tag{5.2}$$

where Δ is the evaporation energy (heat). Equation (5.2) relates the energy Δ to the temperature under the assumption that the preexponential factor A is a universal constant. The temperature of clusters being evaporated can be determined based on this formal relation. Its values obtained by this method are in excellent agreement with experimental data (see Section 2.1).

It is necessary, however, to describe clusters obtained by spraying, laser ablation, photoexcitation, and ionization, besides those produced in nozzle sources. The properties of these small aggregates (clusters) are also controlled by evaporation. The above procedure was further developed and improved in [423–428]. Simulation of the evolution of small systems such as clusters requires different (more general) approaches [424]. (It is worth noting that investigations into cluster evolution were motivated by the necessity to obtain detailed information on the cluster structure). One of such approaches applied in [423] was the 'evaporative ensemble' model. The notion of 'evaporative ensemble' and its properties are defined below.

Cluster temperature was considered on the basis of the theory of monomolecular reactions in [429, 430]. Monomolecular reaction rates are known to be strongly temperature-dependent. This dependence can be used to determine the activation energy, usually interpreted as the minimal amount of energy to be located on the reaction coordinate. In the case of clusters, dissociation (evaporation) processes are considered using energy instead of temperature to describe the system. In particular, it is assumed that the energy E of the medium under consideration is not very high compared with the minimal energy E_0 that must be accumulated to support the reaction. In this context, the use of the notion of 'temperature' appears more justified. Furthermore, the event of interest must always be taken as a monomolecular reaction in the given medium, regardless of the approach chosen to describe the evaporation process [428].

Exact calculations of the evaporation rate constants are reported in [424, 427]. They include estimation of temperature (canonical) rate constants used to obtain microcanonical constants. Computation of microcanonical rate constants is not described here; we only quote the final result directly related to the problem considered in this review. It is shown that the temperature of the evaporating aggregate (cluster) can be extracted from the equation

$$\frac{RT_{\rm cl}}{\Delta E} = \text{const}\,, \tag{5.3}$$

where R is the gas constant and ΔE is the molar vaporization energy. Generally speaking, the 'constant' in the right-hand side of (5.3) is independent of the cluster material; it is actually a slowly descending time constant (because clusters cool). Within a time scale of a few dozen microseconds, calculations give a typical value of the constant $\approx 4 \times 10^{-2}$ [427].

Equation (5.3) can also be represented in the form [428]

$$\frac{\Delta}{k_{\rm B}T_{\rm cl}} \approx \gamma(k)\,, \tag{5.4}$$

where Δ is the evaporation (vaporization) energy per particle. The parameter $\gamma(k)$ in Eqn (5.4) is equal to the inverse constant value in (5.3) and referred to as the Gspann parameter. As mentioned above, $\gamma(k)$ is virtually independent of the cluster size and material. The Gspann parameter shows a weak dependence on time and equals roughly 25 within a typical time scale of several dozen microseconds. A detailed analysis reported recently in [433] showed that the Gspann parameter may be approximately 1.5-fold larger or smaller than the above value, depending on the cluster size, the state density, and the kinetic energy realized during evaporation.

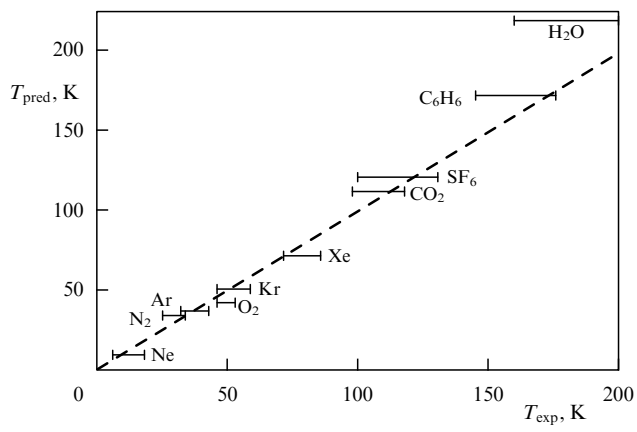

Figure 15. Comparison of cluster evaporation temperatures measured in [434–436] and predicted based on Eqn (5.4) (dashed line) [428].

The above relations can be used to predict the temperature of large clusters, such as those studied by the diffraction method. The thermodynamic data in Eqns (5.3) and (5.4) can be borrowed from standard sources (e.g., [371]).

In Fig. 15, we compare the cluster temperature predicted in [427, 428] and experimental values for large van der Waals clusters obtained by the electron diffraction methods in [434–435]. The dashed line has a unit slope and is far from being the best fit to the experimental data. It can be seen that the predicted results fairly well agree with experimental ones.

One more method to measure the temperature of small clusters was proposed in [427, 428]. According to the authors, the mean kinetic energy of an atom or a molecule leaving the cluster surface may be a measure of the transient state temperature. If the cluster fragmentation process is described in terms of the hard-sphere model, this relation is given by

$$\bar{\varepsilon}^* = k_{\rm B}T^*_{\rm cl}\,, \tag{5.5}$$

where $T^*_{\rm cl}$ is the temperature of the aggregate transient state. We note, however, that the temperature of small clusters measured in this way is lower than the temperature of the parent cluster undergoing fragmentation because part of the cluster energy is spent to maintain monomer evaporation [427, 428]. This method, measuring the cluster temperature from the kinetic energy of the released fragments, is not infrequently used in experiments on cluster excitation by laser irradiation [437] or by collision with a surface [70], and in model calculations [438].

Equations (5.3) and (5.4) are general relations for estimating the temperature in clusters by a variety of methods (gas expansion in nozzle sources, sputtering, laser ablation). They are equally suitable in the case of metastable clusters [424]. Evaporation of at least one atom (molecule) from a cluster is the sole indispensable precondition for the derivation and application of Eqns (5.3) and (5.4). This condition, i.e., the occurrence of a single evaporation act, determines the existence of the 'evaporative ensemble.' However, it cannot be realized in such cases as supersonic gas expansion in nozzle sources when the condensed gas is diluted with an uncondensed one. In this situation, the

resulting clusters have a very low temperature ($T_{cl} \leqslant 1-5$ K), and evaporation kinetics establishes only an upper boundary of the available temperature range.

5.3 Relevant remarks

Several remarks are in order as regards the 'evaporative ensemble' and the temperature of evaporating clusters [423–428].

1. It is assumed for the purpose of derivation of the microcanonical rate constant in the evaporative ensemble [423] that evaporation is accompanied by the loss of monomers. But in certain cases (e.g., with carbon clusters), the loss of several atoms predominates [218, 439–442]. A redefinition of the monomer unit and generalization of the theory are then needed.

2. Emission of radiation in the IR range competes with evaporation at large times [225]. Hence, the necessity to take this energy relaxation channel into account.

3. The principal concept of the microcanonical rate constant $k(E)$ suggests that the equilibrium energy distribution in the system undergoes dissociation (fragmentation). This is not always the case, however. For example, high-frequency molecular oscillations in molecular clusters may long (for several microseconds) remain in disequilibrium with van der Waals vibrations [443]. The temperature given by Eqn (5.5) refers to low-frequency van der Waals modes alone.

4. It is assumed in the derivation of Eqn (5.3) that the evaporation energy is a weakly varying monotonic function of the cluster size. It should be borne in mind, however, that 'magic' clusters, if they exist, have a higher evaporation energy [424, 426, 428].

The evaporative ensemble cannot be characterized by a single fixed temperature because it decreases during evaporation. This fact is of little importance for relatively large clusters ($N \geqslant 10^3$) having rather high heat capacity. For small clusters ($N \leqslant 10$), the notion of 'temperature' should be used only to denote energy, especially the high-energy wing of cluster ensembles from which atoms (molecules) evaporate.

To conclude this section, we note that the concept of the evaporative ensemble allows determining evaporation rates of both neutral and charged clusters [331, 356, 423, 424, 444]. Evaporation rate constants of neutral and ionized water clusters ($N = 10$ and $N = 100$) as functions of temperature in the range 170–250 K were reported in [423]. It is shown that they strongly depend on temperature, especially near the limiting temperature ($T_{cl} \leqslant 190$ K), where rate constants of small clusters ($N = 10$) become vanishingly small ($\leqslant 10^5$ s^{-1}). Evaporation rates for small ion water clusters ($N = 10$) are approximately two orders of magnitude smaller than for neutral clusters. Conversely, evaporation rates of neutral and charged clusters containing $N = 100$ molecules differ by less than 25%. This can be accounted for by the fact that the evaporation process becomes increasingly endothermal with decreasing the cluster ion size due to the enhanced binding energy of cluster molecules.

6. Excitation of clusters upon collision with a solid surface

6.1 General remarks

Collision of accelerated cluster beams and cluster ions with a solid surface is an efficacious method for the rapid and strong excitation of clusters (see [43, 70] and the references therein). Collisions of large ($N \geqslant 10^2-10^6$) high-energy ($E_{col} \geqslant 10-10^3$ eV per particle) clusters with a solid surface within a short span of $\leqslant 50-500$ fs produce a medium with unusually high temperature ($\geqslant 10^4-10^5$ K), density (4–5 times that of a solid body), and pressure ($\geqslant 1-10$ Mbar). The cluster heating rate amounts to $10^{15}-10^{16}$ K s^{-1}. The physicochemical process induced under such extreme conditions and in the collision zone do not occur in thermal equilibrium (ionization, emission of light and charged particles, fragmentation, breakup and formation of chemical bonds, generation of microshock waves, nuclear synthesis, surface bombardment). These processes result from a strong excitation of clusters colliding with the surface; their characteristics are strongly influenced by the cluster velocity, size, and composition, as well as the material and temperature of the surface [70].

When high-energy clusters hit a surface, a large number of atoms are simultaneously incident on its small portion, leading to energy concentration in the collision zone. Indeed, collision of a high-energy cluster with the surface provides a unique opportunity to realize high energy concentration within a small ($\leqslant 5-10$ nm^2) area and to obtain a very high power density ($\geqslant 10^{16}$ W cm^{-2}). The collision of a cluster or multiatomic ion with the surface results in the superposition in time of the same processes that arise from the collision of a single atomic ion with a similar surface. These interactions are accompanied by space–time cooperative and/or coherent effects, accounting for the process rates and outputs unobservable in collisions of single atomic ions. The characteristics and mechanisms of cluster excitation (strong heating) by collisions with surfaces, the resulting cluster temperatures, energy transfer processes, and their outcomes and implications are briefly discussed in Sections 6.2–6.4. The same issues are considered at length in recent review [70].

6.2 Energy transfer in cluster/surface collisions

An important aspect in the description of collisions of high-energy clusters and cluster ions with surfaces is the amount of energy transmitted from a cluster to the surface, which determines the internal temperature of the reflected cluster. This energy can be measured from the recoil energy of intact cluster ions scattered on the surface [43].

The energy of cluster collisions with the surface was controlled in [43] by varying the target potential. If the potential U_{target} applied to the target exceeded the kinetic energy of incident ions, they were elastically reflected without touching the surface. Ion–surface collisions can be initiated when the applied voltage is lower than the kinetic energy of the ions. In other words, the collision energy E_{col} depends on the difference between the mean kinetic energy of incident ions and the target potential U_{target},

$$E_{col} = E_i - eU_{target}\,, \tag{6.1}$$

where e is the elementary charge. Negative collision energies suggest reflection. The recoil energy E_{rec} is given by the difference between the mean kinetic energy of scattered ions E_s and the potential U_{target}:

$$E_{rec} = E_s - eU_{target}\,. \tag{6.2}$$

Figure 16 presents the elastic collision coefficient ε, defined as the ratio of the recoil energy E_{rec} to the collisional

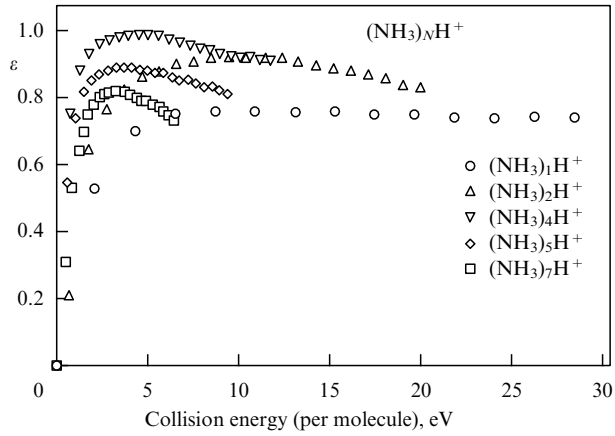

Figure 16. The elastic collision coefficient $\varepsilon = E_{rec}/E_{col}$ for protonated cluster ions of ammonia $(NH_3)_NH^+$ depending on the collision energy [43].

energy E_{col} ($\varepsilon = E_{rec}/E_{col}$) for protonated ammonia clusters $(NH_3)_NH^+$ ($N = 1, 2, 4, 5, 7$), depending on the collision energy. Evidently, cluster ions scattered from the target surface lose a substantial part of their kinetic energy at small collision energies (< 2.5 eV per molecule). At higher collision energies, only a small fraction of the kinetic energy (20–30%) is lost, which suggests substantial elasticity of cluster–surface collisions at high E_{col}. Normally, some 75% of the kinetic energy is retained in the initial cluster ions scattered on the surface. This result is not unexpected for hard-surface materials, e.g., diamond, and agrees with the data obtained by the molecular dynamics method [136, 137, 153]. Thus, the temperature of a scattered cluster depends on the collision energy.

6.3 Formation of microshock waves inside clusters

The collision of clusters and cluster beams with a solid surface at super- and hypersonic velocities produces a microshock wave inside the clusters and in the collision zone, as shown in [445, 446] by computer simulation of molecular dynamics (see also [135]). In Ref. [445], this process was studied using krypton clusters Kr_N ($N = 8-512$) colliding with a platinum surface at the speed $v = 5 \times 10^4 - 10^7$ cm s^{-1} and energy $E^0_{kin} = 10 - 10^6$ eV. Argon clusters Ar_N ($N = 55-555$) in [446] collided with a platinum surface at the speed $v = 10^5 - 10^6$ cm s^{-1}. Cluster–surface interactions were described either by the Lennard–Jones potential [445] or by two potentials, the Lennard–Jones and exp-6 [446] (see also [70]). The collision speed did not exceed $v = 10$ km s^{-1} in order to avoid the necessity of taking effects associated with electron excitation of clusters into account and in order to consider processes in the ground electron state alone. At this speed, the kinetic energy was $E_{kin}/N < 26$ eV per particle.

6.3.1 Energy acquisition in cluster–surface collisions. The evolution of the potential energy of E_p clusters, the temperature T_{cl}, and the cluster–surface interaction energy (CSIE) was examined in [445, 446] (Fig. 17). References [445, 446] report the most characteristic features of the evolution of these parameters. Specifically, their time dependences for the two potentials used in these studies differed by less than 20%. The parameters E_p, E_{cl}, and CSIE began to increase at the moment of collision τ_0. E_p and CSIE maxima practically coincided. The temperature T_{cl} increased to a maximum and

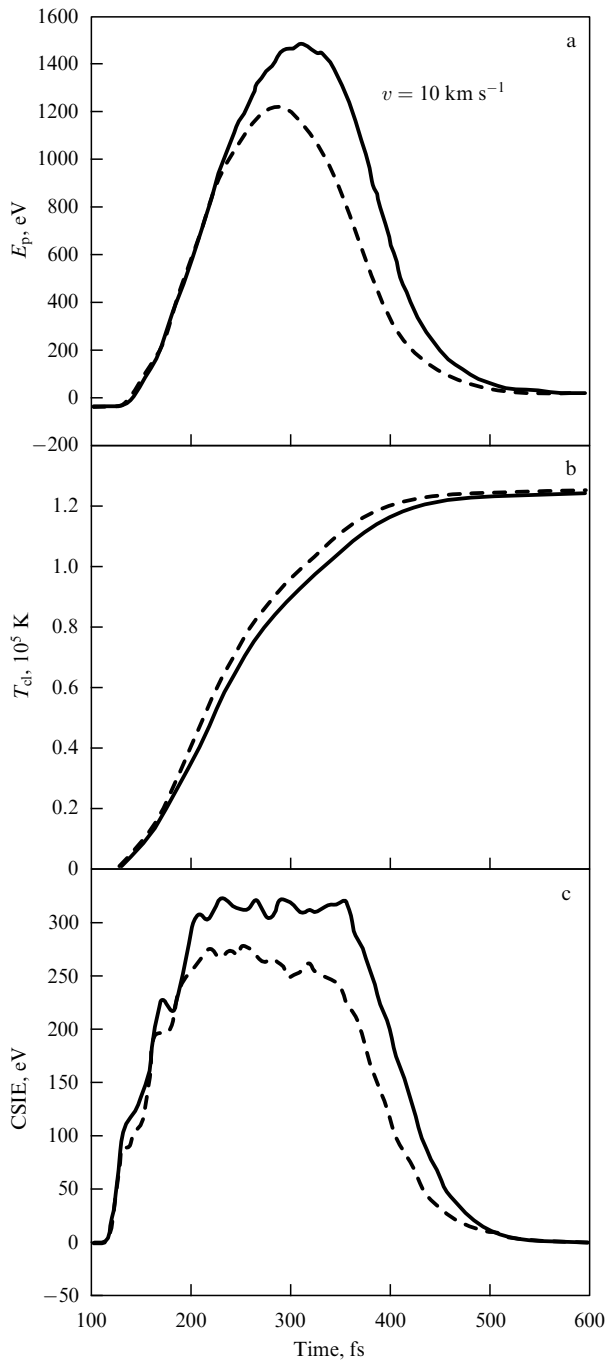

Figure 17. Time evolution of the cluster potential energy (CPE) (a), the cluster temperature T_{cl} (b), and the cluster–surface interaction energy (CSIE) (c) for a collision of cluster Ar_{555} with a platinum surface at the speed 10 km s^{-1} for two model potentials: exp-6 (solid line) and the Lennard–Jones potential (dashed line) [446].

reached the saturation level. The time τ during which a cluster remained near the surface was given by the width of the E_p curve, which was very close to the width of the CSIE curve. The time τ_{max} corresponding to the maximum E_p value determined the cluster energy acquisition time $\tau_{CEA} = \tau_{max} - \tau_0$.

6.3.2 Formation and propagation of a microshock wave. A cluster excited by a collision with a surface is a small-size system existing at extreme temperature and pressure. The cluster temperature may be very high, e.g., as high as

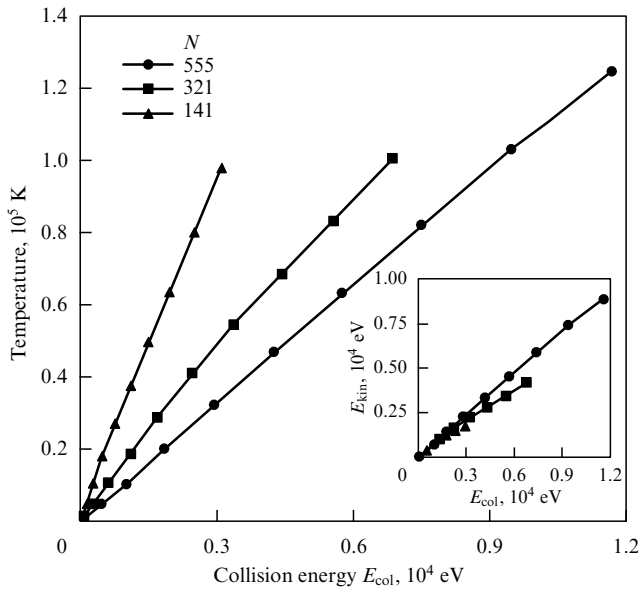

Figure 18. The maximum temperature of Ar_N clusters ($N = 141, 321, 555$) colliding with a Pt surface plotted vs the collision energy. Inset: maximum kinetic energies of the clusters [446].

$T_{cl} = 1.2 \times 10^5$ K at the speed $v \approx 10$ km s^{-1} ($E_{kin}/N = 21$ eV) of Ar_N clusters ($N = 555$) at time moments when the clusters have the maximum potential energy (Fig. 18). The temperature T_{cl} increases linearly as E_{kin} increases and satisfies the relation $T_{cl} = \alpha(E_{kin}/N)$, where $\alpha = (5 \pm 0.5) \times 10^3$ eV^{-1} K; the parameter α is independent of the cluster size for $E_{kin}/N = 0.2 - 22$ eV.

The propagation of a microshock wave inside a cluster was studied in [445, 446], where it was assumed to be composed of many spatial layers, in analogy with continuous media [447]. Immediately before the collision with the surface ($t < 0$), the energy was evenly distributed inside the cluster. It was found (see also [70]) that the collision was followed by the spreading of the high-energy region over the outer layers of the cluster; this process reflects propagation of the microshock wave inside the cluster as it shrinks at the moment of collision. Before E_p reached a maximum value (e.g., up to $t \sim 200$ fs for Ar_{555} at $v = 10$ km s^{-1}), the compression shock wave propagated toward the cluster as a single wave. Thereafter, the primary wave was overlapped by the secondary one that originated near the Pt surface and moved away from it. Eventually, the two waves diverged locally. Collisions of these waves with the surface gave rise to the tertiary and higher-order shock waves whose propagation and reflection resulted in cluster degradation.

The velocity u_s of a shock wave in clusters appears to be linearly dependent on the collision speed v at which the clusters and cluster ions hit a solid surface [446]: $u_s = \eta v$. The parameter η depends on the cluster size. Analysis of the results obtained in [446] shows that the relation $u_s/v = 1 \pm 0.15$ is satisfied for relatively large clusters ($N \geqslant 321$); this means that the velocity of propagation of a microshock wave inside a cluster roughly equals its collision velocity.

6.4 Other processes in clusters upon their collision with a surface

Collisions of high-energy clusters and cluster ions with solid surfaces that occur at extremely high temperature, density, and pressure are accompanied by a variety of other physicochemical processes, such as the ionization of atoms and molecules [448 – 456], the electron emission [457 – 474], the fragmentation of clusters [136, 137, 475 – 492], the breakage and formation of chemical bonds [127 – 146], initiation of reactions with high-energy barriers [138 – 146], nuclear synthesis [119 – 126], light emission [493], the formation of films [7, 147 – 175] and nanostructures with specific properties [159 – 177], and surface bombardment [178 – 196]. All these processes have been considered at some length in recent review [70]. They have important fundamental and practical implications. Investigations into extreme processes inside clusters provide information on homogeneous and heterogeneous processes of energy input and distribution with an ultrashort time scale of the molecular motion.

The ultrafast energy redistribution inside cluster ions during their collisions with a surface provides a basis for the formation of 'superhot' clusters with an energy sufficient to break almost all intermolecular bonds. The method based on the collision of high-energy clusters with a solid surface allows realizing a new regime with the input of 1 – 50 eV of energy per molecule for 10 – 100 fs. This allows inducing intracluster reactions with a high energy barrier, even such as air burning [139, 141, 142]. It may be argued that chemical reactions induced by cluster – surface collisions represent a novel and rather general mechanism in femtosecond chemistry.

The interaction of neutral and ionized cluster beams with a surface is used in macro- and nanotechnologies. Studies on the interaction of metal and superconductor cluster beams with solid surfaces demonstrated [41, 54, 70] that such beams can be used to treat the surfaces, produce thin films, and create essentially new materials.

Metal clusters formed by pure vapor expansion are hot liquid droplets. Due to this, deposition of high-energy cluster beams on the surface yields high-quality films (see, e.g., [7, 54, 68, 70, 295] and Section 2.6). Droplet fluidity accounts for the high cluster mobility at the surface, while the heat brought in with the clusters ensures efficacious, even if locally restricted, annealing. Moreover, deposition of low-energy cluster beams [162 – 175] produces thin films with intercalated solid clusters known as 'materials assembled from clusters' [170 – 173]. Nanonstructures formed by cluster beams, thin films, and other cluster materials have very specific structures and properties of importance for modern technologies.

7. Strong heating of clusters by superpower ultrashort laser pulses

Excitation by superstrong ultrashort laser pulses is the most efficient way to 'instantaneously' and heavily heat clusters [52 – 57, 85 – 111, 494, 495]. Such experiments became possible owing to the creation of superpower laser systems emitting ultrashort pulses [496, 497]. The excitation of clusters by ultrashort laser pulses in the IR range ($\lambda \approx 800$ nm) is known fairly well (see, e.g., [52 – 57]). In what follows, we briefly mention the main processes associated with this excitation mode and the resulting cluster temperatures. The peculiarities of cluster excitation by vacuum UV radiation of a free-electron laser is considered at a somewhat greater length.

We recall that the excitation of clusters by femtosecond laser pulses generates a strongly nonequilibrium plasma. Therefore, temperature may be introduced only for individual plasma components at selected stages of its evolution. On the other hand, consideration of cluster excitation by

ultrashort laser pulses is useful in that it gives a better idea of the methods to reach a high cluster temperature.

Irradiation of large clusters containing thousands of atoms or molecules by an intense ultrashort laser pulse gives rise to strongly excited matter [52–54]. Fast excitation of a cluster in the absence of heat extraction leads to considerable heating of its electron subsystem (to several kiloelectronvolts). Atomic ions are not heated at the onset of laser pulse impact. After a rapid initial multiple ionization by the main pulse component, the cluster ion is an ideal plasma composed of electrons and multicharged atomic ions. A variety of nonequilibrium extreme processes develop in such strongly excited clusters during and after the action of the laser pulse [52–57], e.g., internal and external photoionization, Coulomb and hydrodynamic explosions, generation of high harmonics and X-ray radiation, nuclear synthesis, and production of neutrons.

7.1 Cluster ionization

Typical fluxes of laser energy in experiments on cluster excitation by superstrong ultrashort pulses (see [52–57, 495]) are $10^{16}-10^{20}$ W cm^{-2} at the pulse length $\tau_p \sim 30-300$ fs. The electric field strength in a laser wave is much higher than that in a hydrogen atom (approximately 10^9 W cm^{-1}). Therefore, a laser pulse can ionize cluster atoms due to the above-threshold ionization process. The same is true of the ions being formed. Excitation of clusters by a laser pulse induces a series of processes including (1) internal ionization of cluster atoms giving rise to nanoplasma, (2) heating of quasi-free electrons inside the clusters, (3) external ionization as a result of electron emission by highly ionized clusters, (4) complete fragmentation of the clusters following the Coulomb and/or hydrodynamic explosion. For this reason, the total amount of the absorbed energy strongly depends on the internal ionization rate, which determines the plasma density and, therefore, the plasma heating rate.

Thus, clusters interacting with a laser pulse are transformed into a system of multicharged ions and free electrons [52–54]. Some electrons leave the cluster, which then acquires a positive charge, while others are retained by the cluster self-consistent field. The resultant system of multicharged ions and electrons is unstable and dissociates as a result of ion dispersion. The characteristic time of its disintegration is expressed as [55]

$$\tau_{\rm exp} \sim r_0 \left(\frac{m_{\rm i}}{Zk_{\rm B}T_{\rm e}}\right)^{1/2} \left(\frac{n_0}{n_{\rm e}}\right)^{1/3}, \tag{7.1}$$

where r_0 is the initial cluster radius, Z is the charge of the cluster ion, $T_{\rm e}$ is the cluster electron temperature, $m_{\rm i}$ is the ion mass, and n_0 and $n_{\rm e}$ are the initial and current electron concentration, respectively. Because the system degrades with ion velocities, its disruption time may be much greater than the laser pulse duration. This stage of plasma development affects the pulse properties [52–54]. The character of plasma beam interaction with superstrong ultrashort laser pulses allows the input of large specific energy into the electron subsystem (1–10 keV). In this way, absorption of the laser pulse energy by the cluster beam leads to the formation of specific hot plasma [52–54].

7.2 Coulomb and hydrodynamic explosions

The formation of homogeneous cluster plasma, nuclear synthesis, and generation of neutrons result from the explosion (expansion) of clusters. We consider the mechanism of explosion [55, 91, 498, 499]. A cluster is subject to two forces that cause its expansion during and after the action of the exciting pulse. One of them is the pressure of hot electrons that expand and push cold and heavy ions outside. The characteristic expansion rate is equivalent to the speed of sound in the plasma:

$$v_{\rm exp} \sim \left(\frac{Zk_{\rm B}T_{\rm e}}{m_{\rm i}}\right)^{1/2}. \tag{7.2}$$

The other force arises from the formation of an electric charge in the cluster. Cluster atoms undergo rapid ionization under the effect of a laser field, while electrons and ions concomitantly formed inside the cluster generate a self-consistent field; its interaction with the laser field leads to the ejection of some electrons outside the cluster. The developing charge of the cluster creates an electric field that allows the dispersion of the cluster internal atomic ions, i.e., causes its Coulomb explosion [52–57].

The electron pressure is given by

$$p_{\rm e} = n_{\rm e}k_{\rm B}T_{\rm e}, \tag{7.3}$$

where $n_{\rm e}$ is the concentration of electrons. Hence, the temperature reduction rate of the expanding cluster [55, 91] is

$$\left.\frac{\partial T_{\rm e}}{\partial t}\right|_{\rm exp} = -2\,\frac{T_{\rm e}}{r}\,\frac{\partial r}{\partial t}, \tag{7.4}$$

where r is the cluster radius.

To evaluate the force responsible for cluster expansion under the effect of the accumulated charge, the cluster plasma sphere is regarded [55] as an ideal conductor and the accumulated charge $Q_{\rm e}$ is considered to be concentrated on the cluster surface. The energy accumulated in the spherical 'capacitor' is expressed as

$$E_{Q_{\rm e}} = \frac{Q^2e^2}{2r^2}, \tag{7.5}$$

and therefore the force acting on the unit surface is

$$p_{\rm Coul} = \frac{Q^2e^2}{8\pi r^4}. \tag{7.6}$$

Because of the $1/r^4$ dependence of $p_{\rm Coul}$, the Coulomb force predominates in the case of small clusters. But as the clusters expand, it is replaced by the hydrodynamic force, with the hydrodynamic pressure being proportional to $1/r^3$ (due to $n_{\rm e}$).

We emphasize that a cluster rapidly expands as soon as it is heated to a very high temperature, irrespective of the explosion mechanism [55]. For example, a deuterium cluster measuring 100 Å at the electron temperature 1 keV expands two-fold after a Coulomb explosion for $\leqslant 20$ fs. It is shown [55, 91] that large clusters expand more slowly than small ones. Larger clusters are preferred in the general case for laser excitation because they remain intact during the subsequent heating by a laser pulse and can absorb more of its energy. The expansion affects cluster dynamics due to the decrease in the electron temperature described by Eqn (7.4). Another mechanism of electron cooling is associated with the energy transition from hot to cold electrons in the course of collisional thermalization [52–56].

7.3 Generation of X-ray radiation and neutrons

The excitation of clusters by strong ultrashort laser pulses was used to create an efficacious compact source of X-ray radiation [92 – 103, 495, 500 – 503]. The inhomogeneous hot plasma produced by the absorption of laser light by clusters is composed of multicharged ions and electrons captured by them [52 – 57]. Further plasma evolution gives rise to excited multicharged ions and other excited states and to the emission of shortwave photons. We recall that any hot plasma can emit shortwave radiation [54]. The plasma formed by laser radiation ensures a highly efficient transformation of the laser pulse energy into the X-ray radiation energy (from one to several percent) [52 – 57, 495].

Similar processes occur when the same plasma is used as a source of neutrons [54 – 57, 104 – 111]. In this case, a beam of deuterium clusters is irradiated by a laser pulse. The plasma formed in each cluster has a high electric potential, which accounts for its rapid dispersion under the effect of the cluster self-consistent field, leading to the appearance of energetic ions. The energy of such ions may be as high as dozens of kiloelectronvolts. Collisions of deuterium energetic ions at the next stage of plasma development when it becomes homogeneous after cluster dispersion may cause a thermonuclear reaction with the participation of these ions. Such a scheme cannot be used to construct a fusion reactor because the Lawson criterion for plasma parameters is four to five orders of magnitude smaller than its threshold value for a self-supporting fusion reaction. Nevertheless, it permits creating a source of neutrons based on a beam of deuterium clusters or deuterium-containing molecules [54, 57, 104 – 111].

High-energy ions were for the first time used to generate neutrons from the DD synthesis in [104]. In the experiments, large deuterium clusters formed in a gas-dynamic jet as the gas outflowed from the nozzle. An intense ($\geqslant 10^{16}$ W cm^{-2}) ultrashort (35 ps) laser pulse with the energy 120 mJ (at the pulse repetition rate 10 Hz) was focused into the jet carrying deuterium clusters and rapidly heated them. The resulting cluster explosion gave rise to ions with the energy of several kiloelectronvolts. The plasma filament thus formed had a diameter roughly equal to that of the laser spot in the focus (approximately 200 μm) and a width identical with the width of the deuterium cluster beam ($\approx$ 2 mm). Fast deuterium ions outflowing from exploded clusters collided with ions released from other clusters in the plasma. With the ion energy being sufficiently high (at least several kiloelectronvolts), there is a high probability of DD reactions. A good indicator of this process is one of the channels of DD synthesis, $D + D \rightarrow He^3 + n$, in which neutrons with the energy 2.45 MeV are generated.

The energy of the neutrons was measured by the time-of-flight method. It was found that the time of flight of the neutrons was 46 ns m^{-1}, in agreement with their energy 2.45 MeV. The output was some 1×10^4 neutrons per pulse [104, 105]. Such efficiency (approximately 10^5 neutrons per J of the laser energy) is comparable with that in large-scale installations (see, e.g., [104] and the references therein).

Time-of-flight measurements in [104, 105] were used to determine the burst period in the neutron source (approximately 500 ps) and neutron energy spread (roughly 10%) (Fig. 19). The plasma temperature derived from the broadening of plasma temperature spectra was about 8 keV, in excellent agreement with the results of time-of-flight measurements in experiments with deuterium ions. Thus, studies [104, 105] demonstrated the possibility of obtaining a rather high neutron output in synthetic reactions induced by the interaction of femtosecond laser pulses with deuterium clusters.

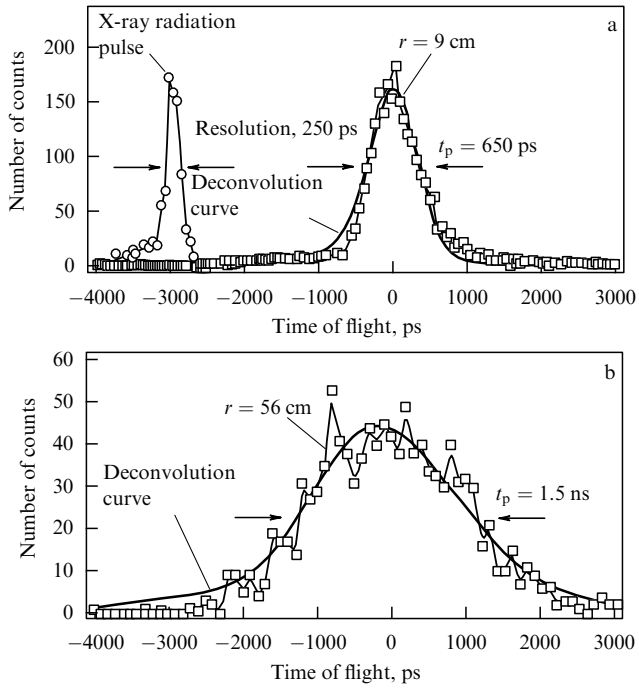

Figure 19. (a) The measured width of a neutron pulse at the distance $r = 9$ cm from the target. The estimated width is $t_p = 650$ ps. The response of the detector shown on the left-hand side of the figure is deduced from the measurement of a hard X-ray radiation pulse from the target. (b) The measured width of a neutron pulse t_p at the distance $r = 56$ cm from the target. The pulse width is $t_p = 1.5$ ns. The detector time resolution is 1.1. ns [106].

We emphasize that the generation of neutrons by strong ultrashort laser pulses has recently attracted the close attention of researchers (see, e.g., [57, 104 – 111] and the reference therein). There is every reason to believe that the combined use of cluster beams and intense ultrashort laser pulses will be instrumental in creating compact sources of X-ray radiation and neutrons.

7.4 Characteristics of cluster excitation by vacuum ultraviolet radiation

7.4.1. Results of observations. Studies on cluster excitation by UV radiation of free electron lasers (FELs) have recently been initiated [504 – 509]. Two large-scale FEL projects are currently being implemented based on particle accelerators at Stanford, USA, and near Hamburg, Germany. The FEL of the latter facility was used to excite clusters in the far UV spectral region. These results are discussed below.

The first experiments were performed in [504] to study interactions between intense FEL radiation (wavelength $\lambda = 98$ nm) and atoms or clusters of xenon chosen because they can be ionized by individual photons with the energy 12.7 eV at the given wavelength (the ionization energy of xenon atoms is 12.1 eV [371]). The atoms and clusters were irradiated by laser pulses with the duration about 100 fs at the power density up to 7×10^{13} W cm^{-2}. The ions being formed were detected with a time-of-flight mass spectrometer.

Very broad ion mass peaks were recorded in these experiments (Fig. 20), suggesting a high kinetic energy of the ions, attributable to Coulomb explosions of clusters. Both the

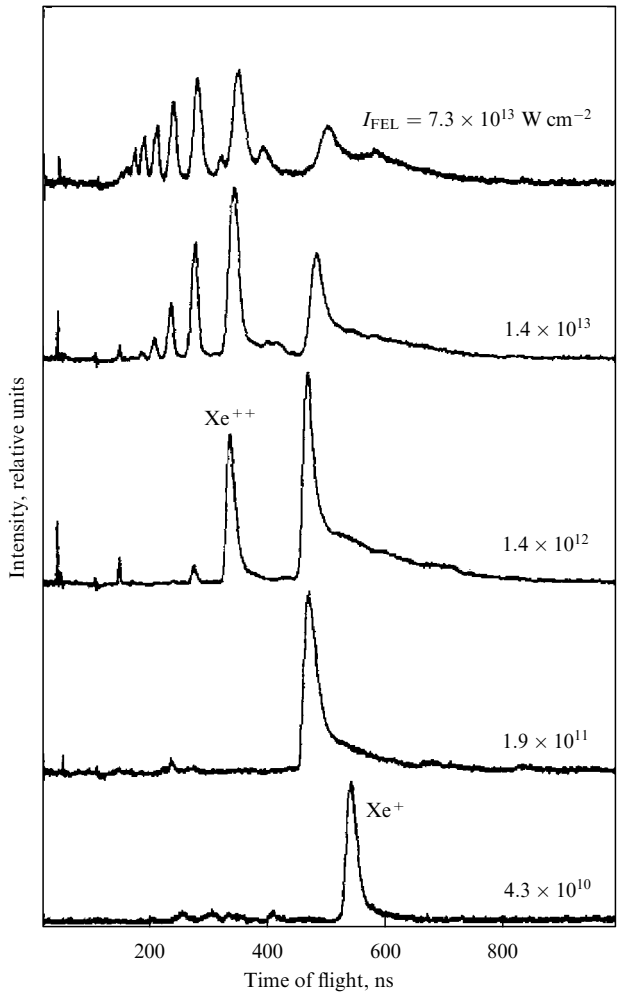

Figure 20. Time-of-flight mass spectra of Xe clusters ($N = 1500$) after their laser UV irradiation by a free electron laser at the wavelength 98 nm and varying laser power density [504].

number of differently charged ions and their kinetic energy strongly depend on the power density of the exciting radiation, as is well apparent from Fig. 20, showing the mass spectra of the ions after excitation of xenon clusters of 1500 molecules. At the highest power density used in the experiment (7×10^{13} W cm^{-2}), ions with the charge up to +8 are detected. The intensity of ion peaks corresponding to multicharged ions sharply decreases with decreasing the power density of exciting radiation. For example, only monocharged Xe^{+} ions with a rather high kinetic energy can be seen at 2×10^{11} W cm^{-2}.

The strong dependence of the signals on the power density of the exciting radiation unequivocally suggests the prevalence of nonlinear optical processes at the power levels used in the experiments. The average charge increases from 1 to approximately 2.5 as the power density increases from 2×10^{11} W cm^{-2} to 7×10^{13} W cm^{-2}. This means that each atom in a cluster of 1500 xenon atoms loses 2 – 3 electrons on the average at the highest power density.

The mean kinetic energy of ions estimated from time-of-flight measurements (see Fig. 20) strongly depends on the cluster size and charge. Xe^{7+} ions have a kinetic energy in excess of 2 keV. In small clusters, it increases with increasing the charge. Such a behavior confirms disintegration of clusters as a result of Coulomb explosion [510]. The data in Fig. 20 allow concluding that the energy of a few hundred electronvolts is absorbed from the laser pulse field.

The effects in clusters associated with their excitation by a shortwave UV radiation [504] are surprising because the Coulomb explosions first occur at the power density 10^{11} W cm^{-2}, which is much smaller than the power necessary for a Coulomb explosion in the IR region. Moreover, the frequency of the exciting radiation is so high that the direct effect of the laser field on electron motion is negligibly small [511]. The experiments being discussed revealed that field-induced ionization prevailing in the overall process of cluster ionization by IR radiation does not substantially contribute to FEL radiation at the wavelength 98 nm, nor does the electron motion induced by the electric field play a key role in these experiments. Therefore, there must be no direct laser-induced ejection of electrons from the clusters. Hence, additional processes and mechanisms of cluster ionization should be taken into consideration to explain absorption, ionization, and the dynamics of cluster explosion under the effect of IR radiation from FEL.

7.4.2. Interpretation of results. The authors of [504] describe cluster ionization as a two-stage process in analogy with the cluster ionization by IR radiation [512, 513]. At the first stage, atoms inside clusters lose electrons (at least one electron each), which thereafter travel freely inside the clusters (internal ionization). At the second stage, these electrons move away from the clusters to infinity (external ionization). Internal ionization is easy to explain, bearing in mind that the energy of FEL photons exceeds the ionization energy of Xe atoms. It appears that valence electrons in the clusters are transferred into excited states (conductivity band). At the power density in excess of 10^{13} W cm^{-2}, this process occurs within the first several femtoseconds after the onset of the FEL pulse impact due to a very large absorption cross section (30 – 50 Mbarn) [514].

To better understand the radiation absorption processes and mechanisms of cluster ionization, the authors of [504] calculated electron motions in Xe_{13} and Xe_{55} clusters accounting for both the forces acting on electrons from ions and cluster electrons and the laser pulse field. It turned out that clusters emit electrons isotropically at the wavelength 98 nm and the power density 10^{14} W cm^{-2} or 10^{16} W cm^{-2}. In contrast, most of them are emitted in the direction of polarization of the pulse field under typical conditions of experiments using optical-range lasers (800 nm, 10^{16} W cm^{-2}). This observation confirms the field-induced ionization of clusters in the second situation. A similar result was obtained in [506] (Fig. 21). The isotropic emission of electrons from a cluster excited by an FEL at 98 nm provides a strong argument in favor of the absence of field-induced ionization. The authors of [504, 506] conclude that electrons undergo multiple scattering inside the cluster and thereby strongly heat it prior to escape.

It was hypothesized in [504] that multicharged ions arise on the cluster surface due to field-induced ionization in the strong Coulomb field of ions contained inside the cluster [515, 516]. The electric field at the surface of a large high-charge cluster is usually 10 – 50 V Å^{-1}, i.e., almost 20 times as strong as the FEL pulse field at the power density 10^{14} W cm^{-2}. A field of some 30 V Å^{-1} is sufficient for Xe^{8+} ions to form [517]. These observations explain the formation of multicharged ions in clusters excited by UV radiation from an FEL (see also [506 – 509]).

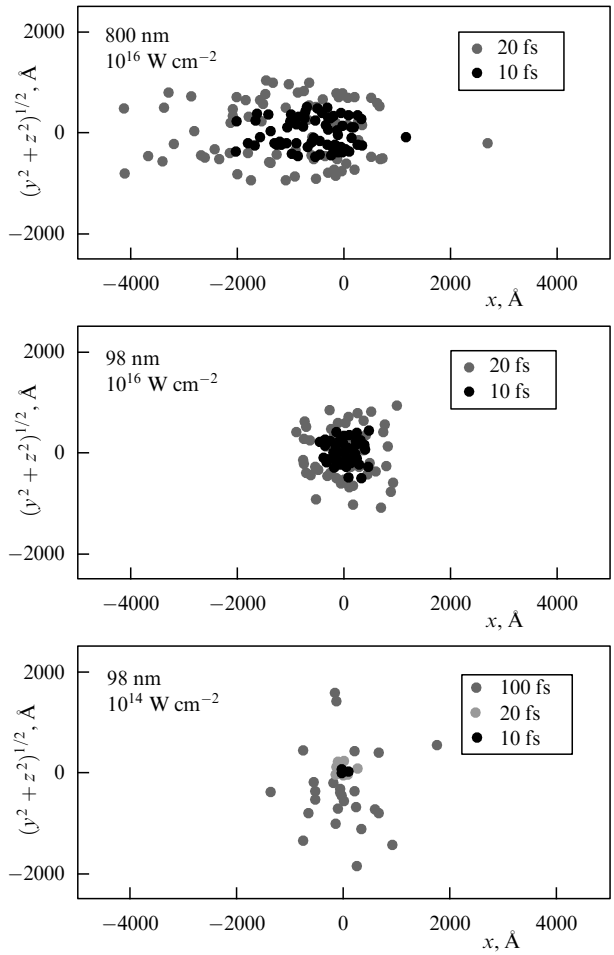

Figure 21. Calculated electron motions and Xe_{13} cluster ionization after IR and soft X-ray irradiation. The trajectories of electrons are computed for 100-fs-long pulses of equal energy at the two irradiation modalities. Positions of electrons are shown at 10, 20, and 100 fs after the onset of laser radiation, whose polarization is parallel to the x axis [506].

Later studies demonstrated the Boltzmann energy distribution of electrons emitted by clusters. The mean temperature of electrons emitted under the effect of UV radiation was only 30 – 40 eV compared to 1 – 10 keV in electrons for IR radiation with the wavelength 800 nm. These data suggest different mechanisms of cluster ionization by IR and UV radiation and confirm that the UV radiation of FELs is a highly efficient tool for cluster excitation.

8. Conclusion

The results of the reviewed studies indicate that the cluster internal temperature is an important characteristic determining many cluster properties, including polarizability, magnetic moment, ionization potential, optical response, structure, configuration, and phasic state. Cluster temperature has a marked effect on physicochemical processes and phenomena involving clusters and cluster beams, such as fragmentation (evaporation) and chemical reaction rates, fragmentation channels, energy relaxation rates, and channels.

There is a variety of methods allowing the cluster temperature to be determined with a rather high degree of accuracy: recording electron diffraction and equilibrium radiation, vibrational – rotational spectroscopy of intracluster molecules, evaporative cooling, measurements of the kinetic energy of fragments resulting from cluster degradation, energy transfer in cluster – atom collisions, and the recoil energy of cluster – surface collisions.

The available methods of cluster excitation (laser excitation, electron impact, cluster heating in a buffer gas discharge, collision of high-energy clusters and cluster ions with a solid surface or between themselves in crossed beams, interaction of clusters with superstrong ultrashort laser pulses) are employed to obtain clusters with very high internal temperatures (up to $10^3 - 10^8$ K). On the other hand, low-temperature clusters of noble gases and molecular clusters (with the temperature $10^{-3} - 10^2$ K) can be produced in nozzle sources and with the use of evaporative stabilization.

It was shown that the upper limiting temperature of large van der Waals clusters from nozzle sources achieved during evaporative stabilization depends on the binding energy of atoms (molecules) inside the clusters. At the same time, nozzle sources in which a carrier gas with a low binding energy is used produce clusters having a significantly lower temperature than that depending on the binding energy.

Fragmentation, emission of charge particles (electrons and ions), and emission in the visible and infrared spectral regions are the main energy relaxation channels in strongly heated clusters. Fragmentation and the emission of electrons greatly contribute to the first stage of cluster cooling, whereas its final stage largely depends on the emission of radiation.

Strong heating of clusters and cluster ions colliding with a surface initiate a variety of extreme processes both in themselves and in the collision zone (emission of light and charged particles, fragmentation, the breakage and formation of chemical bonds, nuclear synthesis, surface bombardment) that do not occur in thermal equilibrium. These processes develop due to strong cluster heating upon their collisions with a surface, which generates a microshock wave both inside the clusters and in the collision zone within a very short time ($\leqslant 1$ ps). Interactions between cluster beams and surfaces may be used to obtain thin films, synthesize new nanostructural materials, and treat their surfaces. As shown in the reviewed publications (see also [70] and the references therein), a major component in many of these processes is the collision energy, a large fraction of which is converted to the cluster internal energy (temperature) during an act of collision.

The excitation of clusters by superstrong ultrashort laser pulses results in a substantial heating of their electron and ion subsystems (to 1 – 100 keV), a Coulomb or hydrodynamic explosion, and the generation of X-ray radiation and neutrons. The available data (see also [70]) indicate that excitations of clusters by ultrashort laser pulses and by collisions with a surface at high velocities ($v \sim 10^6 - 10^7$ cm s^{-1}) have much in common. Specifically, energy inputs, excitation rates ($\sim 10^{13} - 10^{14}$ s^{-1}), and cluster lifetimes relative to the degradation time ($\sim 10^{-13}$ s) are comparable. In either case, clusters emit light and charged particles (electrons and ions), undergo fragmentation, with excitation accompanied by excitation, and give rise to nuclear synthesis and the generation of neutrons. It appears, however, that laser excitation permits realizing greater specific energy inputs per particle [57] and yields larger amounts of denser cluster plasma. For this reason, the excitation of clusters by laser pulses is the method of choice for the production of high-temperature plasma and generation of X-ray radiation and the neutrons.

Experiments on resonance excitation of clusters containing intercalated molecules by strong ultrashort IR laser pulses are important for the investigation of their interaction with intense laser radiation. This inference refers first and foremost to clusters with a low binding energy, such as superfluid helium clusters. Chromophors located in the center of such clusters are efficacious sorbents of laser radiation. Rapid energy acquisition by a cluster due to its absorption by the chromophor and fast relaxation of the vibrational excitation energy may cause strong heating and 'instantaneous' fragmentation (explosion) of the cluster. Small clusters ($N \leqslant 10^3$) may totally disintegrate, giving rise to 'stripped' molecules in the beam. This fact can be used to study the thermal (hydrodynamic) explosion of laser-excited clusters. Selective laser excitation of clusters in a beam permits separating intercalated molecules of different isotopic (component) compositions [72, 385 – 387].

The author thanks V N Lokhman and A N Petin for assistance in drawing figures, A N Makarova and E A Nikolaeva for their help in picking up literature sources. The valuable remarks of the referee are thankfully acknowledged. The work was partly supported by the Russian Foundation for Basic Research (grants No. 06-02-16634 and No. 07-02-00165).

References

1. Pauly H *Atom, Molecule, and Cluster Beams* Vol. 2 *Cluster Beams, Fast and Slow Beams, Accessory Equipment, and Applications* (Springer Ser. on Atomic, Optical, and Plasma Phys., Vol. 32) (Berlin: Springer, 2000)
2. Scoles G (Ed.) *Atomic and Molecular Beam Methods* Vol. 1 (New York: Oxford Univ. Press, 1988)
3. Scoles G (Ed.) *Atomic and Molecular Beam Methods* Vol. 2 (New York: Oxford Univ. Press, 1992)
4. Jena P, Khanna S N, Rao B K (Eds) *Physics and Chemistry of Finite Systems: From Clusters to Crystals* (NATO ASI Series. Ser. C, Vol. 374) (Dordrecht: Kluwer Acad. Publ., 1992)
5. Jortner J, Pullman A, Pullman B (Eds) *Large Finite Systems* (The Jerusalem Symp. on Quantum Chemistry and Biochemistry, Vol. 20) (Dordrecht: D. Reidel, 1987)
6. Sugano S, Nishina Y, Ohnishi S (Eds) *Microclusters* (Springer Ser. in Materials Science, Vol. 4) (Berlin: Springer-Verlag, 1987)
7. Takagi T *Ionized-Cluster Beam Deposition and Epitaxy* (Park Ridge, NJ: Noyes Publ., 1988)
8. Benedek G, Martin T P, Pacchioni G (Eds) *Elemental and Molecular Clusters* (Springer Ser. in Materials Science, Vol. 6) (Berlin: Springer-Verlag, 1988)
9. Aleksandrov M L, Kusner Yu S *Gazodinamicheskie Molekulyarnye, Ionnye i Klastirovannye Puchki* (Executive Ed. E P Velikhov) (Gas-Dynamic Molecular, Ionic and Cluster Beams) (Leningrad: Nauka, 1989)
10. Bernstein E R (Ed.) *Atomic and Molecular Clusters* (Studies in Physical and Theoretical Chemistry, Vol. 68) (Amsterdam: Elsevier, 1990)
11. Billups W E, Giufolini M A (Eds) *Buckminsterfullerenes* (New York: VCH, 1993)
12. Haberland H (Ed.) *Clusters of Atoms and Molecules: Theory, Experiment, and Clysters of Atoms* (Springer Series in Chemical Physics, Vol. 52) (Heidelberg: Springer-Verlag, 1994)
13. Klabunde K J *Free Atoms, Clusters, and Nanoscale Particles* (San Diego: Academic Press, 1994)
14. Kondow T, Kaya K, Terasaki A (Eds) *Structure and Dynamics of Clusters* (Frontiers Science Ser., Vol. 16) (Tokyo: Univ. Acad. Press, 1996)
15. Martin T P (Ed.) *Large Clusters of Atoms and Molecules* (NATO ASI Series, Ser. E, Vol. 313) (Dordrecht: Kluwer Acad., 1996)
16. Yoshimura S, Chang R P H *Supercarbon: Synthesis, Properties, and Applications* (Springer Ser. in Materials Science, Vol. 33) (Heidelberg: Springer-Verlag, 1998)
17. Hirsch A *Fullerenes and Related Structures* (Topics in Current Chemistry, Vol. 199) (Heidelberg: Springer-Verlag, 1998)
18. Smirnov B M *Clusters and Small Particles: in Gases and Plasmas* (New York: Springer, 2000)
19. Campargue R (Ed.) *Atomic and Molecular Beams: The State of the Art 2000* (Berlin: Springer, 2001)
20. Lakhno V D *Klastery v Fizike, Khimii, Biologii* (Clusters in Physics, Chemistry, Biology) (Izhevsk: RKhD, 2001)
21. Havenith-Newen M *Infrared Spectroscopy of Molecular Cluster: An Introduction to Intermolecular Forces* (Berlin: Springer, 2002)
22. Hagena O F "Cluster beams from nozzle sources", in *Molecular Beams and Low Density Gasdynamics* (Gasdynamics, Vol. 4, Ed. P P Wegener) (New York: M. Dekker, 1974)
23. Becker E W *Z. Phys. D* **3** 101 (1986)
24. Hagena O F *Z. Phys. D* **4** 291 (1987)
25. Miller D E "Free jet sources", in *Atomic and Molecular Beam Methods* Vol. 1 (Ed. G Scoles) (New York: Oxford Univ. Press, 1988) p. 14
26. Kappes M, Leutwyler S "Molecular beams of clusters", in *Atomic and Molecular Beam Methods* Vol. 1 (Ed. G Scoles) (New York: Oxford Univ. Press, 1988) p. 380
27. Huisken F *Adv. Chem. Phys.* **81** 63 (1992)
28. Smirnov B M *Usp. Fiz. Nauk* **162** (1) 119 (1992) [*Sov. Phys. Usp.* **35** 37 (1992)]
29. Miller R E "Infrared laser spectroscopy", in *Atomic and Molecular Beam Methods* Vol. 2 (Ed. G Scoles) (New York: Oxford Univ. Press, 1992) p. 192
30. de Heer W A *Rev. Mod. Phys.* **65** 611 (1993)
31. Eletskii A V, Smirnov B M *Usp. Fiz. Nauk* **163** (2) 33 (1993) [*Phys. Usp.* **36** 202 (1993)]
32. Buck U *J. Phys. Chem.* **98** 5190 (1994)
33. Buck U, in *Advances in Atomic, Molecular, and Optical Physics* Vol. 35 (Eds B Bederson, H Walther) (Amsterdam: Elsevier, 1995) p. 121
34. Eletskii A V, Smirnov B M *Usp. Fiz. Nauk* **165** 997 (1995) [*Phys. Usp.* **38** 935 (1995)]
35. Alivisatos A P *J. Phys. Chem.* **100** 13226 (1996)
36. Bacic Z, Miller R E *J. Phys. Chem.* **100** 12945 (1996)
37. Castleman A W (Jr), Bowen K H (Jr) *J. Phys. Chem.* **100** 12911 (1996)
38. Gspann J, in *Large Clusters of Atoms and Molecules* (NATO ASI Series, Ser. E, Vol. 313, Ed. T P Martin) (Dordrecht: Kluwer Acad., 1996)
39. Kohler B et al. *Adv. Chem. Phys.* **101** 83 (1997)
40. Eletskii A V *Usp. Fiz. Nauk* **167** 945 (1997) [*Phys. Usp.* **40** 899 (1997)]
41. Smirnov B M *Usp. Fiz. Nauk* **167** 1169 (1997) [*Phys. Usp.* **40** 1117 (1997)]
42. Valbusa U "Molecular beams in high-energy physics: beam targets", in *Atomic and Molecular Beam Methods* Vol. 1 (Ed. G Scoles) (New York: Oxford Univ. Press, 1988) p. 438
43. Christen W, Even U *J. Phys. Chem. A* **102** 9420 (1998)
44. Herschbach D *Rev. Mod. Phys.* **71** S411 (1999)
45. Smalley R E *Usp. Fiz. Nauk* **168** 323 (1998); *Rev. Mod. Phys.* **69** 723 (1997)
46. Curl R F *Usp. Fiz. Nauk* **168** 331 (1998); *Rev. Mod. Phys.* **69** 691 (1997)
47. Kroto H *Usp. Fiz. Nauk* **168** 343 (1998); *Rev. Mod. Phys.* **69** 703 (1997)]
48. Lifshitz C *Int. J. Mass Spectrom.* **200** 423 (2000)
49. Eletskii A V *Usp. Fiz. Nauk* **170** 113 (2000) [*Phys. Usp.* **43** 111 (2000)]
50. Rakov E G *Usp. Khim.* **69** 41 (2000) [*Russ. Chem. Rev.* **69** 35 (2000)]
51. Smirnov B M *Usp. Fiz. Nauk* **170** 495 (2000) [*Phys. Usp.* **43** 453 (2000)]
52. Krainov V P, Smirnov M B *Usp. Fiz. Nauk* **170** 696 (2000) [*Phys. Usp.* **43** 901 (2000)]
53. Krainov V P, Smirnov M B *Phys. Rep.* **370** 237 (2002)
54. Smirnov B M *Usp. Fiz. Nauk* **173** 609 (2003) [*Phys. Usp.* **46** 589 (2003)]
55. Ditmire T et al. *Phys. Rev. A* **53** 3379 (1996)
56. Ditmire T et al. *Phys. Rev. A* **57** 369 (1998)
57. Zweiback J et al. *Phys. Plasmas* **9** 3108 (2002)
58. Eletskii A V *Usp. Fiz. Nauk* **174** 1191 (2004) [*Phys. Usp.* **47** 1119 (2004)]

59. Kwon Y et al. *J. Chem. Phys.* **113** 6469 (2000)
60. Northby J A *J. Chem. Phys.* **115** 10065 (2001)
61. Callegari C et al. *J. Chem. Phys.* **115** 10090 (2001)
62. Stienkemeier F, Vilesov A F *J. Chem. Phys.* **115** 10119 (2001)
63. Toennies J P, Vilesov A F, Whaley K B *Phys. Today* **54** (2) 31 (2001)
64. Dalfovo F, Stringari S *J. Chem. Phys.* **115** 10078 (2001)
65. Dalfovo F et al. *Rev. Mod. Phys.* **71** 463 (1999)
66. Lugovoj E et al. "Spectroscopy of single molecules and clusters inside superfluid helium droplets", in *Atomic and Molecular Beams: The State of the Art 2000* (Ed. R Campargue) (Berlin: Springer, 2001) p.755
67. Makarov G N *Usp. Fiz. Nauk* **174** 225 (2004) [*Phys. Usp.* **47** 217 (2004)]
68. Yamada I, Toyoda N *Nucl. Instrum. Meth. Phys. Res. B* **232** 195 (2005)
69. Berry R S, Smirnov B M *Usp. Fiz. Nauk* **175** 367 (2005) [*Phys. Usp.* **48** 345 (2005)]
70. Makarov G N *Usp. Fiz. Nauk* **176** 121 (2006) [*Phys. Usp.* **49** 117 (2006)]
71. Dumesh B S, Surin L A *Usp. Fiz. Nauk* **176** 1137 (2006) [*Phys. Usp.* **49** 1113 (2006)]
72. Makarov G N *Usp. Fiz. Nauk* **176** 1155 (2006) [*Phys. Usp.* **49** 1131 (2006)]
73. Eletskii A V *Usp. Fiz. Nauk* **177** 233 (2007) [*Phys. Usp.* **50** 225 (2007)]
74. Kapitza P L *Zh. Eksp. Teor. Fiz.* **11** 1, 581 (1941)
75. Pi M, Mayol R, Barranco M *Phys. Rev. Lett.* **82** 3093 (1999)
76. Pörtner N, Toennies J P, Vilesov A F *J. Chem. Phys.* **117** 6054 (2002)
77. Chin S A, Krotscheck E *Phys. Rev. B* **52** 10405 (1995)
78. Sindzingre P, Klein M L, Ceperley D M *Phys Rev. Lett.* **63** 1601 (1989)
79. Casas M et al. *Z. Phys. D* **35** 67 (1995)
80. Rama Krishna M V, Whaley K B *J. Chem. Phys.* **93** 746 (1990)
81. Rubahn H-G *Nanophysik und Nanotechnologie* (Stuttgart: Teubner Verlag, 2002)
82. Fahrner W *Nanotechnologie und Nanoprozesse* (Berlin: Springer, 2003)
83. Edelstein A S, Cammarata R C (Eds) *Nanomaterials: Synthesis, Properties, and Applications* (Bristol: Institute of Physics Publ., 1996)
84. Barnett R N, Landman U *Nature* **387** 788 (1997)
85. Ditmire T et al. *Nature* **386** 54 (1997)
86. Last I, Jortner J *J. Phys. Chem. A* **102** 9655 (1998)
87. Springate E et al. *Phys. Rev. A* **61** 044101 (2000)
88. Auguste T et al. *J. Quant. Spectrosc. Radiat. Transf.* **71** 147 (2001)
89. Skobelev I Yu et al. *Zh. Eksp. Teor. Fiz.* **121** 88 (2002) [*JETP* **94** 73 (2002)]
90. Maltsev A, Ditmire T *Phys. Rev. Lett.* **90** 053002 (2003)
91. Parra E et al. *J. Opt. Soc. Am. B* **20** 118 (2003)
92. McPherson A et al. *Nature* **370** 631 (1994)
93. Dobosz S et al. *Phys. Rev. A* **56** R2526 (1997)
94. Ditmire T et al. *Appl. Phys. Lett.* **71** 166 (1997)
95. Stenz C et al. *Kvantovaya Elektron.* **30** 721 (2000) [*Quantum Electron.* **30** 721 (2000)]
96. Junkel-Vives G C et al. *J. Quant. Spectrosc. Radiat. Transf.* **71** 417 (2001)
97. Skobelev I Yu et al. *Zh. Eksp. Teor. Fiz.* **121** 1124 (2002) [*JETP* **94** 1063 (2002)]
98. Magunov A I et al. *Laser Part. Beams* **21** 73 (2003)
99. Fukuda Y et al. *Pis'ma Zh. Eksp. Teor. Fiz.* **78** 146 (2003) [*JETP Lett.* **78** 115 (2003)]
100. Fukuda Y et al. *Laser Part. Beams* **22** 215 (2004)
101. Ivanova E P, Ivanov A L *Zh. Eksp. Teor. Fiz.* **127** 957 (2005) [*JETP* **100** 844 (2005)]
102. Kim K Y et al. *Phys. Rev. E* **73** 066403 (2006)
103. Smirnov M B, Becker W *Phys. Rev. A* **74** 013201 (2006)
104. Ditmire T et al. *Nature* **398** 489 (1999)
105. Zweiback J et al. *Phys. Rev. Lett.* **84** 2634 (2000)
106. Zweiback J et al. *Phys. Rev. Lett.* **85** 3640 (2000)
107. Last I, Jortner J *J. Phys. Chem. A* **106** 10877 (2002)
108. Madison K W et al. *J. Opt. Soc. Am. B* **20** 113 (2003)
109. Madison K W et al. *Phys. Plasmas* **11** 270 (2004)
110. Madison K W et al. *Phys. Rev. A* **70** 053201 (2004)
111. Buersgens F et al. *Phys. Rev. E* **74** 016403 (2006)
112. Campbell E E B et al. *Phys. Rev. Lett.* **70** 263 (1993)
113. Schulte J et al. *Phys. Lett. A* **198** 51 (1995)
114. Schmidt R, Seifert G, Lutz H O *Phys. Lett. A* **158** 231 (1991)
115. Seifert G, Schmidt R, Lutz H O *Phys. Lett. A* **158** 237 (1991)
116. Farizon B, Farizon M, Gaillard M J *Int. J. Mass Spectrom.* **192** 259 (1999)
117. Campbell E E B et al. *C. R. Physique* **3** 341 (2002)
118. Smirnov B M *Pis'ma Zh. Eksp. Teor. Fiz.* **81** 8 (2005) [*JETP Lett.* **81** 6 (2005)]
119. Beuhler R J, Friedlander G, Friedman L *Phys. Rev. Lett.* **63** 1292 (1989)
120. Leonas V B *Usp. Fiz. Nauk* **160** (11) 135 (1990) [*Sov. Phys. Usp.* **33** 956 (1990)]
121. Beuhler R J et al. *J. Phys. Chem.* **94** 7665 (1990)
122. Vandenbosch R et al. *Nucl. Instrum. Meth. Phys. Res. B* **88** 116 (1994)
123. Fallavier M et al. *Phys. Rev. Lett.* **70** 1022 (1993)
124. Fallavier M et al. *Nucl. Instrum. Meth. Phys. Res. B* **88** 122 (1994)
125. Shapiro M H, Tombrello T A *Phys. Rev. Lett.* **65** 92 (1990)
126. Fortov V E et al. *Int. J. Impact Eng.* **17** 323 (1995)
127. John P M St, Beck R D, Whetten R L *Phys. Rev. Lett.* **69** 1467 (1992)
128. Beauregard J N, Mayne H R *Surf. Sci. Lett.* **280** L253 (1993)
129. Beauregard J N, Mayne H R *J. Chem. Phys.* **99** 6667 (1993)
130. Mair C et al. *J. Chem. Phys.* **111** 2770 (1999)
131. Christen W, Even U *Eur. Phys. J. D* **9** 29 (1999)
132. Yasumatsu H et al. *J. Chem. Phys.* **105** 9509 (1996)
133. Yasumatsu H, Terasaki A, Kondow T *J. Chem. Phys.* **106** 3806 (1997)
134. Yasumatsu H et al. *Surf. Rev. Lett.* **3** 901 (1996)
135. Schek I et al. *Chem. Phys. Lett.* **257** 273 (1996)
136. Schek et al. *J. Chem. Phys.* **101** 8596 (1994)
137. Raz T et al. *J. Chem. Phys.* **101** 8606 (1994)
138. Raz T, Levine R D *Chem. Phys. Lett.* **226** 47 (1994)
139. Raz T, Levine R D *J. Am. Chem. Soc.* **116** 11167 (1994)
140. Raz T, Levine R D *J. Phys. Chem.* **99** 13713 (1995)
141. Raz T, Levine R D *J. Phys. Chem.* **99** 7495 (1995)
142. Raz T, Levine R D *Chem. Phys. Lett.* **246** 405 (1995)
143. Gupta M, Walters E A, Blais N C *J. Chem. Phys.* **104** 100 (1996)
144. Qi L, Sinnott S B *J. Phys. Chem. B* **101** 6883 (1997)
145. Kornweitz H, Raz T, Levine R D *J. Phys. Chem. A* **103** 10179 (1999)
146. Nguyen T-N V et al. *J. Chem. Phys.* **119** 7451 (2003)
147. Yamada I, Usui H, Takagi T *J. Phys. Chem.* **91** 2463 (1987)
148. Takagi T *Pure Appl. Chem.* **60** 781 (1988)
149. Sosnowski M, Yamada I *Nucl. Instrum. Meth. Phys. Res. B* **46** 397 (1990)
150. Huq S E, McMahon R A, Ahmed H *Semicond. Sci. Technol.* **5** 771 (1990)
151. Takaoka G H, Ishikawa J, Takagi T *J. Vac. Sci. Technol. A* **8** 840 (1990)
152. Yamada I, Takaoka G H *Jpn. J. Appl. Phys.* **32** 2121 (1993)
153. Cleveland C L, Landman U *Science* **257** 355 (1992)
154. Haberland H, Insepov Z, Moseler M *Phys. Rev. B* **51** 11061 (1995)
155. Kraft J et al. *Surf. Coat. Technol.* **158–159** 131 (2002)
156. Haberland H et al. *Suf. Rev. Lett.* **3** (1) 887 (1996)
157. Haberland H et al. *Nucl. Instrum. Meth. Phys. Res. B* **80–81** 1320 (1993)
158. Haberland H et al. *J. Vac. Sci. Technol. A* **12** 2925 (1994)
159. Cheng H-P, Landman U *J. Phys. Chem.* **98** 3527 (1994)
160. Bromann K et al. *Surf. Sci.* **377–379** 1051 (1997)
161. Palmer R E, Pratontep S, Boyen H-G *Nature Mater.* **2** 443 (2003)
162. Fuchs G et al. *Phys. Rev. B* **44** 3926 (1991)
163. Mélinon P et al. *Int. J. Mod. Phys. B* **9** 339 (1995)
164. Perez A et al. *J. Phys. D: Appl. Phys.* **30** 709 (1997)
165. Mélinon P et al. *Phys. Rev. B* **58** 16481 (1998)
166. Mélinon P et al. *C. R. Physique* **3** 273 (2002)
167. Mélinon P et al. *J. Chem. Phys.* **107** 10278 (1997)
168. Perez A et al. *Mater. Trans.* **42** 1460 (2001)
169. Gaudry M et al. *Phys. Rev. B* **67** 155409 (2003)
170. Khanna S N, Jena P *Phys. Rev. Lett.* **69** 1664 (1992)
171. de Heer W A, Milani P, Châtelain A *Phys. Rev. Lett.* **65** 488 (1990)
172. Khanna S N, Linderoth S *Phys. Rev. Lett.* **67** 742 (1991)
173. Palpant B *Phys. Rev. B* **57** 1963 (1998)
174. Harbich W, Fedrigo S, Buttet J *Chem. Phys. Lett.* **195** 613 (1992)

175. Harbich W, Fedrigo S, Buttet J *J. Chem. Phys.* **96** 8104 (1992)
176. Jena P, Khanna S N, Rao B K *Surf. Rev. Lett.* **3** 993 (1996)
177. Rao B K, Khanna S N, Jena P *J. Cluster Sci.* **10** 477 (1999)
178. Haberland H et al. *J. Vac. Sci. Technol. A* **10** 3266 (1992)
179. Orloff J *Rev. Sci. Instrum.* **64** 1105 (1993)
180. Gspann J *Z. Phys. D* **20** 421 (1991)
181. Henkes P R W, Klingelhöfer R *Vacuum* **39** 541 (1989)
182. Gspann J *Microelectron. Eng.* **27** 517 (1995)
183. von Blanckenhagen P, Gruber A, Gspann J *Nucl. Instrum. Meth. Phys. Res. B* **122** 322 (1997)
184. Gruber A, Gspann J *J. Vac. Sci. Technol. B* **15** 2362 (1997)
185. Gruber A, Gspann J, Hoffmann H *Appl. Phys. A* **68** 197 (1999)
186. Rattunde O et al. *J. Appl. Phys.* **90** 3226 (2001)
187. Bromann K et al. *Science* **274** 956 (1996)
188. Akizuki M et al. *Surf. Rev. Lett.* **3** 891 (1996)
189. Qiang Y et al. *Surf. Coat. Technol.* **100 – 101** 27 (1998)
190. Yamaguchi Y, Gspann J *Eur. Phys. J. D* **16** 103 (2001)
191. Yamaguchi Y, Gspann J, Inaba T *Eur. Phys. J. D* **24** 315 (2003)
192. Yamada I, Matsuo J, Toyoda N *Nucl. Instrum. Meth. Phys. Res. B* **206** 820 (2003)
193. Insepov Z et al. *Nucl. Instrum. Meth. Phys. Res. B* **206** 846 (2003)
194. Xirouchaki C *Vacuum* **73** 123 (2004)
195. Aoki T, Matsuo J *Nucl. Instrum. Meth. Phys. Res. B* **255** 265 (2007)
196. Zimmermann S, Urbassek H M *Nucl. Instrum. Meth. Phys. Res. B* **255** 208 (2007)
197. Grisenti R E et al. *Phys. Rev. Lett.* **85** 2284 (2000)
198. Mandrich M L, Reents W D (Jr), Bondebey V E, in *Atomic and Molecular Clusters* (Ed. E R Bernstein) (Amsterdam: Elsevier, 1990)
199. Haberland H, in *Clusters of Atoms and Molecules: Theory, Experiment, and Clusters of Atoms* (Ed. H Haberland) (Heidelberg: Springer-Verlag, 1994)
200. Pauly H "High-Energy Beam Sources", in *Atomic and Molecular Beam Methods* Vol. 1 (Ed. G Scoles) (New York: Oxford Univ. Press, 1988) p. 124
201. Landau L D, Lifshitz E M *Statisticheskaya Fizika* Ch. 1 (Statistical Physics) (Moscow: Nauka, 1976) [Translated into English (Oxford: Pergamon Press, 1980)]
202. Vekhter B et al. *J. Chem. Phys.* **106** 4644 (1997)
203. Berry R S, Smirnov B M *Zh. Eksp. Teor. Fiz.* **125** 414 (2004) [*JETP* **98** 366 (2004)]
204. Bixon M, Jortner J *J. Chem. Phys.* **91** 1631 (1989)
205. Labastie P, Whetten R L *Phys. Rev. Lett.* **65** 1567 (1990)
206. Wales D J *Mol. Phys.* **78** 151 (1993)
207. Wales D J, Berry R S *Phys. Rev. Lett.* **73** 2875 (1994)
208. Umirzakov I H *Phys. Rev. E* **60** 7550 (1999)
209. Schmidt M et al. *Phys. Rev. Lett.* **86** 1191 (2001)
210. Gobet F et al. *Phys. Rev. Lett.* **89** 183403 (2002)
211. Reyes-Nava J A, Garzón I L, Michaelian K *Phys. Rev. B* **67** 165401 (2003)
212. Harms J et al. *J. Mol. Spectrosc.* **185** 204 (1996)
213. Brink D M, Stringari S *Z. Phys. D* **15** 257 (1990)
214. Vostrikov A A, Dubov D Yu, Agarkov A A *Pis'ma Zh. Eksp. Teor. Fiz.* **63** 915 (1996) [*JETP Lett.* **63** 963 (1996)]
215. Agarkov A A et al. *Eur. Phys J. D* **9** 331 (1999)
216. Vostrikov A A, Agarkov A A, Dubov D Yu *Zh. Tekh. Fiz.* **70** (7) 102 (2000) [*Tech. Phys.* **45** 915 (2000)]
217. Vostrikov A A, Dubov D Yu, Agarkov A A *Teplofiz. Vys. Temp.* **39** 26 (2001) [*High Temp.* **39** 22 (2001)]
218. Foltin M et al. *J. Chem. Phys.* **98** 9624 (1993)
219. Wan Z et al. *J. Chem. Phys.* **99** 5858 (1993)
220. Rohlfing E A *J. Chem. Phys.* **89** 6103 (1988)
221. Mitzner R, Campbell E E B *J. Chem. Phys.* **103** 2445 (1995)
222. Heszler P, Carlsson J O, Demirev P *J. Chem. Phys.* **107** 10440 (1997)
223. Frenzel U et al. *Z. Phys. D* **40** 108 (1997)
224. Farges J et al. *Surf. Sci.* **106** 95 (1981)
225. Gspann J *Z. Phys. D* **3** 143 (1986)
226. Gspann J, in *Physics of Electronic and Atomic Collisions* (Ed. S Datz) (Amsterdam: North-Holland, 1982) p. 79
227. Frenkel J *Kineticheskaya Teoriya Zhidkostei* (Kinetic Theory of Liquids) (Moscow – Leningrad: Izd. AN SSSR, 1945) [Translated into English (Oxford: The Univ. Press, 1946) Ch. 1]
228. Miller T M, Bederson B, in *Advances in Atomic and Molecular Physics* (Eds D R Bates, I Esterman) (New York: Academic Press, 1977)
229. Tikhonov G et al. *Phys. Rev. A* **64** 063202 (2001)
230. Knight W D et al. *Phys. Rev. B* **31** 2539 (1985)
231. Manninen M, Nieminen R M, Puska M J *Phys. Rev. B* **33** 4289 (1986)
232. Moullet I et al. *Phys. Rev. Lett.* **65** 476 (1990)
233. Guan J et al. *Phys. Rev. B* **52** 2184 (1995)
234. Calaminici P, Jug K, Köster A M *J. Chem. Phys.* **111** 4613 (1999)
235. Kronik L, Vasiliev I, Chelikowsky J R *Phys. Rev. B* **62** 9992 (2000)
236. Kümmel S, Akola J, Manninen M *Phys. Rev. Lett.* **84** 3827 (2000)
237. Ashcroft N W, Mermin N D *Solid State Physics* (New York: Holt, Rinehart and Winston, 1976) [Translated into Russian (Moscow: Mir, 1979)]
238. Moro R et al. *Science* **300** 1265 (2003)
239. Moro R et al. *Phys. Rev. Lett.* **93** 086803 (2004)
240. Ginzburg V L *J. Supercond.* **13** 665 (2000)
241. Ginzburg V L *Usp. Fiz. Nauk* **174** 1240 (2004) [*Phys. Usp.* **47** 1155 (2004)]
242. Andreev A F *J. Supercond.* **12** 197 (1999)
243. Andersen K E et al. *Phys. Rev. B* **73** 125418 (2006)
244. Andersen K E et al. *Phys. Rev. Lett.* **93** 246105 (2004)
245. Fa W, Luo Ch, Dong J *Phys. Rev. B* **71** 245415 (2005)
246. Knickelbein M B *J. Chem. Phys.* **118** 6230 (2003)
247. Xu X et al. *Phys. Rev. B* **75** 085429 (2007)
248. Simonds J L *Phys. Today* **48** (4) 26 (1995)
249. Landau L D, Lifshitz E M *Elektrodinamika Sploshnykh Sred* (Electrodynamics of Continuous Media) (Moscow: Nauka, 1982) [Translated into English (Oxford: Pergamon Press, 1984)]
250. Kittel Ch *Introduction to Solid State Physics* 5th ed. (New York: Wiley, 1976) [Translated into Russian (Moscow: Nauka, 1978)]
251. Khanna S N, Linderoth S *Phys. Rev. Lett.* **67** 742 (1991)
252. Gerlach W, Stern O *Z. Phys.* **9** 349 (1922)
253. Billas I M L et al. *Phys. Rev. Lett.* **71** 4067 (1993)
254. Billas I M L, Châtelain A, de Heer W A *Surf. Rev. Lett.* **3** 429 (1996)
255. Billas I M L, Châtelain A, de Heer W A *Science* **265** 1682 (1994)
256. Billas I M L, Châtelain A, de Heer W A *J. Magn. Magn. Mater.* **168** 64 (1997)
257. Hirt A et al. *Z. Phys. D* **40** 160 (1997)
258. Pastor G M, Hirsch R, Mühlschlegel B *Phys. Rev. B* **53** 10382 (1996)
259. Mahendran M *Solid State Sci.* **7** 325 (2005)
260. Lyalin A, Solov'yov A V, Greiner W *Phys. Rev. A* **74** 043201 (2006)
261. Polesya S et al. *Europhys. Lett.* **74** 1074 (2006)
262. Mattis D C *The Theory of Magnetism* (Berlin: Springer-Verlag, 1988)
263. Knickelbein M B *J. Chem. Phys.* **125** 044308 (2006)
264. Serrano-Guisan S et al. *Nature Mater.* **5** 730 (2006)
265. Pacheco J M, Schöne W-D *Phys. Rev. Lett.* **79** 4986 (1997)
266. Ellert C et al. *Phys. Rev. Lett.* **75** 1731 (1995)
267. Reiners Th et al. *Chem. Phys. Lett.* **215** 357 (1993)
268. Hahn M Y, Whetten R L *Phys. Rev. Lett.* **61** 1190 (1988)
269. Zabel T, Garcia M E, Bennemann K H *Eur. Phys. J. D* **7** 219 (1999)
270. Chang H-C et al. *Israel J. Chem.* **39** 231 (1999)
271. Wang Y-S et al. *J. Am. Chem. Soc.* **120** 8777 (1998)
272. Jiang J-C et al. *J. Am. Chem. Soc.* **122** 1398 (2000)
273. Thompson J M, Bulgac A *Z. Phys. D* **40** 462 (1997)
274. Selby K et al. *Phys. Rev. B* **43** 4565 (1991)
275. Martin T P et al. *J. Chem. Phys.* **100** 2322 (1994)
276. Schmidt M et al. *Nature* **393** 238 (1998)
277. Haberland H et al. *Phys. Rev. Lett.* **94** 035701 (2005)
278. Berry R S, Jellinek J, Natanson G *Phys. Rev. A* **30** 919 (1984)
279. Beck T L, Jellinek J, Berry R S *J. Chem. Phys.* **87** 545 (1987)
280. Smirnov B M *Usp. Fiz. Nauk* **177** 369 (2007) [*Phys. Usp.* **50** 354 (2007)]
281. Bulgac A *Czech. J. Phys.* **48** 697 (1998)
282. Li Y, Blaisten-Barojas E, Papaconstantopoulos D A *Phys. Rev. B* **57** 15519 (1998)
283. Bréchignac C et al. *Phys. Rev. Lett.* **89** 183402 (2002)
284. Bréchignac C et al. *Phys. Rev. A* **68** 063202 (2003)
285. Sizun M, Aquillon F *Phys. Chem. Chem. Phys.* **3** 5225 (2001)
286. Sizun M, Aquillon F, Sidis V *J. Chem. Phys.* **123** 074331 (2005)
287. Hervieux P A et al. *J. Phys. B: At. Mol. Opt. Phys.* **34** 3331 (2001)
288. Babikov D et al. *Chem. Phys. Lett.* **316** 129 (2000)
289. Ho J et al. *J. Chem. Phys.* **99** 140 (1993)
290. Boyukata M et al. *Int. J. Mod. Phys. C* **16** 295 (2005)

291. Gée C et al. *J. Phys. Chem.* **100** 13421 (1996)
292. Gée C et al. *J. Chem. Phys.* **107** 4194 (1997)
293. Lugovoj E, Toennies J P, Vilesov A *J. Chem. Phys.* **112** 8217 (2000)
294. Lallement A et al. *Chem. Phys. Lett.* **189** 182 (1992)
295. Yamaguchi N et al. *Thin Solid Films* **345** 34 (1999)
296. Yamaguchi N, Terashima K, Yoshida T *J. Mater. Sci. Lett.* **17** 2067 (1998)
297. Ross J, Andres R P *Surf. Sci.* **106** 11 (1981)
298. Buffat Ph, Borel J-P *Phys. Rev. A* **13** 2287 (1976)
299. Yamada I et al., in *Proc. 6th Symp. on Ion Sources and Ion Assisted Technology, Tokyo, 1982,* p. 47
300. Farges J et al. *J. Chem. Phys.* **84** 3491 (1986)
301. Farges J, Raoult B, Torchet G *J. Chem. Phys.* **59** 3454 (1973)
302. Farges J et al. *J. Chem. Phys.* **78** 5067 (1983)
303. Lee J W, Stein G D *Surf. Sci.* **156** 112 (1985)
304. Lee J W, Stein G D *J. Phys. Chem.* **91** 2450 (1987)
305. van de Waal B W, Torchet G, de Feraudy M-F *Chem. Phys. Lett.* **331** 57 (2000)
306. Torchet G, de Feraudy M-F, Loreaux Y *J. Mol. Struct.* **486** 261 (1999)
307. Kovalenko S I et al. *J. Cryst. Growth.* **191** 553 (1998)
308. Bartell L S et al. *J. Phys. Chem.* **91** 2498 (1987)
309. Beniere F M et al. *J. Phys. Chem.* **97** 10472 (1993)
310. Torchet G, de Feraudy M-F, Raoult B *J. Chem. Phys.* **103** 3074 (1995)
311. Holland R J et al. *J. Chem. Phys.* **88** 7952 (1988)
312. Kovalenko S I et al. *Fiz. Nizk. Temp.* **20** 961 (1994) [*Low Temp. Phys.* **20** 758 (1994)]
313. Kovalenko S I et al. *Fiz. Nizk. Temp.* **24** 481 (1998) [*Low Temp. Phys.* **24** 364 (1998)]
314. Calvo F, Torchet G, de Feraudy M-F *J. Chem. Phys.* **111** 4650 (1999)
315. Torchet G et al. *J. Chem. Phys.* **81** 2137 (1984)
316. Torchet G et al. *J. Chem. Phys.* **105** 3671 (1996)
317. Gafner Yu Ya et al. *Fiz. Tverd. Tela* **47** 1304 (2005) [*Phys. Solid State* **47** 1353 (2005)]
318. Jellinek J, Srinivas S, Fantucci P *Chem. Phys. Lett.* **288** 705 (1998)
319. Branz W et al. *Chem. Phys. Lett.* **328** 245 (2000)
320. Branz W et al. *Phys. Rev. B* **66** 094107 (2002)
321. Farges J et al. *J. Phys.* (Paris) **38** (C2 – 7) 47 (1977)
322. Farges J et al., in *Rarefied Gas Dynamics*: *Technical Papers* (Prog. in Astronautics and Aeronautics, Vol. 51, Ed. J L Potter) (New York: Am. Inst. of Aeronautics and Astronautics, 1977) p. 1117
323. van de Waal B W *J. Chem. Phys.* **90** 3407 (1989)
324. van de Waal B W *Z. Phys. D* **20** 349 (1991)
325. Euken A, Schroder E *Z. Phys. Chem. B* **41** 307 (1938)
326. Calvo F, Torchet G *J. Cryst. Growth* **299** 374 (2007)
327. Bartell L S, Huang J *J. Phys. Chem.* **98** 7455 (1994)
328. Huang J, Bartell L S *J. Phys. Chem.* **99** 3924 (1995)
329. Johari G P *J. Chem. Phys.* **122** 194504 (2005)
330. Ju S-P, Yang S-H, Liao M-L *J. Phys. Chem. B* **110** 9286 (2006)
331. Caleman C, van der Spoel D *J. Chem. Phys.* **125** 154508 (2006)
332. Kuo J-L, Klein M L *J. Chem. Phys.* **122** 024516 (2005)
333. Svanberg M, Pettersson J B C *J. Phys. Chem. A* **102** 1865 (1998)
334. Christie R A, Jordan K D *J. Phys. Chem. B* **106** 8376 (2002)
335. McDonalds S, Singer S J, Ojamae L *J. Phys. Chem. A* **102** 2824 (1998)
336. Miyazaki M et al. *Science* **304** 1134 (2004)
337. Shin J-W et al. *Science* **304** 1137 (2004)
338. Wong R L, Paech K, Williams E R *Int. J. Mass. Spectrom.* **232** 59 (2004)
339. Klein M L, Venables J A (Eds) *Rare Gas Solids* Vol. II (London: Academic Press, 1977)
340. Farges J *J. Cryst. Growth* **31** 79 (1975)
341. Torchet G, Docteures-Sciences Thesis (Paris: Paris Univ., 1978)
342. Frenzel U et al. *Surf. Rev. Lett.* **3** 505 (1996)
343. Heszler P, Carlsson J O, Demirev P *Phys. Rev. B* **53** 12541 (1996)
344. Mitzner R, Campbell E E B *Surf. Rev. Lett.* **3** 759 (1996)
345. Wan Z, Christian J F, Anderson S L *J. Chem. Phys.* **96** 3344 (1992)
346. Frenzel U, Roggenkamp A, Kreisle D *Chem. Phys. Lett.* **240** 109 (1995)
347. Bohren C F, Huffman D R *Absorption and Scattering of Light by Small Particles* (New York: Wiley, 1983)
348. Westergren J et al. *J. Chem. Phys.* **107** 3071 (1997)
349. Westergren J et al. *J. Chem. Phys.* **109** 9848 (1998)
350. Westergren J et al. *Nanostruct. Mater.* **12** 281 (1999)
351. Westergren J, Nordholm S, Rosén A *Eur. Phys. J. D* **22** 81 (2003)
352. Kolodney E, Budrevich A, Tsipinyuk B *Phys. Rev. Lett.* **74** 510 (1995)
353. Campbell E E B, Ulmer G, Hertel I V *Z. Phys. D* **24** 81 (1992)
354. Klots C E *Chem. Phys. Lett.* **186** 73 (1991)
355. Steger H et al. *Chem. Phys. Lett.* **234** 455 (1995)
356. Klots C E *Z. Phys. D* **20** 105 (1991)
357. Radi P P et al. *Chem. Phys. Lett.* **174** 223 (1990)
358. Sandler P, Lifshitz C, Klots C E *Chem. Phys. Lett.* **200** 445 (1992)
359. Allamandola L J, Thielens G G M, Barker J R *Astrophys. J. Suppl. Ser.* **71** 733 (1989)
360. Bethune D S et al. *Chem. Phys. Lett.* **179** 181 (1991)
361. Ievlev D N et al. *Rev. Sci. Instrum.* **74** 3031 (2003)
362. Branz W, Ph.D. Thesis (Stuttgart: Univ. of Stuttgart, 2001)
363. Weber B, Scholl R *J. Illumin. Eng. Soc.* **21** (2) 93 (1992)
364. Scholl R, in *Physics and Chemistry of Finite Systems*: *From Clusters to Crystals* Vol. 2 (NATO ASI Series, Ser. C, Vol. 374, Eds P Jena, S N Khanna, B K Rao) (Dordrecht: Kluwer Acad. Publ., 1992) p. 1275
365. Weber B, Scholl R *J. Appl. Phys.* **74** 607 (1993)
366. Smirnov B M *Phys. Scripta* **51** 380 (1995)
367. Smirnov B M *Phys. Scripta* **53** 608 (1996)
368. Smirnov B M *Teplofiz. Vys. Temp.* **34** 512 (1996) [*High Temp.* **34** 506 (1996)]
369. Scholl R, Notour G, in *Phenomena in Ionized Gases* (AIP Conf. Proc., Vol. 363, Eds K H Becker, W E Carr, E E Kunhardt) (Woodbury, NY: AIP, 1996) p. 373
370. Heintel M, Neiger M, Scholl R *Contrib. Plasma Phys.* **38** 419 (1998)
371. Lide D R (Ed.) *CRC Handbook of Chemistry and Physics 74th ed.* (Boka Raton: CRC Press, 1993 – 1994)
372. Ascencio J A et al. *Surf. Sci.* **396** 349 (1998)
373. Borman V D et al. *Zh. Eksp. Teor. Fiz.* **130** 984 (2006) [*JETP* **103** 850 (2006)]
374. Dolbec R et al. *Phys. Rev. B* **70** 201406 (2004)
375. Sibener S J, Hislop P, in *LBL Report, Part VII, Advanced Isotope Separation Technology* (1978) p. 470
376. Klekamp A, Umbach E *Surf. Sci.* **249** 75 (1991)
377. Makarov G N, Petin A N *Pis'ma Zh. Eksp. Teor. Fiz.* **83** 115 (2006) [*JETP Lett.* **83** 87 (2006)]
378. Makarov G N, Petin A N *Chem. Phys. Lett.* **426** 464 (2006)
379. Makarov G N, Petin A N *Kvantovaya Elektron.* **36** 889 (2006) [*Quantum Electron.* **36** 889 (2006)]
380. Makarov G N, Petin A N *Zh. Eksp. Teor. Fiz.* **130** 804 (2006) [*JETP* **103** 697 (2006)]
381. Makarov G N, Petin A N *Optika Spektrosk.* **102** 438 (2007) [*Opt. Spectrosc.* **102** 388 (2007)]
382. Hartmann M et al. *Phys. Rev. Lett.* **75** 1566 (1995)
383. Grebenev S, Toennies J P, Vilesov A F *Science* **279** 2083 (1998)
384. McDowell R et al. *Spectrochim. Acta A* **42** 351 (1986)
385. Lokhman V N, Makarov G N *Chem. Phys. Lett.* **398** 453 (2004)
386. Lokhman V N, Makarov G N *Zh. Eksp. Teor. Fiz.* **127** 570 (2005) [*JETP* **100** 505 (2005)]
387. Lokhman V N, Makarov G N *Khim. Fiz.* **26** (4) 7 (2007)
388. Pawlow P *Z. Phys. Chem.* **65** 1, 545 (1909)
389. Takagi M *J. Phys. Soc. Jpn.* **9** 359 (1954)
390. Lindeman F A *Z. Phys.* **11** 609 (1910)
391. Hansen J-P, Verlet L *Phys. Rev.* **184** 151 (1969)
392. Berry R S *Sci. Am.* **263** (2) 50 (1990)
393. Etters R D, Kaelberer J *Phys. Rev. A* **11** 1068 (1975)
394. Kaelberer J B, Etters R D *J. Chem. Phys.* **66** 3233 (1977)
395. Berry R S et al. *Adv. Chem. Phys.* **90** 75 (1988)
396. Zhou Y et al. *J. Chem. Phys.* **116** 2323 (2002)
397. Garrigos R, Cheyssac P, Kofman R *Z. Phys. D* **12** 497 (1989)
398. Lai S L et al. *Phys. Rev. Lett.* **77** 99 (1996)
399. Martin T P *Phys. Rep.* **273** 199 (1996)
400. Jortner J et al., in *The Chemical Physics of Atomic and Molecular Clusters*: *Proc. of the Intern. School of Physics 'Enrico Fermi'. Course LI* (New York: Academic Press, 1971) p. 73
401. Berry R, in *Clusters of Atoms and Molecules*: *Theory, Experiment, and Clusters of Atoms* (Springer Series in Chemical Physics, Vol. 52) (Ed H Haberland) (Springer-Verlag, Berlin, 1994) Ch. 2.8

402. Schmidt M et al. *Phys. Rev. Lett.* **79** 99 (1997)
403. Bertsch G *Science* **277** 1619 (1997)
404. Schmidt M et al. *Phys. Rev. Lett.* **87** 203402 (2001)
405. Schmidt M et al. *Phys. Rev. Lett.* **90** 103401 (2003)
406. Krishnamurty S et al. *Phys. Rev. B* **73** 045406 (2006)
407. Breaux G A et al. *Phys. Rev. Lett.* **94** 173401 (2005)
408. Neal C M, Starace A K, Jarrold M F *J. Am. Soc. Mass Spectrom.* **18** 74 (2007)
409. Labastie P, Whetten R L *Phys. Rev. Lett.* **65** 1567 (1990)
410. Ercolessi F, Andreoni W, Tosatti E *Phys. Rev. Lett.* **66** 911 (1991)
411. Ju N, Bulgac A *Phys. Rev. B* **48** 2721 (1993)
412. Smirnov B M *Phys. Scripta* **50** 427 (1994)
413. Hervieux P A, Gross D H E *Z. Phys. D* **33** 295 (1995)
414. Calvo F, Spiegelmann F *J. Chem. Phys.* **112** 2888 (2000)
415. Aguado A et al. *J. Phys. Chem. B* **105** 2386 (2001)
416. Berry R S, Smirnov B M *J. Chem. Phys.* **118** 5979 (2003)
417. Ding F, Rosén A, Bolton K *Phys. Rev. B* **70** 075416 (2004)
418. Teng Y et al. *J. Phys Chem. B* **111** 2309 (2007)
419. Duan H et al. *Chem. Phys.* **333** 57 (2007)
420. Zhukov A V, Kraynyukova A, Cao J *Phys. Lett. A* **364** 329 (2007)
421. Shvartsburg A A, Jarrold M F *Phys. Rev. Lett.* **85** 2530 (2000)
422. Joshi K, Kanhere D G, Blundell S A *Phys. Rev. B* **66** 155329 (2002)
423. Klots C E *J. Chem. Phys.* **83** 5854 (1985)
424. Klots C E *Z. Phys. D* **5** 83 (1987)
425. Klots C E *J. Chem. Phys.* **90** 4470 (1989)
426. Klots C E *Z. Phys. D* **21** 335 (1991)
427. Klots C E *Nature* **327** 222 (1987)
428. Klots C E *J. Phys. Chem.* **92** 5864 (1988)
429. Robinson P J, Holbrook K A *Unimolecular Reactions* (London: Wiley, 1972) [Translated into Russian (Moscow: Mir, 1975)]
430. Eyring H, Lin S H, Lin S M *Basic Chemical Kinetics* (New York: Wiley, 1980)
431. Marcus R A *J. Chem. Phys.* **20** 359 (1952)
432. Klots C E *J. Phys. Chem.* **75** 1526 (1971)
433. Hansen K, Campbell E E B *Int. J. Mass Spectrom.* **233** 215 (2004)
434. Torchet G et al. *J. Chem. Phys.* **79** 6196 (1983)
435. Valente E J, Bartell L S *J. Chem. Phys.* **79** 2683 (1983)
436. Valente E J, Bartell L S *J. Chem. Phys.* **80** 1451 (1984)
437. Brockhaus P et al. *Phys. Rev. A* **59** 495 (1999)
438. Jundt G et al. *Chem. Phys. Lett.* **370** 504 (2003)
439. Beck R D et al. *Chem. Phys. Lett.* **257** 557 (1996)
440. O'Brien S C et al. *J. Chem. Phys.* **88** 220 (1988)
441. DeMuro R L, Jelski D A, George T F *J. Phys. Chem.* **96** 10603 (1992)
442. Vandenbosch R *J. Phys. Chem.* **99** 14686 (1995)
443. Magnera T F, David D E, Michl J *Chem. Phys. Lett.* **123** 327 (1986)
444. Andersen J U et al. *Eur. Phys. J. D* **24** 191 (2003)
445. Even U, Schek I, Jortner J *Chem. Phys. Lett.* **202** 303 (1993)
446. Schek I, Jortner J *J. Chem. Phys.* **104** 4337 (1996)
447. Zel'dovich Ya B, Raizer Yu P *Fizika Udarnykh Voln i Vysokotemperaturnykh Gidrodinamicheskikh Yavlenii* (Physics of Shock Waves and High-Temperature Hydrodynamic Phenomena) 2nd ed. (Moscow: Nauka, 1966) [Translated into English (Mineola, NY: Dover Publ., 2002)]
448. Vostrikov A A, Dubov D Yu, Predtechenskii M R *Zh. Tekh. Fiz.* **56** 1393 (1986) [*Sov. Phys. Tech. Phys.* **31** 821 (1986)]
449. Vostrikov A A, Dubov D Yu, Predtechenskii M R *Zh. Tekh. Fiz.* **57** 760 (1987) [*Sov. Phys. Tech. Phys.* **32** 459 (1987)]
450. Vostrikov A A, Dubov D Yu, Predtechenskiy M R *Chem. Phys. Lett.* **139** 124 (1987)
451. Vostrikov A A, Dubov D Yu, Predtechenskii M R *Zh. Tekh. Fiz.* **58** 1897 (1988) [*Sov. Phys. Tech. Phys.* **33** 1153 (1988)]
452. Vostrikov A A, Dubov D Yu *Z. Phys. D* **20** 61 (1991)
453. Vostrikov A A et al. *Z. Phys. D* **40** 542 (1997)
454. Gephardt C R, Schröder H, Kompa K-L *Nature* **400** 544 (1999)
455. Andersson P U, Pattersson J B C *Z. Phys. D* **41** 57 (1997)
456. Andersson P U, Pattersson J B C *J. Phys. Chem.* **102** 7428 (1998)
457. Even U et al. *Phys. Rev. Lett.* **56** 965 (1986)
458. De Lange P J, Renkema P J, Kommandeur J *J. Phys. Chem.* **92** 5749 (1988)
459. Yeretzian C, Hansen K, Whetten R L *Science* **260** 652 (1993)
460. Leisner T et al. *Z. Phys. D* **20** 127 (1991)
461. Amrein A, Simpson R, Hackett P *J. Chem. Phys.* **95** 1781 (1991)
462. Yeretzian C, Whetten R L *Z. Phys. D* **24** 199 (1992)
463. Campbell E E B, Ulmer G, Hertel I V *Phys. Rev. Lett.* **67** 1986 (1991)
464. John P M St, Whetten R L *Chem. Phys. Lett.* **196** 330 (1992)
465. John P M St, Yeretzian C, Whetten R L *J. Phys Chem.* **96** 9100 (1992)
466. Hendell E, Even U *J. Chem. Phys.* **103** 9045 (1995)
467. Töglhofer K et al. *J. Chem. Phys.* **99** 8254 (1993)
468. Töglhofer K et al. *Nucl. Instrum. Meth. Phys. Res. B* **88** 44 (1994)
469. Baudin K et al. *Nucl. Instrum. Meth. Phys. Res. B* **117** 47 (1996)
470. Billebaud A et al. *Nucl. Instrum. Meth. Phys. Res. B* **112** 79 (1996)
471. Aumayr F et al. *Int. J. Mass Spectrom. Ion Process.* **163** 9 (1997)
472. Aumayr F et al. *Int. J. Mass Spectrom. Ion Process.* **174** 317 (1998)
473. Winter H P *Phys. Rev. A* **56** 3007 (1997)
474. Fallavier M *Nucl. Instrum. Meth. Phys. Res. B* **112** 72 (1996)
475. Hendell E et al. *Phys. Rev. Lett.* **75** 2670 (1995)
476. Christen W et al. *Int. J. Mass Spectrom. Ion Process.* **174** 35 (1998)
477. Christen W, Even U *Eur. Phys. J. D* **24** 283 (2003)
478. Farizon B et al. *Int. J. Mass Spectrom. Ion Process.* **164** 225 (1997)
479. Ehlich R, Westerburg M, Campbell E E B *J. Chem. Phys.* **104** 1900 (1996)
480. Ouaskit S et al. *Int. J. Mass Spectrom. Ion Process.* **139** 141 (1994)
481. LeBrun T et al. *Phys. Rev. Lett.* **72** 3965 (1994)
482. Farizon B et al. *Nucl. Instrum. Meth. Phys. Res. B* **88** 86 (1994)
483. Zimmermann S, Urbassek H M *Eur. Phys J. D* **39** 423 (2006)
484. Raz T, Even U, Levine R D *J. Chem. Phys.* **103** 5394 (1995)
485. Raz T, Levine R D *J. Chem. Phys.* **105** 8097 (1996)
486. Raz T, Levine R D *Chem. Phys.* **213** 263 (1996)
487. Lifshitz C, Louage F *J. Phys. Chem.* **93** 5633 (1989)
488. Wei S, Tzeng W B, Castleman A W (Jr) *J. Chem. Phys.* **92** 332 (1990)
489. Wei S, Tzeng W B, Castleman A W (Jr) *J. Chem. Phys.* **93** 2506 (1990)
490. Beck R D et al. *Chem. Phys. Lett.* **187** 122 (1991)
491. Beck R D et al. *J. Phys. Chem.* **95** 8402 (1991)
492. Mowrey R C et al. *J. Phys. Chem.* **95** 7138 (1991)
493. Gross A, Levine R D *J. Phys. Chem. A* **107** 9567 (2003)
494. Shao Y L et al. *Phys. Rev. Lett.* **77** 3343 (1996)
495. Smirnov M B et al. *Zh. Eksp. Teor. Fiz.* **125** 1283 (2004) [*JETP* **98** 1123 (2004)]
496. Perry M D, Mourou G *Science* **264** 917 (1994)
497. Kryukov P G *Kvantovaya Elektron.* **31** 95 (2001) [*Quantum Electron.* **31** 95 (2001)]
498. Lezius M et al. *Phys. Rev. Lett.* **80** 261 (1998)
499. Hutchinson H *Science* **280** 693 (1998)
500. McPherson A et al. *Phys. Rev. Lett.* **72** 1810 (1994)
501. Ditmire T et al. *Phys. Rev. Lett.* **75** 3122 (1995)
502. Dobosz S et al. *Pis'ma Zh. Eksp. Teor. Fiz.* **68** 454 (1998) [*JETP Lett.* **68** 485 (1998)]
503. Abdallah J (Jr) et al. *Phys. Rev. A* **68** 063201 (2003)
504. Wabnitz H et al. *Nature* **420** 482 (2002)
505. Kapteyn H C, Ditmire T *Nature* **420** 467 (2002)
506. Schulz J et al. *Nucl. Instrum. Meth. Phys. Res. A* **507** 572 (2003)
507. Laarmann T et al. *Phys. Rev. Lett.* **92** 143401 (2004)
508. Laarmann T et al. *Phys. Rev. Lett.* **95** 063402 (2005)
509. de Castro A R B et al. *J. Electron Spectrosc. Relat. Phenomena* **144** 3 (2005)
510. Rusek M, Lagadec H, Blenski T *Phys. Rev. A* **63** 013203 (2000)
511. Brewczyk M, Rzazewski K *J. Phys. B: At. Mol. Opt. Phys.* **32** L1 (1999)
512. Last I, Jortner J *Phys. Rev. A* **60** 2215 (1999)
513. Krainov V P, Roshchupkin A S *J. Phys. B: At. Mol. Opt. Phys.* **34** L297 (2001)
514. Samson J A R *Phys. Lett.* **8** 107 (1964)
515. Rose-Petruck C et al. *Phys. Rev. A* **55** 1182 (1997)
516. Last I, Jortner J *Phys. Rev. A* **62** 013201 (2000)
517. Augst S et al. *Phys. Rev. Lett.* **63** 2212 (1989)